universität wien

MASTERARBEIT / MASTER'S THESIS

Titel der Masterarbeit / Title of the Master's Thesis

Investigating the mechanism of host translation shut off by human rhinovirus 2A proteinases

verfasst von / submitted by

Öykü Üzülmez

angestrebter akademischer Grad / in partial fulfilment of the requirements for the degree of

Master of Science (MSc)

Wien 2017 / Vienna 2017

Studienkennzahl lt. Studienblatt / Degree programme code as it appears on the student record sheet:	A 066 863
Studienrichtung lt. Studienblatt / Degree programme as it appears on the student record sheet:	Masterstudium Biologische Chemie
Betreut von / Supervisor:	Ao. Univ.-Prof. Dr. Timothy Skern

ACKNOWLEDGEMENT

I would like spare this page to thank everyone who supported me through this journey.

I owe my supervisor Prof. Tim Skern a debt of gratitude for accepting me to his lab, for encouraging me about my job, for showing me how it is done.

I want to thank every Skernling who ever passed by to our lab. Especially, I was lucky to be tutored by Martina Aumayr, who introduced me to the laboratory work. Thank you for helping me whenever I needed. We were a crowded lab with many smiling faces: Nina Bobik, Amelie Schoenenwald, Daniel Azar, Sofiya Fedosyuk, and Gustavo Arruda Bezerra. Thank you all for being supportive, for cheering me up about ITC, for being friends rather than just colleagues.

I would also like to thank to all of my friends, for putting so much stress on my shoulders by believing in me unconditionally! Special thanks go to Ceren Bilgilier, for many things: Thank you for being such an amazing friend for 14 years, for your support, for listening me when I had mood swings about my experiments, but particularly for bringing me food while I was writing this thesis.

Ve son olarak canım aileme teşekkür etmek istiyorum. Annem'e ve Babam'a: Bana inandığınız için, hep destek olduğunuz için, yaptığım bilimi anlamak istediğiniz için, ve beni koşulsuz sevdiğiniz için çok teşekkürler. Kardeşim'e: Sana abla olmak yaptığım en zor ve en güzel işlerden biri. İyi ki senin ablanım. Benimle gurur duyduğunu her fırsatta dile getirdiğin için çok teşekkür ederim.

TABLE OF CONTENTS

ABSTRACT

Picornavirus term originates from the words “pico” (means small quantity in Spanish) and RNA. These are non-enveloped, small, genomic RNA containing viruses that are responsible for the common cold. Human rhinoviruses belong to the *Enterovirus* genus within the *Picornaviridae* family. An icosahedral capsid protects the viral genes encoded within the positive sense single-stranded RNA. The virus translates a single polyprotein from one large open-reading frame, which is later processed by viral proteinases into mature viral proteins. First, HRV $2A^{pro}$ cleaves itself from the polyprotein co-translationally between its N-terminal domain and the C-terminal domain of the preceding VP1 protein. Subsequently, other cleavages are performed by other viral proteinases ($3C^{pro}$ and $3CD^{pro}$) to result in eleven mature proteins.

The genetic divergence, replication site, and disease associations are responsible for the division of HRVs into three species, namely the genetic groups A, B, C. We wanted to investigate the major differences between the $2A^{pro}$ from genetic groups A and B. Therefore, we performed *in vitro* biochemical and biophysical interaction experiments with $2A^{pro}$ from HRV1A and HRV4 against eukaryotic initiation factors to elucidate the structural homology of the proteinases.

First, we expressed the recombinant $2A^{pro}$ from the HRV1A serotype. The active proteinase was tested with eukaryotic initiation factors (eIF4E and $eIF4GII_{551-745}$: residues between 551-745 covering the eIF4E binding site and the $2A^{pro}$ cleavage site), as eIF4G is cleaved in cells that are infected with HRV. We certified that the $2A^{pro}$ from HRV1A and HRV2 cleave the $eIF4GII_{551-745}$ at the same rate. The inactive (C106A) purified proteinase was used for binding studies with eukaryotic initiation factors. We found that the binding interactions were very similar between HRV1A $2A^{pro}$ and HRV2 $2A^{pro}$. We confirmed ternary complex formation with HRV1A $2A^{pro}$/eIF4E/$eIF4GII_{551-745}$ as it was published for the HRV2 $2A^{pro}$; this is expected due to 86.3 % shared sequence homology. eIF4E is capable of forming a binary complex with the $2A^{pro}$ whereas $eIF4GII_{551-745}$ cannot. These results coincide for both $2A^{pro}$ from the genetic group A (Aumayr et al., 2015). Moreover, both proteinases were measured as homodimers with 32 kDa molecular mass using static light scattering (Aumayr et al., 2015). The ternary complex with HRV1A $2A^{pro}$ indicated a higher oligomeric state than 1:1:1. This complex has 133 kDa measured molecular mass, which could be explained by a double ternary complex. Isothermal titration calorimetry measured the dissociation constant as 1 μM for the ternary complex. This interaction is stronger than eIF4E/$2A^{pro}$ binding, which is 7 μM.

As the next step, we tried to express recombinant HRV4 $2A^{pro}$. However, we could not produce enough from this protein; therefore, we developed a DNA construct that encodes N-terminal extension to the $2A^{pro}$. The hexahistidine tag followed by the eight VP1 amino acid residues at the N-terminal domain of the proteinase enhanced the expression level. We tested the purified wild-type HRV4 His_6VP1_8 $2A^{pro}$ for enzymatic activity together with the initiation factors. Interestingly, HRV4 His_6VP1_8

$2A^{pro}$ did not cleave the $eIF4GII_{551-745}$ within 2 h, even though 10 times more active proteinase was used when with HRV1A $2A^{pro}$. The poor recognition of eIF4E and $eIF4GII_{551-745}$ by the genetic group B $2A^{pro}$ was also confirmed by binding studies. There is no complex formation between (inactive) HRV4 His_6VP1_8 $2A^{pro}$ C110S and the initiation factors. We observed a possible *cis* cleavage of the proteinase at the VP1-$2A^{pro}$ junction. The inactivation with Ser might have preserved a small amount of nucleophilic characteristic at the active site, which we observe from the detected wild-type length second $2A^{pro}$ band on SDS-PAGE analyses. Important findings about the HRV4 His_6VP1_8 $2A^{pro}$ indicated that this proteinase is a monomer unlike HRV1A $2A^{pro}$ and HRV2 $2A^{pro}$ (Aumayr et al., 2015). The shared sequence homology between HRV4 $2A^{pro}$ and HRV1A $2A^{pro}$ is around 39 % and therefore different structural behavior can be expected. Nevertheless, we know that coxsackievirus (CV) B4 $2A^{pro}$ from the same genus is also a monomer (Baxter et al., 2006); this too shares 39 % amino acid sequence homology. Interestingly, CVB4 $2A^{pro}$ is capable of forming a ternary complex but not a binary complex with either of the initiation factors (Aumayr et al., 2015). To summarize, there are remarkable structural and behavioral differences between the $2A^{pro}$ from genetic group A and B that affect the efficiency of host translation shut off.

ZUSAMMENFASSUNG

Der Begriff Picornaviren stammt von dem Wort “pico” (bedeutet geringe Menge in Spanisch) und RNA. Diese sehr kleinen Viren sind verantwortlich für Schnupfen und Erkältung, und besitzen keine Hülle. Sie weisen eine Ikosahedrale Symmetrie auf und genomische RNA auf. Humane Rhinoviren (HRV) gehören zu der Familie der *Picornaviridae* innerhalb der Gattung Enteroviren. Die einzelsträngige RNA ist vom Ikosahedralen Kapsid umhüllt, um die viralen Gene zu stützen. Es gibt nur einen offenen Leserahmen, von dem ein einzelnes Polyprotein abgelesen wird. Das Polyprotein wird danach prozessiert, um erwachsene virale Proteine zu erhalten. Zunächst spaltet sich wahrend der Translation HRV $2A^{pro}$ vom Polyprotein ab. Diese Prozessierung wird zwischen dem N-Terminus der Proteinase und dem C-Terminus des davorliegenden Proteins VP1 durchgeführt. Die restlichen Schritte der Prozessierung werden bei den anderen Proteinasen $3C^{pro}$ und $3CD^{pro}$ durchgeführt, daher liegen schlussendlich elf fertig prozessierte virale Proteine vor.

Es gibt drei Arten von humanen Rhinoviren (genetische Gruppen A, B, C), die nach Krankheitssymptomen, der genetischen Divergenz und dem Ort der Replikation klassifiziert werden. In dieser Arbeit wird der Unterschied zwischen $2A^{pro}$ aus unterschiedlichen genetischen Gruppen (A und B) vergleichen. Deswegen haben wir *in vitro* biochemische und biophysikalische Experimente durchgeführt mit $2A^{pro}$ von HRV1A und HRV4 durchgeführt, um die strukturelle Homologie zu verstehen.

Zunächst haben wir rekombinante $2A^{pro}$ des HRV1A Subtyps durch Überexpression erzeugt. Die Aktivität der Proteinase wurde mit den eukaryotischen Initiationsfaktoren getestet (eIF4E und $eIF4GII_{51-745}$: Aminosäurereste zwischen 551-745 besitzen den Bindungsort der eIF4E und die Prozessierungsstelle der $2A^{pro}$). Wir konnten bestätigen, dass die $2A^{pro}$ bei den Subtypen HRV1A und HRV2 gleich effizient ist. Die inaktivierte (C106A) HRV1A $2A^{pro}$ wurde für die Bindungsstudien benutzt. Hier fanden wir heraus, dass die Fähigkeit der Bindungsinteraktion für beide Proteinasen der genetischen Gruppe A gleichartig ist. Die Proteinasen von HRV1A und HRV2 sind in ihrer Aminosäurensequenz zu 86.3 % ident. Eine Folge davon ist die Bildung eines ternären Komplexes mit HRV1A $2A^{pro}$/eIF4E/$eIF4GII_{551-745}$, wie es auch für die HRV2 $2A^{pro}$ bestätigt wurde (Aumayr et al., 2015). eIF4E bildet einen binären Komplex mit der Proteinase, $eIF4GII_{551-745}$ allerdings nicht. Die Ergebnisse stimmen mit jenen der HRV2 $2A^{pro}$ überein (Aumayr et al., 2015). Wir fanden mittels statischer Lichtstreuung heraus, dass HRV1A $2A^{pro}$ aus zwei Monomeren besteht und 32 kDa wiegt. Die Dimerisierung der HRV2 $2A^{pro}$ wurde auch von Aumayr et al. publiziert. Der dreifache Komplex aus HRV1A $2A^{pro}$/eIF4E/$eIF4GII_{551-745}$ ließ auf einen höheren oligomeren Zustand mit 133 kDa molekularer Masse schließen. Diese Masse Ließe sich durch einen doppelten ternären Komplex erklären. Wir haben die Thermodynamik der Wechselwirkung mit Isothermer Titrationskalorimetrie gemessen. Einerseits wurde eine Dissoziationskonstante von 1 μM für den ternären Komplex gemessen, andererseits fanden wir 7 μM für die HRV1A $2A^{pro}$/eIF4E Komplexe.

Außerdem haben wir die Überexpression der rekombinanten HRV4 $2A^{pro}$ versucht. Dafür wurde eine Verlängerung am N-Terminus der HRV4 $2A^{pro}$ eingefügt, weil wir nicht genügenden Proteine vom Wildtyp erhalten konnten. Ein Hexahistidin-Tag gefolgt von acht Aminosäuren von VP1 am N-Terminus der Proteinase, verbesserte das Level der Expression. Die aktive HRV4 His_6VP1_8 $2A^{pro}$ wurde zusammen mit Initiationsfaktoren auf enzymatische Aktivität getestet. Wir konnten zeigen, dass $eIF4GII_{551-745}$ von der aktiven Proteinase innerhalb von zwei Stunden nicht prozessiert wird, auch wenn HRV4 His_6VP1_8 $2A^{pro}$ zehnfach konzentrierte als HRV1A $2A^{pro}$ war. Die Bindungsstudien zeigten auch, dass eIF4E und $eIF4GII_{551-745}$ von der $2A^{pro}$ der genetischen Gruppe B schlecht erkannt werden. Es wird kein ternären Komplex zwischen der inaktiven (C110S) HRV4 His_6VP1_8 $2A^{pro}$ und den Initiationsfaktoren aufgebaut. Weder eIF4E, noch $eIF4GII_{551-745}$ bilden Komplexe mit der Proteinase. Trotzdem haben wir eine mögliche Selbstprozessierungsreaktion bei der C110S Mutante von HRV4 His_6VP1_8 $2A^{pro}$ an der VP1-$2A^{pro}$-Region beobachtet. Die Substitution des aktiven Cysteins durch Serin konserviert vermutlich die schwache nucleophile Natur, die für die Selbstprozessierungsreaktion verantwortlich ist. SDS-PAGE Analysen zeigten eine möglicherweise selbstprozessierte zweite $2A^{pro}$-Bande mit Masse des Wildtyps. Ein wichtiges Ergebnis ist die monomere Natur der $2A^{pro}$ von HRV4 His_6VP1_8 im Unterschied zu den dimeren HRV1A $2A^{pro}$ und HRV2 $2A^{pro}$ (Aumayr et al., 2015). Die nur 39 % der Aminosäurensequenz zwischen beiden $2A^{pro}$ von HRV4 und HRV1A ident sind, erwarteten wir keine gleiche Struktur. Allerdings besteht die (CV) B4 $2A^{pro}$ des Coxsackie-Virus,

welcher zu der Gattung *Enteroviren* gehört, aus einem Monomer (Baxter et al., 2006) und ist auch 39 % identisch zur $2A^{pro}$ von HRV4 His_6VP1_8. Dennoch kann die CVB4 $2A^{pro}$ einen ternären Komplex, allerdings keinen binären Komplex mit den Initiationsfaktoren bilden (Aumayr et al., 2015). Zusammenfassend gibt es bemerkenswerte strukturelle und Verhaltensunterschiede zwischen dem $2A^{pro}$ aus der genetischen Gruppe A und B, die die Abschaltung der Host-Translation beeinträchtigen.

1 INTRODUCTION

1.1 Picornaviruses

Picornaviruses, belonging to the family of *Picornaviridae*, represent small, non-enveloped and spherical viruses. Their single-stranded positive sense genomic RNA (~ 7.5 kb) is protected by the surrounding T=3 icosahedral capsid (see figure 1.1), composed of 12 pentameric and 20 hexameric capsids in ~ 30 nm diameter. The structural VP1, VP2, VP3 and VP4 proteins are commissioned to protect the viral genome, which encodes viral proteins needed for maintaining the life cycle (Hogle et al., 1985; Rossmann et al., 1985; Desk Encyclopedia of General Virology, 2010).

The first discovery of a picornavirus member was foot-and-mouth disease virus (FMD) dating back to 1898 by Friedrich Loeffler (Rott & Siddell, 1998). The family harbors other well-known viruses such as; rhinovirus (RV) (formerly known as human rhinovirus: HRV), poliovirus (PV), hepatitis A virus (HAV).

According to the international committee on taxonomy of viruses (ICTV), there are 31 genera belonging to *Picornaviridae* family (ICTV master species list, 2015) (website accessed on November 20, 2016). These genera are: *Aphthovirus, Aquamavirus, Avihepatovirus, Avisivirus, Cardiovirus, Cosavirus, Dicipivirus, Enterovirus, Erbovirus, Gallivirus, Hepatovirus, Hunnivirus, Kobuvirus, Kunsagivirus, Limnipivirus, Megrivirus, Mischivirus, Mosavirus, Oscivirus, Parechovirus, Pasivirus, Passerivirus, Potamipivirus, Rosavirus, Sakobuvirus, Salivirus, Sapelovirus, Senecavirus, Sicinivirus, Teschovirus,* and *Tremovirus*. The diseases emerging from picornaviruses vary from severe conditions such as hepatitis to milder ones such as the common cold (Jiang et al., 2014).

1.1.1 Human rhinovirus (HRV)

HRVs were first isolated from the patients with common cold symptoms dating back 60 years. The characteristic clinical symptoms that are associated with HRV concern both the upper and the lower respiratory tract and even unusual parts like the middle ear fluid (in the case of acute otitis media). Infectious HRV are responsible about 50 % of the common cold cases, affecting both adults and children. In school-aged children, HRV is found to be associated with cystic fibrosis and asthma exacerbations in up to 70 % of the cases (Turner, 2007).

HRV are transmitted mainly by direct contact with eye or nose and by aerosols via the respiratory tract. Viral replication is optimal between temperatures of 33 – 35°C (Mclntyre et al., 2013; Foxman et al., 2014). There are rapid detection methods using real-time PCR assays; however, there are no vaccines or antiviral treatment applications to prevent HRV infections to date (Do et al., 2010; Royston & Tapparel, 2016).

1.1.2 Taxonomy

HRV are classified into three genetic groups harboring 80, 32, and 55 serotypes within HRV-A, HRV-B, and HRV-C, respectively. In total more than 150 serotypes are known at present (http://www.picornaviridae.com/). The classification of these genetic groups is determined according to their sequence homologies, capsid properties, and genome organization. Serotyping is established with cross-neutralization assays in cell culture.

Species Rhinovirus-A and Rhinovirus-B are together divided into two further groups namely the minor group and major group which depending on the receptors that are recognized by the viruses. The minor group consists of twelve HRV-A types which bind to low-density lipoprotein receptors (LDLR) whereas the major group consists of the remaining types from HRV-A and HRV-B that recognize the intercellular adhesion molecule-1 (ICAM-1). Recent findings on receptor recognition of Rhinovirus-C species suggest that viral binding and vigorous replication is associated with cadherin-related family member 3 (CDHR3) (Bochkov et al., 2015). Classification can also be explained with *p*-distance values, which corresponds to a proportion (*p*) of nucleotide sites at which two different sequences are compared are different. According to *p*-distance comparisons in the VP1 region, the minimum needed nucleotide divergence thresholds for separating inter- from intra-serotype are 13 % for HRV-A and HRV-C, 12 % for HRV-B type viruses (Blaas & Fuchs, 2016; Mclntyre et al., 2013; Bochkov et al., 2015). Formerly, the classification between rhinovirus species A and B were established by comparison of rather conserved VP4/VP2 regions (Simmonds et al., 2010).

1.2 Virion

1.2.1 Capsid

Picornaviral capsid assembly and viral protein mapping was first investigated using techniques and equipment such as electron density maps, chemical labeling of the surface particles, crosslinking agents or crosslinking with UV-light. Human rhinovirus 14 was the first discovered atomic resolution structure within the animal viruses, with 3.0 Å resolution (Rossmann et al., 1985). Electron density map was used to solve the structure of virus crystals (see figure 1.1) . Subsequently, the three-dimensional structure of the poliovirus was resolved by X-ray crystallographic methods, with 2.9 Å resolution (Hogle et al., 1985). Lonberg-Holm and his colleagues labeled VP1-4 virion polypeptides from poliovirus and human rhinovirus type 2 with [^{3}H]acetic anhydride in order to investigate surface properties of the native virions; in both cases they found that VP1 was labeled at most when compared to VP2 and VP3. On the other hand, VP4 was not labeled at all which proved its role in the inner shell

(Lonberg-Holm & Butterworth, 1976). Moreover, Mengo virus was treated with cross-linking agents such as dithiobis(succinimidyl propionate) (DSP) in order to reveal interactions between adjacent pentameres that are building up and stabilizing the capsid of the virion (Horden et al., 1979). A remarkable discovery was published by Wetz & Habermehl in 1982 about cross-linking of the poliovirus RNA to the capsid polypeptides using UV light. RNA-protein cross-links produced by low radiation (approx. 5%) were analyzed on SDS-polyacrylamid gels after being freed from unbound protein. Results concluded that the smallest polypeptide VP4 was the most abundant one attached to the RNA, followed by VP2 and VP1. On the other hand, only trace amounts of VP3 was bound to the RNA (Wetz & Habermehl, 1982).

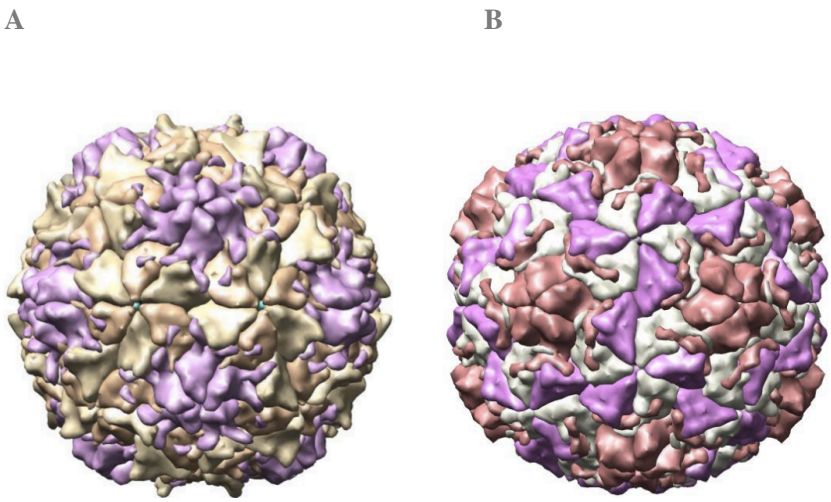

Figure 1.1 The icosahedral symmetry of capsids are depicted for poliovirus type 1 (figure A) and human rhinovirus 14 (figure B). Models were accessed from protein databank (PDB accession codes; poliovirus type 1: 1PO1, human rhinovirus 14: 4RHV).

The viral capsid proteins are VP0, VP1 and VP3. As the last step of assembly, VP0 is cleaved into VP2 and VP4; thus, the RNA inclusion into a fully assembled capsid is accomplished. VP1, VP2, and VP3 are around 30 kDa with their C-termini exposed and located at the outer shell. VP4 is rather small (10 kDa) and covers the interior of the shell. The spherical capsid with T=3 icosahedral symmetry and 300 Å diameter is composed of 60 promoters as described by Caspar and Klug in 1962. Each promoter carries one copy of each capsid protein. Star-shaped plateau is found at the fivefold axis and consists of 5 promoters. There is a depression called canyon around this star-shaped plateau. Each promoter is found at a central threefold axis. (see figure 1.2) (Jacobson et al., 1970; Holge et al., 1985; Rossman et al., 1985).

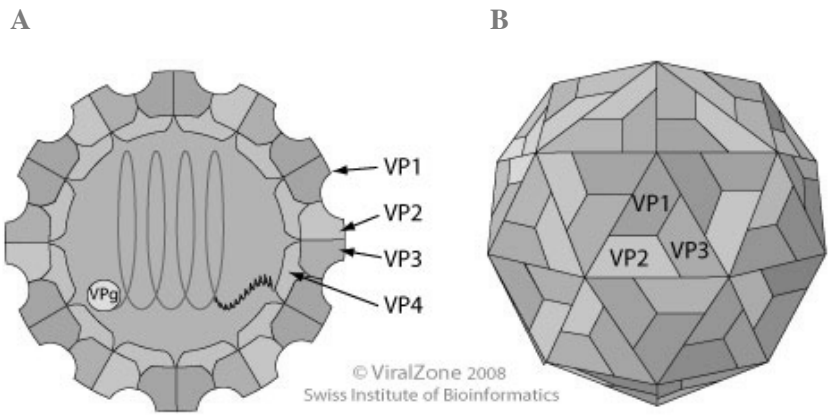

Figure 1.2 T=3 icosahedral symmetry of the *Enterovirus* genus and organization of the capsid. A, cross-section in which the VP4 capsid protein covers the interior, while VP1, VP2 and VP3 are positioned at the outer shell. The genomic single stranded viral RNA is visualized by line connected to viral protein genome-linked (VPg) at 5' end. The polyA tail at the 3' end is illustrated in a zigzag line which is connected to VP4. B, tightly packed VP1, VP2, VP3 and VP4 (inside) in the triangular promoter, a building block for the capsid. A pentameric capsomere consists 5 promoters (figure from http://viralzone.expasy.org).

Each VP is remarkably identical within the core organization, bearing 8-stranded an anti-parallel ß-barrel with two flexible α-helices in the form of wedge-shaped barrel. Nevertheless, there is no significant sequence homology between VP1, VP2 and VP3 (Desk Encyclopedia of General Vrology, 2010; Introduction to Protein Structure, 1999). Due to tight packing of large sequences of VP1, VP2 and VP3 into a promoter, depressions and protrusions are formed. The depressions are 25 Å deep and 12-30 Å wide and located on the surface. They are called the cleft or canyon, and serve as the ICAM-1 receptor binding site for cell entry (see figure 1.3). Immune recognition is prevented since an antibody with 35 Å diameter could not simply fit in this cleft (Rossman et al., 1985).

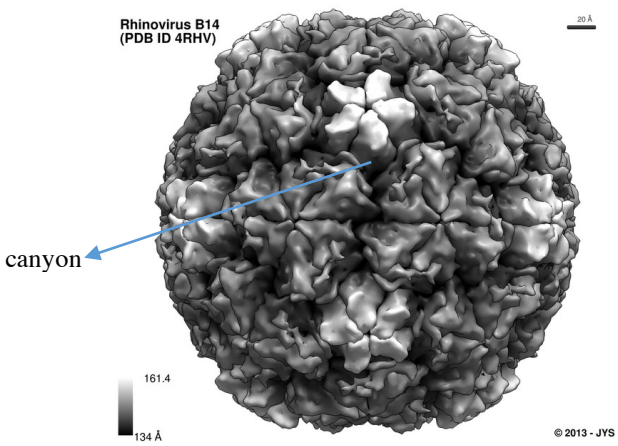

Figure 1.3 Visualization of the capsid surface of HRV14 based on X-ray crystallography. The receptor binding site, namely the canyon, is indicated by an arrow. The star-shaped pentameric capsomere, depressions and protrusions are visible and scaled with color-code at bottom right. Picture from www.virology.wisc.edu (©Jean-Yves Sgro 2013)

1.2.2 Genome

The picornaviral genome is a single-stranded, positive sense RNA, around 7500 nucleotides long. This study concerns 2 serotypes from human rhinovirus within the *Picornaviridae* family; HRV1A and HRV4. Their genome sizes are given below (see table 1.1).

Table 1.1 Viral genome length of two serotypes from human rhinovirus that were studied in this project.

virus	genome length	genbank
HRV 1A	7098 bp	KC894169.1
HRV4	7212 bp	DQ473490.1

Unlike the cellular mRNA, the viral genomic RNA is uncapped at 5' end and there is a protein namely 'viral protein genome-linked' (VPg) which is covalently bound to genome with an assignment to act as primer to initiate the RNA replication (Flanegan et al., 1977; Lee et al., 1997). The VPg connection was investigated by Ambros & Baltimore (1978) using ^{32}P and [^{3}H]tyrosine. A tyrosine residue from VPg is linked to 5' uridine of the viral genome through a phosphodiester bond. The 5' untranslated region (UTR) is around 630 nucleotides long in HRVs (Pilipenko et al., 1990) and harbors significant secondary structures including poly(C) tract (a spacer region), internal ribosomal entry site (IRES) and cis-active RNA elements (cre) that are responsible for converting VPg into $VPgpUpU_{OH}$ and thereby initiating the viral replication (Steil & Barton, 2009). The first 100 nucleotides of the 5' end of enteroviruses form a cloverleaf structure (see figure 1.4) which plays a crucial role in viral growth and organization of the viral proteins such as ribonucleoprotein complexes (RNPs) (Andino et al., 1990). The IRES region is strongly structured and critical for picornaviruses since it promotes cap-independent translation to the virus (Borman & Jackson, 1992). Entero- and rhinoviruses harbor the

IRES type I with a high sequence conservation within the group. On the other hand, there is little sequence homology when compared to IRES type II and IRES type III (Pilipenko et al., 1989).

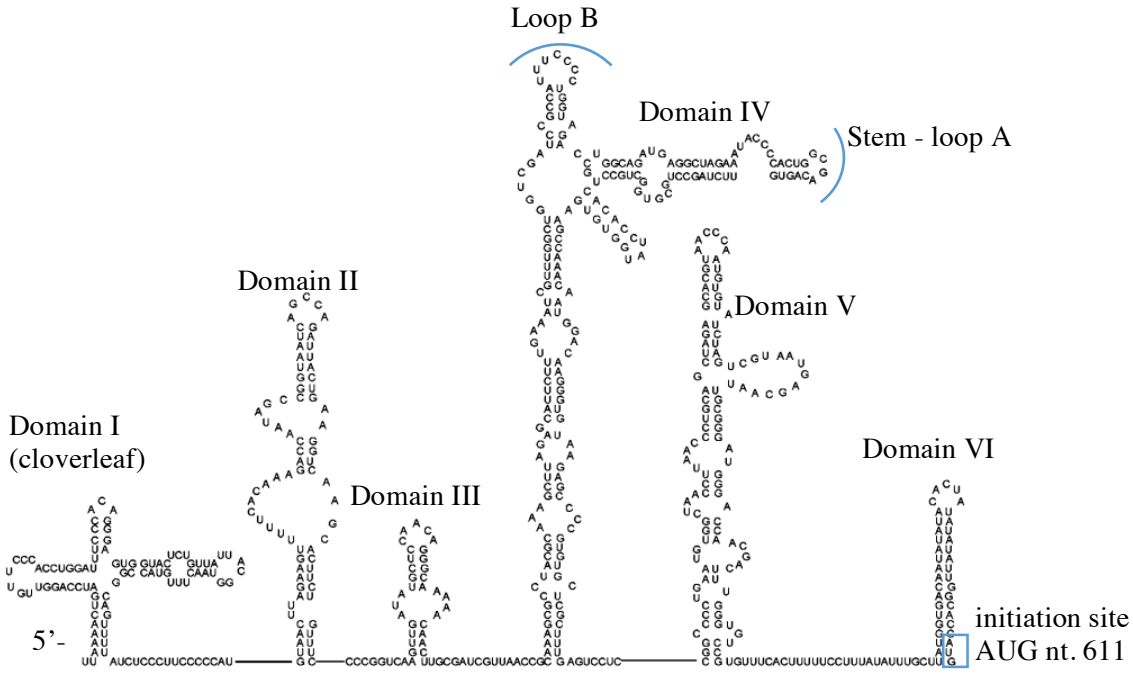

Figure 1.4 Representation of HRV2 5'-UTR with its secondary structures. The cloverleaf-structured domain is attached at the 5' end, which regulates both the translation and replication (Gamarnik & Andino, 1998) and continues with IRES domains II-VI. The ORF starts at the indicated AUG codon at nucleotide position 611. Figure modified from Anderson et al., 2007.

The enteroviral HRV genome encodes a single polyprotein of 250 kDa from one open reading frame consisting of three regions P1-P3, which are then processed into 11 mature proteins (see figure 1.5). P1 is responsible for encoding the coat proteins VP1-VP4, whereas P2 and P3 generate the proteolytically active enzymes and other accessory proteins related to genomic assembly (Rueckert & Wimmer, 1984; Handbook of Proteolytic Enzymes, 2013). Picornaviral short 3'-UTR (40 -60 base) region harbors the poly(A) tail (~ 74 adenosine long) and the ORF termination. There are unbranched stems present at 3'-UTR as well, however their function is unknown at present (Palmenberg et al., 2009; Ahlquist & Kaesberg, 1979).

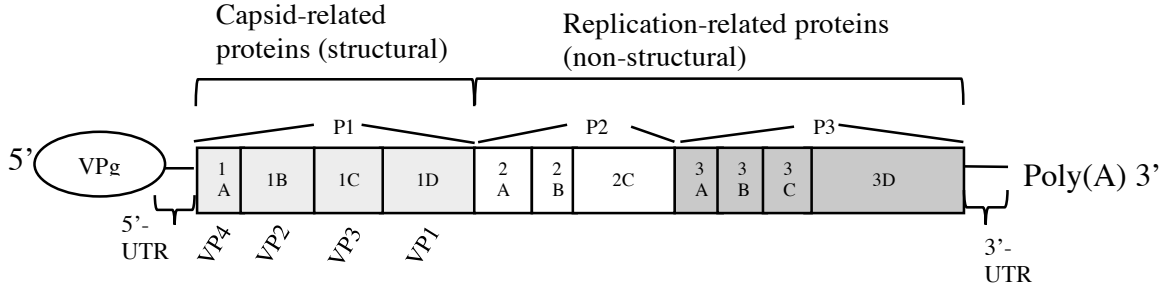

Figure 1.5 Schematic of human rhinovirus genome organization. 5'-UTR is covalently linked to VPg and 3'-UTR terminates with poly(A) tail. Proteins synthesized after the processing cascade are indicated as 1ABCD, 2ABC and 3ABCD with their precursor proteins P1-P3 indicated above. Figure adopted from Ian M. Mackay (www.virologydownunder.blogspot.com.au).

1.3 Picornaviral Life Cycle

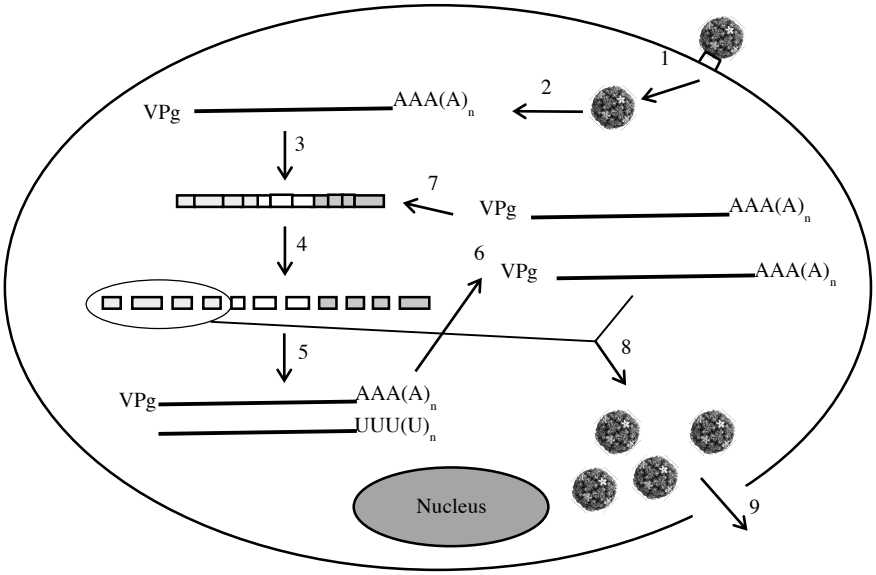

Figure 1.6 Schematic overview of a picornaviral life cycle from invasion to reproduction of the virus. (1) Viral attachment to the cell membrane via appropriate receptor binding. (2) Release of viral RNA by uncoating. (3) Translation of the structural and non-structural proteins. (4) Proteolytic processing of the polyprotein. (5) Negative sense RNA synthesis. (6) Viral replication and positive sense RNA synthesis. (7) Translation of the newly synthesized positive sense strands. (8) Merging the structural proteins with newly synthesized genomic RNA and encapsidation. (9) Cell lysis and the release of progeny. Figure adapted from Zoll et al., 2009.

1.3.1 Attachment and entry

To invade a cell, human rhinoviruses carry out receptor-specific attachment first (see figure 1.6). There are three kinds of receptors associated with cell entry are known at present. The first data about the receptor recognition from the minor group was obtained by Mischak et al. with co-purified HRV2 and receptor from plasma membranes of HeLa cells (Mischak et al., 1988). Later in 1994, further experiments identified the receptor as low density lipoprotein receptor (LDL-R) (Hofer et al., 1994). In 2000, Hewat et al. visualized the interaction between HRV2 with very low density lipoprotein receptor (VLDL-R), a member of LDL-R family, using cryo-electron microscopy and X-ray crystallography upon binding of the receptor directly onto the star-shaped dome of the fivefold symmetry axis (Hewat et al., 2000) (see figure 1.7). The virus is internalized in early endosomes upon cell attachment. Due to acidic pH, the receptor is dissociated and recycled. Later the virus is transferred into the late endosomes where the structural modifications occur receptor-independently at acidic pH (Prchla et al., 1994). Even

though the uncoating is a receptor-independent event, evidences suggest that ß-propeller domains of LDL-R and LRP (low density lipoprotein related protein) are involved in the transfer of the virus into the late endosomes (Fuchs & Blaas, 2010). One of the serotypes that was investigated in this study, HRV1A, belongs to the minor group as well and harbors a highly conserved Lys residue within the receptor binding site (K224) (Neubauer et al., 1987)

On the other hand, major group HRVs recognize intercellular adhesion molecule 1 (ICAM-1) belonging to the immunoglobulin superfamily or heparin sulphate when ICAM-1 is not present (Greve et al., 1989; Vlasak et al., 2005). The ICAM-1 binding site differs remarkably from LDL-R, as it is located at the 'canyon', that is at the depressions surrounding fivefold axis plateau (see figure 1.7). Moreover, ICAM-1 receptors catalyze the capsid modifications inside of the late endosomes, at pH < 5.3. Later, VP1 residues from the N-terminus of HRV induce the release of virus from late endosomes which indicates a sharp contrast with the immobilized minor group HRV upon receptor binding (Prchla et al., 1994; Neubauer et al., 1987). Corresponding residues for receptor binding site in major group, including HRV4, shows a pattern of mostly negative charge; thus it is presumably unfavorable to recognize negatively charged LDL (Vlasak et al., 2003).

Recently discovered HRV-C use the cadherin-related family member 3 (CDHR3) for cell entry. Unlike minor or major group receptors, it is assumed that 3 out of 6 domains of CDHR3 dock onto two promoters on the star-shaped dome of the viral capsid (Bochkov et al., 2015) (see figure 1.7). To date, no data about the uncoating and RNA release pathways of this group is available.

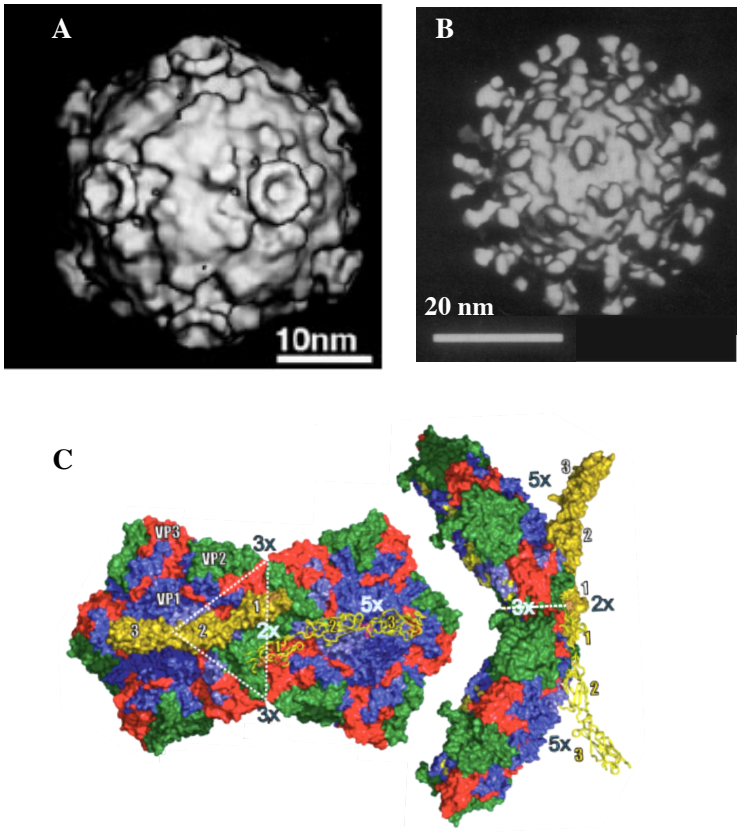

Figure 1.7 Variable receptor binding positions on the viral capsid of minor group, major group and HRV-C. (A) Cryo-EM map of HRV2-MBP-V1-3 complex. MBP stands for maltose binding protein and V1-3 are the ligand-binding repeats of VLDL-R. Figure shows the positioning of a minor group receptor onto 5fold axis plateau rather than onto canyon region (Figure taken from Hewat et al., 2000). (B) Stereoview of HRV16-D1D2 complex captured using cryo-EM. D1D2 are the ICAM-1 domains associated in binding. This type of binding from the major group viruses happens on the canyon region, the depression around the 5fold axis (figure taken from Olson et al., 1993). (C) The suggested structural model of binding between RV-C15 and its receptor CDHR3. Duplicated pentameric capsomere is depicted with an imaginary triangle representing a single promoter in colors; blue for VP1, green for VP2 and red for VP3. Receptor molecules depicted in yellow show the suggested docking model of the domains 1-3 of CDHR3. The next figure shows a rotated version (x= 90 °, y= 90°). In contrast to minor and major groups, this attachment hypothesizes an abutting interaction between the viral capsid and domains 1 and 2 of CDHR3, and leaving domain 3 flanking (figure taken from Bochkov et al., 2015).

1.3.2 Translation and self-processing of the polyprotein

The non-capped viral RNA can be immediately translated due to its positive sense. The distinct picornaviral translation mechanism via IRES motif locating at the secondary structures at 5' end of the genome provides a great advantage in case of host cell shut off (see chapter 1.5.2). The non-capped nature of enterovirus genus was first identified in poliovirus by Nomoto et al. (Nomoto et al., 1976). In order to produce progeny viruses, the encoded viral proteins are needed for new assembly. Thus, the translation of viral RNA needs to be performed first (Fields' Virology). The 5'-linked VPg (see chapter

1.2.2) is removed prior to translation in poliovirus by a DNA repair enzyme 5'-tyrosyl-DNA phosphodiesterase-2 (TDP2) (Virgen-Slane et al., 2012); VPg is presumably not required for translation (Ambros & Baltimore, 1980).

The IRES-dependent translation is mediated by canonical eukaryotic initiation factors (eIFs). Combining the purified 40S ribosomal subunit with Met-tRNA, eIF2, eIF3, eIF4F (consists of eIF4A, eIF4E, eIF4G), ATP, and GTP lead to *in vitro* reconstruction of IRES-mediated 48S pre-initiation complex. eIF4G, a central element of this complex, is recruited during type I IRES-dependent translation to bind directly to IRES region with its central domain (Pestova et al., 1996; de Breyne et al., 2009). However, in cap-dependent translation, eIF4G is the scaffolding element with its N-terminal and C-terminal domains bound to eukaryotic mRNA from m^7GDP cap to poly(A) tail, circularizing it, and forming 43S pre-initiation complex (Lamphear et al., 1995). eIF4G is one crucial element that is in common for cap-dependent & –independent translation machinery and is a substrate for picornaviral $2A^{pro}$ (Gradi et al., 1998b). Hence, eIF4G cleavage reduces the competition for translation during viral infection, as intact eIF4G is required for cap-dependent host translation.

Translation initiation of poliovirus mRNA emerging from internal ribosome entry site at 5'-UTR of the genome was shown by the groups of Pelletier & Sonenberg and Wimmer (Pelletier & Sonenberg, 1988; Jang et al., 1988). Later, Borman et al. studied the picornavirus family in order to elucidate the differences between IRES types. Type I IRES-driven *in vitro* translation of rhinoviruses were found as the least efficient between other types (Jackson & Kaminski, 1995). However, they may be upregulated by supplementation with reticulocyte lysates with HeLa cell proteins and/or $2A^{pro}$, which is an essential proteinase from enteroviruses (see chapter 1.4) (Borman et al., 1995). The cleavage of canonical eIF4G by picornaviral $2A^{pro}$ affect the cap-independent translation of viral mRNAs. Interestingly, the up- or down regulatory $2A^{pro}$ effect on the IRES-driven translation was variable according to IRES-type. The IRES type II-driven translation is not affected as much by $2A^{pro}$ when compared to IRES type I (Borman et al., 1997). Conversely, the picornaviral $2A^{pro}$ inhibits hepatitis A virus (HAV)-IRES-dependent translation, as it requires intact eIF4G (Borman & Kean, 1997).

Viral mRNA translation is not straight forward; it has even more factors that complicate the process that are called IRES trans-acting factors (ITAFs). They may promote, inhibit or may not be necessary for the translation from a certain type of IRES (Flather & Semler, 2015). For example; the polypyrimidine tract-binding protein 1 (PTBP1) was the first nuclear-resident protein found to enhance IRES-dependent translation from HRV2 RNA (Hunt & Jackson, 1999). Translation promotion occurs upon the modulation of the eIF4G by PTBP1 (Kafasla et al., 2010). Moreover, the serine/arginine-rich splicing factor 3 (SRSF3) is also is associated with IRES type I and involved in the promotion of translation (Bedard et al., 2007). However, beside those ITAFs discussed above, there are translation inhibitory nuclear-resident proteins as well. The double-stranded RNA binding protein 76 is an example

for inhibiting the translation initiation from HRV2 IRES (Merrill et al., 2006, Merrill & Gromeier, 2006).

The picornaviral genome is translated from a single open reading frame into a single polyprotein which is cleaved into its functional components by virally encoded proteinases; $2A^{pro}$, L^{pro} and $3C^{pro}$ or $3CD^{pro}$. The primary cleavages are performed co-translationally by $2A^{pro}$ that is encoded within enteroviruses and by L^{pro}, which is found in erbo- and aphthoviruses. They do not only process the polyprotein; they also cleave eIF4G to inhibit host cell translation machinery (Toyoda et al., 1986; Fields' Virology).

First, $2A^{pro}$ cleaves itself co-translationally from its N-terminus and the C-terminus of the preceding protein, which frees the structural protein-encoding P1 from the polyprotein (see figure 1.5). However, the further separation of 2A/2B junction is unclear in HRV. After the primary cleavage by $2A^{pro}$, the remainder of the self-processing is performed by $3C^{pro}$ or $3CD^{pro}$ (Palmenberg, 1982). The $3C^{pro}$ releases itself from the polyprotein like $2A^{pro}$ and has cleavage preferences for Gln-Gly for example in poliovirus; however, the $3C^{pro}$ from other picornaviruses cleaves the dipeptide bonds of Gln-Ser, Gln-Ile, Gln-Asn, Gln-Ala, Gln-Thr and Gln-Val as well (Fields' Virology). Following the cleavage between P2 and P3 by $3C^{pro}$, the polyprotein is processed into P1, P2, and P3 precursor proteins. P1 is cleaved into VP0, VP1 and VP3 by $3CD^{pro}$. VP0 is an immature procapsid component that is later processed into VP2 and VP4 by an unknown mechanism (Jacobson & Baltimore, 1968). However, the role of a conserved His residue was proposed to be involved in the VP0 cleavage by Curry et al. (1997).

1.3.3 Viral replication

The picornavirus genome encodes various viral proteins that are needed for the replication. The positive-stranded HRV genome is used as a template during both replication and translation. Collis et al. conducted experiments to understand both *cis*- and *trans*-acting elements that play a role during the replication using various deletion subclones, both in-frame and out-of-frame, in P1-P3 region. Their findings indicated that $2A^{pro}$ was a *trans*-acting protein for replication (Collis et al., 1992) beside its *cis*-acting features during polyprotein processing (see chapter 1.3.2). Each copy of viral RNA is translated prior to replication (Kuge et al., 1986; Collis et al., 1992; Novak & Kirkegaard, 1994) and therefore it is important to understand the down-regulation of the translation when needed. The switch from translation to RNA replication was investigated by Barton et al. (1999). They used toxins that either "freeze" the ribosomes on mRNAs or dissociate them from the mRNA to inhibit protein synthesis. The requirement of the clearance of translating ribosomes from viral RNA templates for initiating negative-strand synthesis was established (Barton et al., 1999). Moreover, the interaction of 3CD precursor protein with stem-loop D at the cloverleaf at 5'-UTR inhibits the translation of viral proteins. Consistent with that data, the cloverleaf structure was found to upregulate the viral translation (Gamarnik &

Andino, 1998). Removal of the 3'-terminal poly(A)-tail dramatically decreases the infectivity of the poliovirus (Spector & Baltimore, 1974) and the homopolymeric adenine sequences are required rather than heteropolymeric sequences (Sarnow, 1988).

A surprising result showed that positive-strand is used for both negative- and positive-strand synthesis (Vogt & Andino, 2010) (see figure 1.8) in contrast to findings by Novak & Kirkegaard that suggested solely negative-strand was used (Novak & Kirkegaard, 1991). The requirement of both RNA structures at the 5'-UTR and the 3'-UTR for negative-strand synthesis leads to hypothesis of RNA circularization. In 1993, a ribonucleoprotein complex was detected at the 5'-terminus of the poliovirus RNA. This complex was found to be involved with the cloverleaf structure from 5'-UTR, which comprises the recruited polymerase in the form of 3CD precursor protein and 36 kDa ribosome-associated cellular protein (Andino et al., 1993). Later in 1994, Harris et al. found the 3CD/cloverleaf complex in the presence of 3AB, the VPg precursor. The uridylylation of VPg is also associated with 5' cloverleaf structure (Lyons et al., 2001). The 3AB binds to cloverleaf structure only through 3CD. Furthermore, the 3CD/3AB interacts with 3'-terminal sequences of poliovirus RNA (Harris et al., 1994). The poly(rC)-binding protein 2 (PCBP2) forms a complex with cloverleaf structure at the 5'-UTR too, while it forms a ternary complex in the presence of purified 3CD. Mutations at the cloverleaf structure diminish of PCBP2 binding and decrease RNA replication (Parsley et al., 1997). Finally, the circularization theory was better explained through the interaction between poly(A)-binding protein 1 (PABP1) with viral 3CD protein which is bound to the 5' end of RNA and PCBP (Herold & Andino, 2001). Experiments conducted on poliovirus genome explained the genomic circularization during the negative-strand synthesis via protein-protein and protein-RNA interactions.

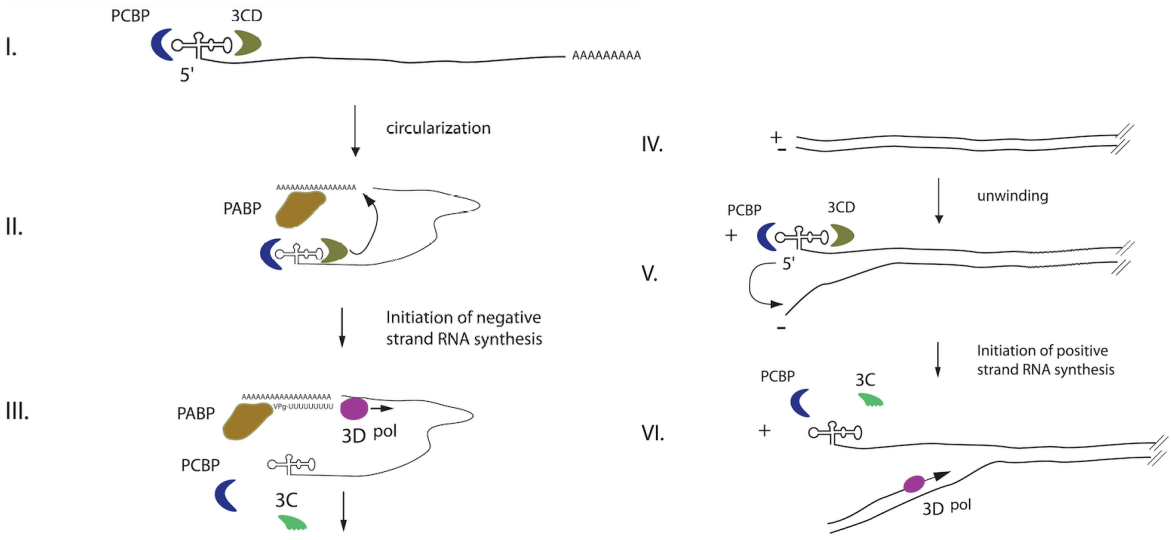

Figure 1.8 (I) The initiation of negative-strand synthesis upon the PCBP and 3CD precursor protein binding to 5' cloverleaf structure. (II) Circularization of genomic RNA through the ternary interaction between poly(A)-binding protein, 3CD, and PCBP. (III) The $3D^{pol}$ starts the synthesis of negative strand using the uridylylated VPg as a primer. (IV) The intermediate double strand is formed. (V) Unwinding of the intermediate positive-negative strand duplex RNA

thereby the formation of cloverleaf structure at the 5' end of positive strand. The 3CD precursor protein and PCBP binds to the cloverleaf structure at the positive-strand, which in turn, triggers the positive-strand synthesis from the 3' end of the negative-strand. (VI) The uridylylated Vpg acts as a primer and binds to the 3'-poly(A) tail of the negative-strand and thus starts the synthesis of positive-strand RNA by the $3D^{pol}$. Picture taken from Vogt & Andino, 2010.

1.3.4 Virus assembly and release

Capsid proteins are encoded within the P1 region. The first step of the capsid formation requires the processing of the P1 region. P1 is separated from P2 and further cleaved by $3CD^{pro}$ into the capsid proteins VP0, VP3 and VP1 (see chapter 1.3.2). The 5S promoters are self-assembly competent to form 14S pentamers (Palmenberg, 1982). The further assembly of 14S particles was first hypothesized by Rombaut et al., and the formation of 80S empty procapsids were observed (Rombaut et al., 1984; 1991). However, the stability of the formation of procapsids and viral subunits seems to be temperature- and pH-dependent. The 80S sedimenting particles which are alkaline dissociable into slower-sedimenting subunits differ from the 80S procapsids that are rather stable (Maraongiu et al., 1981). Interestingly, the 80S procapsids dissociate into 14S pentamers upon freezing overnight, and the freeze-dissociated particles are capable of reassociate (Onodera & Philips, 1987). The discrepancy concerning the stability of all 80S particles add fuel to the debate of whether they are used as reservoir. Later in 1994, the rapid conformational changes were observed in 14S pentamers upon RNA binding (Nugent & Kirkegaard, 1995). This finding eliminated the need for an empty procapsid for RNA packaging, which was suggested in 1968 by Jacobson & Baltimore. The final morphological change happens when the immature 150S provirion changes into the fully infectious 160S virion upon the maturation cleavage of VP0 into VP2 and VP4 (see chapter 1.3.2) (see figure 1.9). Mature and infectious virus is released from the cell by cell lysis (Fields' Virology).

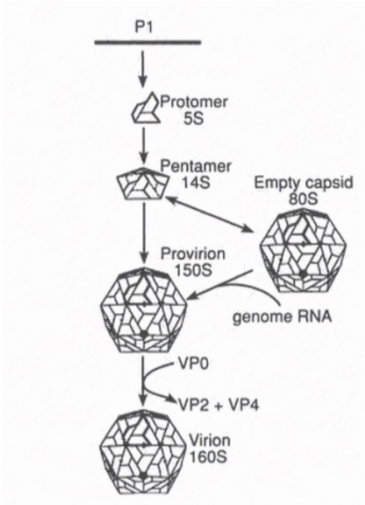

Figure 1.9 Assembly of the picornavirus virion. The capsid precursor P1 is freed from P2 and further processed into VP0, VP3 and VP1 by the $3CD^{pro}$. The 5S Promoters self-assemble into 14S pentamers. The 80S empty capsid is composed of twelve pentamers and with the addition of genomic RNA, it forms 150S provirion. The final step of the morphogenesis occurs via VP0 cleavage into VP2 and VP4 by an unknown mechanism. Then, the fully infectious 160S

virion is formed. Another suggested pathway is the assembly of the pentameres around the genomic RNA in order to form 150S provirion, skipping the 80S empty encapsidation step. This hypothesis suggests that 80S empty capsids are storage units. It is still a matter of debate whether the pentamers interact directly with the genomic RNA or first form the empty capsid. Picture taken from Fields' Virology.

1.4 $2A^{pro}$

1.4.1 Function

The polyprotein is around 2180 aa long and normally it is not detected intact in infected cells. The picornain 2A proteinase ($2A^{pro}$) plays a major role in processing of the polyprotein. It is responsible from the first proteolytic cleavage of the polyprotein as it separates the structural protein-encoding P1 region from the P2 region, which encodes the non-structural proteins. The intramolecular (*cis*) and co-translational cleavage occurs between the N-terminus of $2A^{pro}$ and the C-terminus of the adjacent region VP1 at the Tyr-Gly site. (Toyoda et al., 1986; Sommergruber et al., 1989). The C-terminus of $2A^{pro}$ is freed from adjacent protein 2B by $3C^{pro}$ (Lawson & Semler, 1992; Lee et al., 2014).

Beside its crucial function at polyprotein processing, the $2A^{pro}$ also targets the host cell protein synthesis by cleaving both homologues of eIF4G (eIF4GI and eIF4GII) (see chapter 1.5.2), to achieve complete shut off of the cap-dependent translation (Gradi et al., 1998b). The poliovirus $2A^{pro}$ was shown to cleave poly(A)-binding protein (PABP) (Joachims et al., 1999). Gustin and Sarnow observed accumulates of nuclear proteins in cytoplasma upon infection of the cells with rhinovirus. This accumulation was correlated with the degraded NPC components Nup153 and p62 (Gustin & Sarnow, 2002). Later, the electron microscopy findings showed that $2A^{pro}$ is responsible for the alterations occurring in nuclear pore complexes (NPC) (Belov et al., 2004). Moreover, the RNA polymerase II transcription efficiency was found to be decreased in correlation to transient $2A^{pro}$ expression in COS-1 monkey kidney cells (Davies et al., 1991).

1.4.2 Structure

The $2A^{pro}$ encoded by enteroviruses is within the group of cysteine proteinases (König & Rosenwirth, 1988), due to sequence homology with other known cysteine proteinases and nucleophilic cysteine at their active center (Lloyd et al., 1986). The first suggestions of trypsin-type ß-barrel folds within the structure (Bazan & Fletterick, 1988; Gorbalenya et al., 1989; Sommergruber et al., 1997) were later established in 1999 (Petersen et al., 1999). Petersen and colleagues solved the crystal structure of HRV2 $2A^{pro}$ at a 1.95 Å resolution using multi-wavelength anomalous dispersion technique (MAD). The superimposition of HRV2 $2A^{pro}$ with another chymotyripsin-like proteinase from *Streptomyces griseus* showed a reasonable alignment, although barely sequence homology. When

compared to *Streptomyces griseus* proteinase B (SGPB), only four N-terminal ß-strands superimpose (bI2, cI, eI2, and fI) and the strands correspond to aI, bI1, dI, and eI1 within the N-terminus of SGPB are lacking in HRV2 $2A^{pro}$. Yet, the N-terminal domain alterations are rather common and flexible amongst chymotrypsin-like folded proteineases with examples of five-stranded ß-barrel (Choi et al., 1991) and four-stranded ß-sheet by HRV2 $2A^{pro}$.

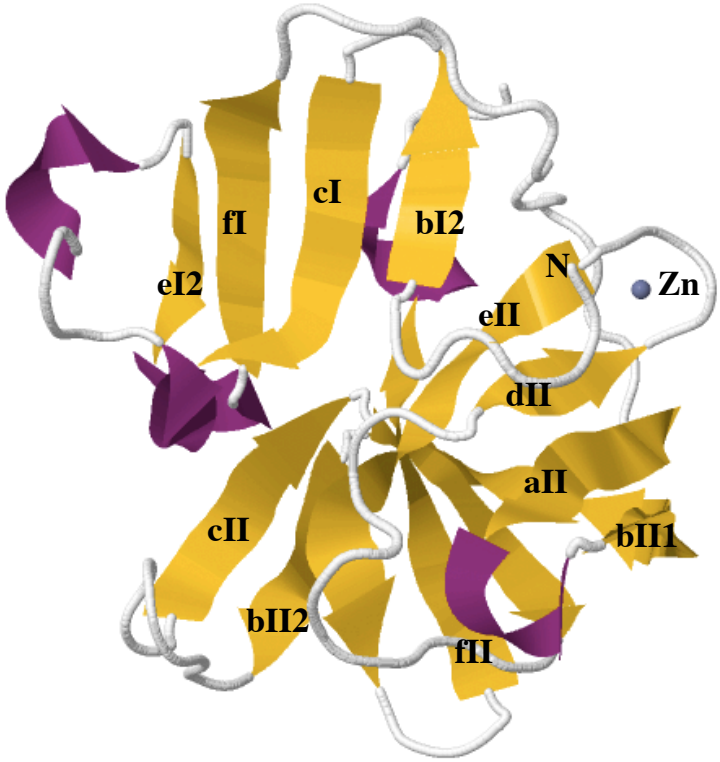

Figure 1.10 Schematic of ribbon diagram of 2A cysteine proteinase from human rhinovirus 2. The ß-strands (yellow) are labelled with Roman numeral I for the N-terminal and with Roman numeral II for the C-terminal domain. The N terminus end is indicated with 'N' and the structural element zinc ion is indicated wirh 'Zn' as a grey sphere. The short 3_{10} helices are depicted in purple. Model accessed from protein databank. (PBD 2HRV) doi: 10.2210/pbd2hrv/pbd

The N-terminal domain harbors two residues of the catalytic triad (Sommergruber et al., 1997): His18 (the general base) and Asp35. The His18 is located at a short 3_{10} helix, between the strands cI and eI2 (see figure 1.10). Asp35 is located in between the following strands eI2 and fI. The nucleophilic Cys106 residue of the triad is however located at the C-terminal domain in between sequential type II ß turns, preceding the strand dII. The catalytic triad is built up via hydrogen-bonds between Asp35 (hydrogen acceptor) and $His18N^{\delta 1}$ and as well as the main-chain amid nitrogen (hydrogen donors). Additional hydrogen-bonds between hydrogen acceptor Asp35 and hydrogen donors Asn16, Tyr86 and Thr121 strengthen the structure. The network also harbors an interaction between Thr121 and Gln91, in which the latter acts as a hydrogen acceptor (see figure 1.11 A). These residues are crucial for the rhinoviral $2A^{pro}$ and therefore highly conserved among serotypes. In addition, a thiolate-imdazolium

interaction between the catalytically active residues His18 and Cys106 was shown (Sarkany et al., 2000).

The nucleophilic attack from Cys106 to the scissile peptide bond of the substrate generates a negatively charged tetrahedral transition molecule which is preserved in the oxyanion hole (see figure 1.10 B). The oxyanion hole harbors the residues Asp105, Glu102, His63, and Lys62 and is located at the type II reverse ß turn prior to the nucleophilic Cys106. Maintenance of the structure is again via hydrogen-bonds between Asp105 and the main-chain amid nitrogen of Lys62, His63, and Glu102. Additionally, there is a possible salt bridge interaction between the His63 hydrogen at $N^{\delta 1}$ position and Asp105 carboxylic anion. Mutations at this site (D105S or D105N) are not tolerated and inactivate the enzyme (Sommergruber et al., 1997).

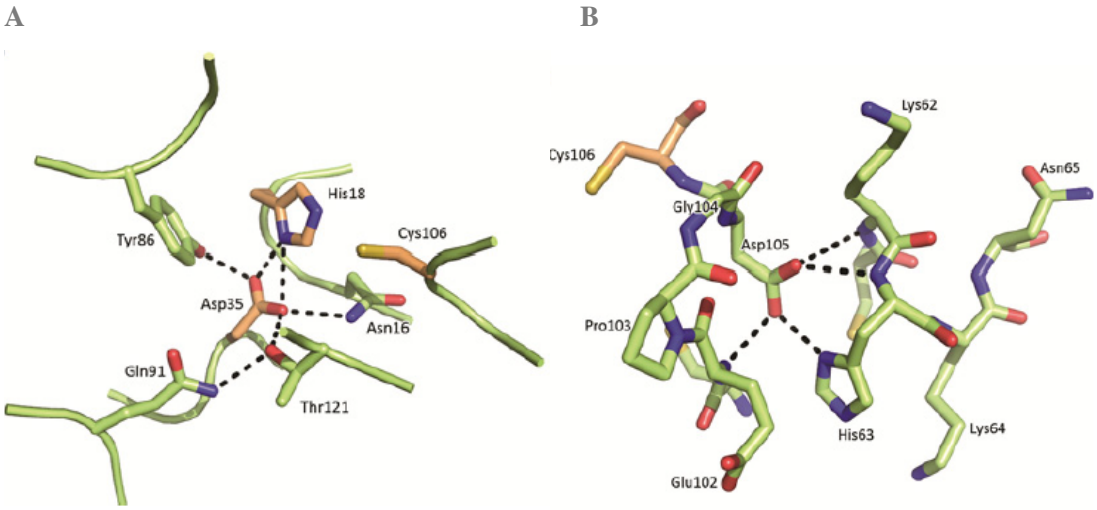

Figure 1.11 Schematic of HRV2 $2A^{pro}$ X-ray structure details of catalytic triad (A) involving residues His_{18}, Asp_{35}, and C_{106}. Figure B shows the oxyanion hole and the residues involved in H-bond network: Lys_{62}, His_{63}, Glu_{102}, and Asp_{105}. Elements are distinctive by color: C (green or orange), O (red), N (blue). The dashed lines (black) represent H-bond network. Picture taken from David Neubauer, Dissertation 2013.

Moreover, the $2A^{pro}$ recruits a Zn ion to stabilize its fold and for substrate specificity (Sommergruber et al., 1994b; Voss et al., 1995). The tetrahedral coordination of the Zn ion is associated with four highly conserved residues (figure 1.12): Cys52 and Cys54 from the interdomain loop, which connect the N- and C-terminal domains, and Cys112 and His114 located at the hairpin loop between the strands dII and eII. The zinc ion is coordinated with three sulfurs (2.3 Å distance) and one nitrogen (2.0 Å distance). Structural maintenance is provided by the connection of interbarrel loop to the turn between ß-strands dII and eII and may compensate for the truncated N-terminal domain. It may also serve as an alternative to disulfide bridge, which is present in chymotrypsin at Cys136 and Cys201 and adjacent to Zn-binding domain of $2A^{pro}$ (Tsukada & Blow, 1985). However, there is a predicted intermolecular disulfide bridge (Cys138-Cys138) (Petersen et al., 1999) building up a dimerization interphase between monomers (Liebig et al., 1993).

1.4.3 Substrate specificity

The substrate specificity of human rhinovirus $2A^{pro}$ from HRV2 and HRV14 are well-studied and representatives of genetic group A and B. Formerly, the studies on HRV2 $2A^{pro}$ indicated the requirement of a minimum 9-mer (from P8 to P1') for a cleavable asymmetric peptide. The key sequence Thr-X*Gly (P2-P1*P1') (nomenclature from Schechter and Berger, 1967, asterisk indicates the scissile peptide bond) was proposed by Sommergruber and his colleagues as a template for self-cleavage (Sommergruber et al., 1992). A classification attempt was made using group-specific proteinase inhibitors (number of inhibitors against metalloproteinases, Asp proteinases, Ser proteinases, Cys proteinases, Cys/Ser proteinases) on HRV2 $2A^{pro}$. Unfortunately, many of the inhibitors did not abolish the activity; however, some from each group did abolish activity activity with various IC_{50} values. Due to high sequence variety in the $2A^{pro}$ within subtypes, no proteinase inhibitor-dependent classification could be made. The sequence alignments of $2A^{pro}$ from HRV1A and HRV4, that were studied in this project, are compared with HRV2 $2A^{pro}$ in figure 1.13, to clarify the differences.

Table 1.2 The cleavage sites on *cis* and *trans* substrates (eIF4GI and eIF4GII) of the $2A^{pro}$ from HRV2, HRV1A and HRV4. Cleavage position between P1 and P1' is indicated with an arrow. P10-P1 amino acid sequences correspond to preceding protein. P1'-P10' amino acid sequences correspond to either $2A^{pro}$ or *trans* substrates eIF4GI/II. Sequences taken from NCBI. (HRV2: CAA26181.1, HRV1A: AKF02546.1, HRV4: ABF51184.1, eIF4GI: NP_886553.3 (source: *Homo sapiens*), eIF4GII: AAC02903.2 (source: *Homo sapiens*))

	P10				P5				P1	↓ P1'				P5'				P10'
HRV2 $2A^{pro}$ (*cis*)	I	V	T	R	P	I	I	T	T	A	G	P	S	D	M	Y	V	H	V	G
HRV1A $2A^{pro}$ (*cis*)	I	V	R	R	N	T	I	T	T	A	G	P	S	D	L	Y	V	H	V	G
HRV4 $2A^{pro}$ (*cis*)	I	K	T	R	E	S	I	N	T	Y	G	L	G	P	R	F	G	G	V	H
eIF4GI (*trans*)	N	L	G	R	T	T	L	S	T	R	G	P	P	R	G	G	P	G	G	E
eIF4GII (*trans*)	G	G	R	G	V	P	L	L	N	V	G	S	R	R	S	Q	P	G	Q	R

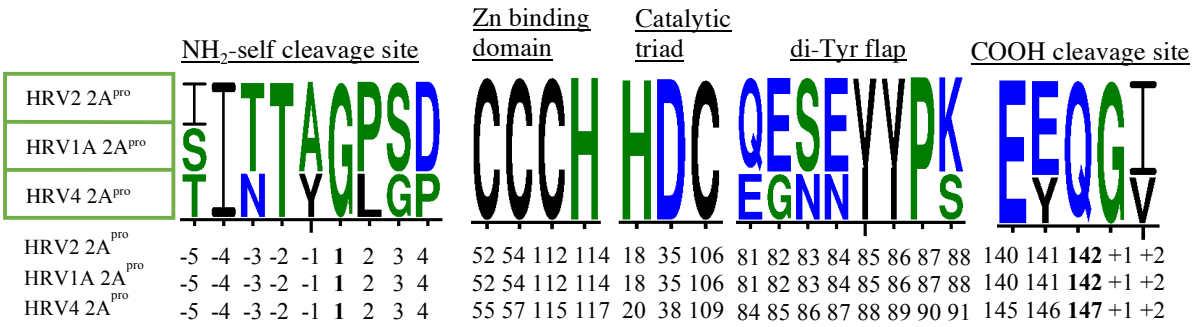

Figure 1.12 Schematic of WebLogo depictions (Crooks et al., 2004) of important rhinoviral $2A^{pro}$ sequences from different serotypes. The $2A^{pro}$ from HRV1A and HRV4 are shown in comparison with HRV2 $2A^{pro}$, a better studied ortholog. The residue heights correspond to relative amino acid occupancies at the corresponding site and are divided into 3 serotypes from top to bottom; HRV2, HRV1A, HRV4. The corresponding amino acid residues are indicated for each serotype below the WebLogo depictions. The residue numbers -5 to -1 indicate the preceding protein sequences (VP1) and +1 to +2 indicate the $2A^{pro}$ sequences. Cleavage site residue numbers of the $2A^{pro}$ are indicated in bold. Figure adapted from Lee et al., 2014

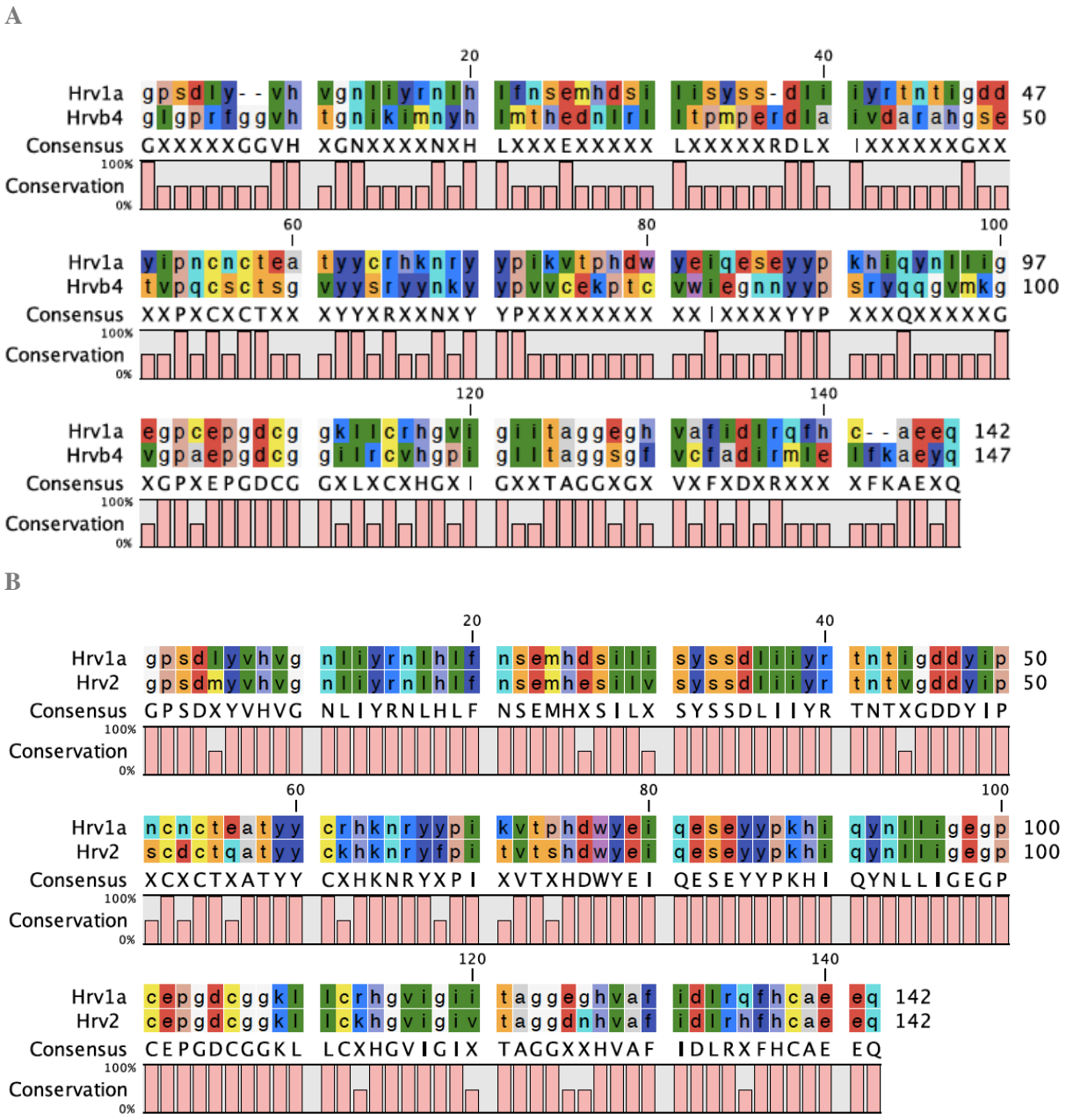

C

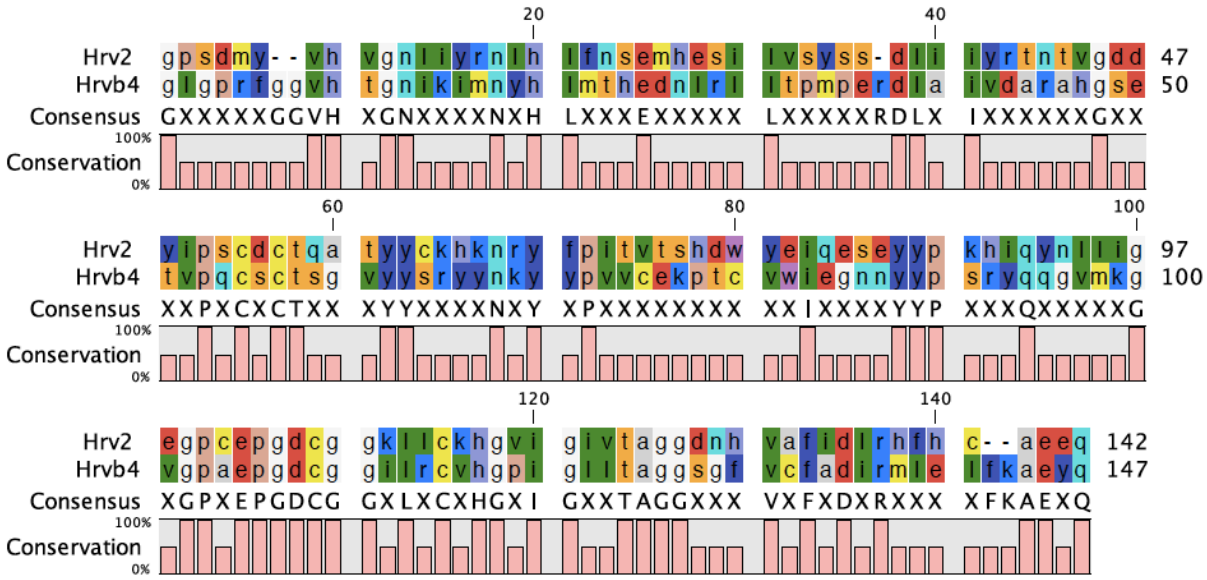

Figure 1.13 The amino acid sequence alignment of 2A^{pro} between rhinoviruses from different genetic groups (HRV1A 2A^{pro} and HRV4 2A^{pro}) is shown in figure A. The alignment of HRV1A 2A^{pro} with HRV2 2A^{pro} is sown in figure B, which shows the high sequence homology. Figure C gives the alignment of HRV2 2A^{pro} with HRV4 2A^{pro}. The remarkable amino acid sequence homology between HRV2 and HRV1A (in figure B) is clear when compared to figures A and B. The bars underneath alignment indicate conservation of the given residue. The right column of numbers indicates the sequence length. Alignments were made by using CLC Genomics Workbench 9. (NCBI accession codes HRV1A: AKF02546.1, HRV4: ABF51184.1, HRV2: CAA26181.1)

The intermolecular substrate specificity experiments were performed with synthesized peptides and the HRV2 2A^{pro}. Petersen et al. (1999) mentioned a substrate binding cleft S4 site, described as a narrow and hydrophobic pocket, which allows residues such as Ile or Leu inside (Sommergruber et al., 1992). Charged residues such as Lys or Asp at the P4 position of a synthetic peptide are neither tolerated nor cleaved by HRV2 2A^{pro} (Sommergruber et al., 1994a). Table 1.2 shows the distribution of Ile and Leu at the P4 position of *cis* and *trans* substrates.

Thr and Asn occupy the P3 site of the VP1-2A^{pro} joint whereas, Ser and Lys are found at this position by eIF4GI and eIF4GII, respectively (see table 1.2). This position was not found crucial for the cleavage efficiency, since the side chain faces probably towards the solvent as shown in the figure 1.14.

In general, P2 position harbors mainly Thr but other residues such as Asn or Ser can be found within *cis* and *trans* substrates as well. The 2A^{pro} that are studied in this thesis (HRV1A 2A^{pro} and HRV4 2A^{pro}) both have Thr at this site (see figure 1.12) although, they share very low sequence homology in general (figure 1.13 A). Substitutions of Thr with all other amino acids (except for Trp, Cys and Met) were found to be deleterious. Sommergruber et al. (1992) explained the prerequisite Tyr85 turn for making a space for ThrP2 binding. The crucial hydrogen-bonding between Ser83 and ThrP2 is depicted in figure 1.14.

The $2A^{pro}$ processing occurs between the positions P1 and P1' (see table 1.2). There is an oxyanion hole within chymotrypsin-like proteinases that preserves the negative charge on the P1 carbonyl oxygen upon substrate binding (see figure 1.14). P1 site substitution of Ala with Met resulted in enhanced cleavage ($(V_{max}/K_m)_{rel}$) of a synthetic peptide. And cleavage efficiencies are comparable with the wild-type HRV2 $2A^{pro}$ when TyrP1 and PheP1 are used (Petersen et al., 1999). An explanation for this phenomenon is the narrow and flat properties of the S1 pocket. The eII strand and oxyanion hole residues together form a pocket-kind of a shape, namely the S1 site, where the conserved substrate residues (either *cis* or *trans*) such as Ala docks inside. On the other hand, P1 site is greatly occupied by Tyr within group B HRVs (as in HRV4 in table 1.2). Possibly burying a large surface area, such as the side chains of Tyr and Phe, is favorable. In general; Ala, Val, Phe, Tyr are the most abundant amino acids found at P1 position within the group A and B.

Among all enteroviral $2A^{pro}$ the Gly residue at the P1' position is strictly conserved and therefore, was thought to be essential for a cleavage activity both *cis* and *trans* (Petersen et al., 1999). Mutational analyses showed that P1'Gly substitutions with Glu, Lys, Thr, or Trp abolished the self-processing (Skern et al., 1991). Moreover, when Phe, Thr, Asp, or Lys were substituted at this site, no peptide cleavage was observed (Sommergruber et al., 1992). Petersen et al. (1999) proposed that the GlyP1' must locate itself at S1 site during the *cis* cleavage, because C-terminal of the VP1 is covalently attached to the GlyP1' immediately prior to cleavage. The VP1-$2A^{pro}$ junctions of HRV2, HRV1A, and HRV4 have Gly at this position as well as the two homologues of eIF4G (see table 1.2).

The P2' site is occupied by Pro within the group A and by Lys within the group B. Eukaryotic initiation factors eIF4GI and eIF4GII bear Pro and Ser at this position, respectively (see table 1.2).

To sum up, a common motif sequence Ile-X-Thr-X*Gly (P4-P3-P2-P1*P1') is found among the VP1-$2A^{pro}$ junctions among the human rhinovirus subtypes that are compared through this study (table 1.2).

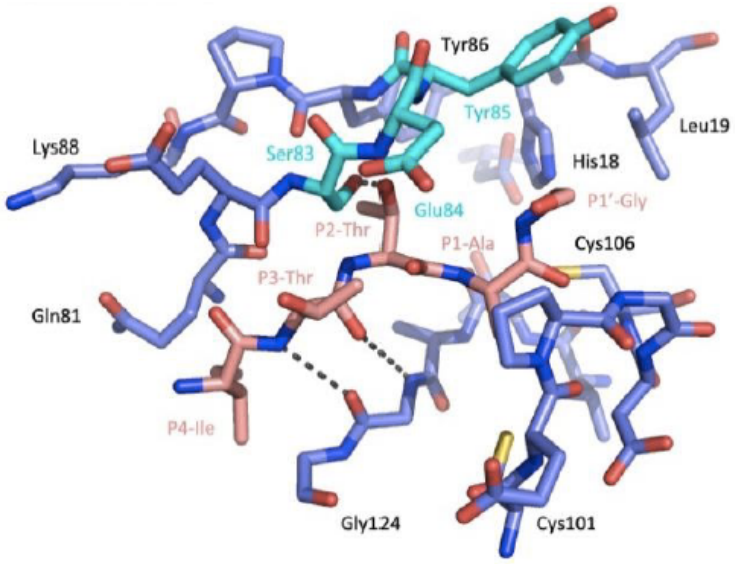

Figure 1.14 Schematic of the substrate interaction with HRV2 $2A^{pro}$. The pentapeptide substrate harbors residues Ile-Thr-Thr-Ala*Gly corresponding to P4-P3-P2-P1*P1' (depicted in pink). Dashed lines indicate the hydrogen bonds between Ser83 (from dityrosine flap) from the $2A^{pro}$ (blue) and P2Thr from the substrate (pink). In the original free enzyme, Tyr85 (light blue) loads on the His18; however, it is rotated away in order to form a hydrogen bond between the proteinase and the substrate (Petersen et al., 1999). Picture taken from Aumayr M., Masterarbeit, 2012.

1.5 Virus-host interaction

Picornaviruses have developed many strategies to overcome the immune signal and survive. In general, picornaviral proteinases are capable of inhibiting the cellular trafficking, host cell replication, transcription, translation, and post-translational modifications. As described in detail in chapter 1.3.2, viral translation makes use of the inhibition of host cell translation, especially with the cleavage of eIF4G. The specific binding of eIF4G to the IRES region in poliovirus (de Breyne et al., 2009) and in encephalomyocarditis virus (Pestova et al., 1996) are identified. Interestingly, the C-terminal domain of eIF4G (in the absence of N-terminal domain) is capable of reinforcing the viral protein synthesis (Ohlmann et al., 1996). The enteroviral proteinases responsible for the canonical initiation factor eIF4G cleavage are not conserved and exhibit different strategies to invade a cell. Enteroviral $2A^{pro}$ are responsible for the cleavage, whereas leader proteinase (L^{pro}) is recruited by aphthoviruses. On the other hand, cardiovirus $2A^{pro}$ inhibit the host cell translation yet in a different manner (Whitton et al., 2005). Cardiovirus $2A^{pro}$ translocates itself into the nucleus and alter the ribosome functioning in the favor of IRES-driven translation (Aminev et al., 2013). Oppositely, hepatitis A viruses seem to be rather non-cytopathic and they do not interfere with the host cell translation (Gauss-Müller & Deinhardt, 1984).

In addition, the host cell transcription is as well scaled down by picornaviruses. Although picornaviral life cycle goes on in the cytoplasm, recent studies on poliovirus infected cells showed that the virally encoded 3CD protein is capable of entering to the nucleus, where it frees itself from the 3D protein. Two hours after the infection, the $3C^{pro}$ rapidly inhibits all three RNA polymerases in the nucleus (Sharma et al., 2004; Dasgupta et al., 2003; Kaariainen & Ranki, 1984). This is a strategy to outnumber the host RNA molecules.

The picornaviral RNA replication and translation are dependent on the nuclear-resident proteins such as 5'-tyrosyl-DNA phosphodiesterase-2 (removes the VPg from viral genomic RNA for enabling replication) (Virgen-Slane et al., 2012), nucleolin (promotes viral translation) (Waggoner & Sarnow, 1998; Izumi et al., 2001), or PABP1 & PCBP2 that are crucial for the recognition of circularized templates by $3D^{pol}$ (Gamarnik & Andino, 1997, 2000; Parsley et al., 1997). Therefore, picornaviruses relocate these proteins from their nuclear habitat into cytoplasm where viral replication takes place. Nucleopore complexes (NPC) facilitate the trafficking between nucleus and cytoplasm. The PV and HRV $2A^{pro}$ degrade Nup62, Nup98, Nup153, and Nup214 nucleoporins within NPC (Gustin & Sarnow, 2001, 2002; Park et al., 2010; Watters & Palmenberg, 2011). Moreover, Nup153, Nup214, Nup358 are

degraded by either $3C^{pro}$ $3CD^{pro}$ from HRV 16 (Ghildyal et al., 2009). The increased permeability of the nuclear envelope result in an accumulation of nuclear-resident proteins in the cytoplasm (Flather & Semler, 2015).

1.5.1 Host cell translation shut off

Host cell protein synthesis is immediately shut off upon an infection. Eukaryotic translation machinery consists of several steps that are catalyzed by eukaryotic initiation factors (eIFs). The eukaryotic mRNA is recognized through its 5' cap structure by eIF4E (the cap-binding protein). First findings on the viral attack was observed with the degradation of a 220 kDa protein complex (Etchison et al., 1982). This degradation was associated with the inhibition of host translation in poliovirus infected cells. Later, the FMDV Lb^{pro} and the $2A^{pro}$ from HRV and CVB were associated with the specific cleavage of eIF4G scaffolding protein (Devaney et al., 1988; Liebig et al., 1993; Kirchweger et al., 1994). Beside many other cellular targets explained above, viral proteinases target for eIF4G (p220), a scaffolding component of eIF4F complex, which recruits ribosomes to the eukaryotic mRNA (Gingras et al., 1999). In figure 1.15, eIF4G is shown to connect 5'- and 3'-ends of the eukaryotic mRNA. The 5'-terminal cap structure is recognized by eIF4E, which interacts with the N-terminal domain of eIF4G (Sonenberg et al., 1978; Svitkin et al., 2005). Moreover, the N-terminal domain also interacts with the polyA-tail via PABP (Imataka et al., 1998). On the other hand, C-terminal domain connects with the eIF4A (RNA helicase) and eIF3. When the eIF4F complex (consists of eIF4A, eIF4G, eIF4E) is formed, the pre-initiation complex 43S triggers the translation. The ternary complex of Met-$tRNA_i^{Met}$, eIF2, and eIF2-bound GTP with 40S ribosomal subunit together yield the 43S pre-initiation complex (Dever, 1999; The Pathway and Mechanism of Initiation of Protein Synthesis). The 43S pre-initiation complex scans the 5'-UTR of mRNA for an AUG initiation codon in a 5' to 3' direction. When the starting codon is recognized, the 48S initiation complex is formed. Following the dissociation of eIF1 and the hydrolysis of eIF2-bound GTP via P_i release, 60S subunit joins to 48S initiation complex. The larger 80S ribosomal subunit recruits the dissociated pre-initiation factors which leads to the initiation of the protein synthesis (Jackson et al., 2010). As the eIF4G harbors binding sites for eIF4E, eIF4A, eIF3 and PABP, it is a desirable substrate for the viral proteinases to cleave. After the cleavage of eIF4G, enhanced viral protein production take-over the cell, leading to apoptosis (Borman & Kean, 1997; Gingras et al., 1999).

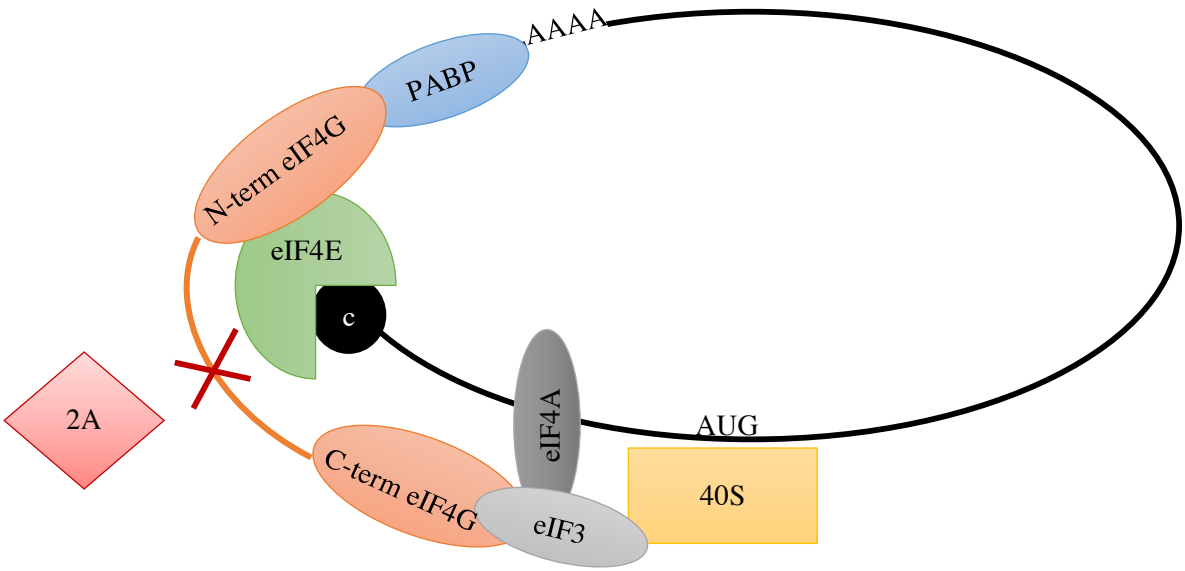

Figure 1.15 Schematic of host cell translation shut off by picornaviral $2A^{pro}$. The 5' mRNA cap is indicated as a black cirle with 'c'. PABP stands for poly(A)-binding protein. The cleavage of eIF4G occurs at the interdomain connecting N- and C-terminal domains together. After the cleavage, eIF4G is no longer capable of recruiting 40S ribosomal unit to the mRNA. (Picture modified from Aumayr M., 2013 Dissertation)

There are two homologs of eIF4G, namely the eIF4GI and eIF4GII, and both are cleaved by picornaviral proteinases in order to inhibit eukaryotic mRNA translation (Gradi et al., 1998a). Lamphear et al. published the cleavage sites of eIF4GI in rabbit and human orthologs, both being between the Arg and Gly (see table 1.2 for human eIF4GI cleavage site) (Lamphear et al., 1993). However; in 2004, experiments conducted with both FMDV L^{pro} and HRV $2A^{pro}$ revealed the cleavage sites of eIF4GII differed 1 amino acid sequence between the two proteinases (Gly_{700}/Ser_{701} for L^{pro} and Val_{699}/Gly_{700} for $2A^{pro}$) (figure 1.16). These experiments also presented that $2A^{pro}$ cleavage does not require the ArgP1, since it corresponds to ValP1 for eIF4GII (Gradi et al., 2004) (see table 1.2 and figure 1.16). Haghighat et al. claimed the binary complex of eIF4E/eIF4G is a better substrate for HRV2 $2A^{pro}$ (1996). The cap-dependent translation in Krebs-2 ascites cells was inhibited when treated with $2A^{pro}$ yet could be restored upon the addition of intact eIF4G.

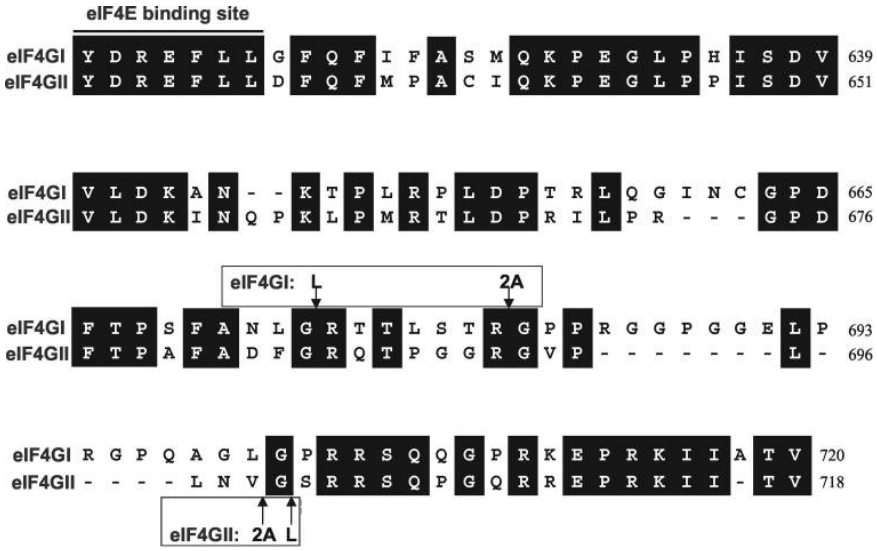

Figure 1.16 Sequence comparison between eIF4GI and eIF4GII is represented including the cleavage sites by proteinases $2A^{pro}$ (HRV) and L^{pro} (FMDV), and eIF4E binding site. The predicted scissile peptide bonds from *in vitro* cleavage assays are indicated with arrows. Conserved residues are highlighted in black. (Figure modified from Gradi et al., 2004)

2 AIMS OF STUDY

This thesis focuses on the structural differences of $2A^{pro}$ from HRV1A (group A) and HRV4 (group B) serotypes. The low sequence homology shared between genetic groups complicates an efficient antiviral drug design. Therefore, it is crucial to understand the discrepancies between different genetic groups.

We aimed to establish protocols of recombinant $2A^{pro}$ expression in bacterial culture and protein purification for both proteinases by following the methods that were described previously (Liebig et al., 1993). The fundamental goal was to elucidate structural properties of recombinant purified $2A^{pro}$ from two serotypes, which belong to different genetic groups (group A and B). Therefore, *in vitro* biochemical and biophysical experiments were done. The $2A^{pro}$ are well-known through co-translational self-processing and *trans* cleavage of eIF4G to shut off the host cell protein synthesis. We aimed to measure binding characteristics of $2A^{pro}$ with two initiation factors, namely the eIF4E (murine) and the eIF4GII (human). Aumayr et al. published that the cleavage of $eIF4GII_{551-745}$ by HRV2 $2A^{pro}$ cannot be as efficient without the presence of eIF4E (Aumayr et al., 2015). A shorter version of eIF4GII was used ($eIF4GII_{551-745}$), following the protocol in Aumayr et al. 2015 that comprises the binding site for eIF4E as well as the *trans* processing region for $2A^{pro}$. *In vitro* biochemical experiments with the wild-type proteinases from HRV1A and HRV4 would elucidate the proteolytic activity against initiation factors, which is the initial goal of the virus during infection. The inactivation of the proteinase was necessary for doing kinetic measurements with stable interactions. The inactive $2A^{pro}$ form HRV1A and HRV4 were incubated with initiation factors to observe possible binary or ternary complex formations. The HRV2, a well-studied pioneer, belongs to the genetic group A as HRV1A. Hence, we expected similar behavior against the initiation factors for genetic group A members. On the other hand, the genetic group B virus HRV4 was expected to behave differently, due to low sequence homology between the genetic groups (39 %). Furthermore, the exact molecular mass of $2A^{pro}$ and the formed complexes were revealed via static light scattering (SLS). The genetic group A proteinase from HRV2 was found to be a homodimer by Aumayr et al.; accordingly, we needed to compare HRV1A $2A^{pro}$ and HRV4 $2A^{pro}$. The possible ternary and binary complexes were also measured by SLS to reveal the oligomeric state. We further wanted to describe the complex formations in the means of dissociation constant (K_D) values, which were conducted using isothermal titration calorimetry (ITC).

3 MATERIALS AND METHODS

3.1 Buffers and solutions

- 2 x TY medium: 16 g/L Tryptone, 10 g/L Yeast extract, 85.5 mM NaCl in dH_2O. Final pH was adjusted to 7 with NaOH.
- Luria Bertani medium: 25 g/L in dH_2O.
- Terrific broth medium: 12 g/L trypton, 24 g/L yeast extract, 0.004 % Glycerol (Sigma-Aldrich), 10 % phosphate buffer dissolved in dH_2O.
- Phosphate buffer: 0.72 M K_2HPO_4, 0.17 M KH_2PO_4 in dH_2O
- RF1 solution: 100 mM KCl, 100 mM $MnCl_2$, 30 mM $K(CH_3COO)$, 10 mM $CaCl_2$, 15 % (w/v) Glycerol in dH_2O. Final pH was adjusted to 5.8 with HCl.
- RF2 solution: 10 mM MOPS, 10 mM KCl, 75 mM $CaCl_2$, 15 % (w/v) Glycerol in dH_2O. Final pH was adjusted to 6.08 with KOH.
- Saturated $(NH_4)_2SO_4$ solution: 4.1M $(NH_4)_2SO_4$ in dH_2O.
- Buffer A: 50 mM Tris-HCl, pH 8.0, 50 mM NaCl, 1 mM EDTA pH 8.0, 5 mM DTT (Applichem), 5 % glycerol in dH_2O.
- Buffer A without DTT pH 9.0: 50 mM Tris/HCl pH 8.0, 50 mM NaCl, 1 mM EDTA pH 8.0, 5 % glycerol in dH_2O. Final pH was adjusted to 9.0 with 10N NaOH.
- MonoQ elution buffer: 50 mM Tris-HCl, pH 8.0, 1 M NaCl, 1 mM EDTA pH 8.0, 5 mM DTT, 5 % glycerol in dH_2O.
- MonoQ elution buffer pH 9.0: 50 mM Tris-HCl, pH 8.0, 1 M NaCl, 1 mM EDTA pH 8.0, 5 mM DTT, 5 % glycerol in dH_2O. Final pH was adjusted to 9.0 with 10N NaOH.
- Hepes buffer: 20 mM Hepes/KOH pH 7.4, 150 mM KCl, 1 mM EDTA, 5 mM DTT in dH_2O.
- Hepes buffer without DTT: 20 mM Hepes/KOH pH 7.4, 150 mM KCl, 1 mM EDTA in dH_2O.
- Histrap binding/equilibration buffer: 50 mM Tris/HCl pH 8.0, 50 mM NaCl, 20 mM imidazole
- Histrap binding/equilibration buffer pH 9.0: 50 mM Tris/HCl pH 8.0, 50 mM NaCl, 20 mM imidazole in dH_2O. Final pH was adjusted to 9.0 with 10 N NaOH.
- Histrap elution buffer: 50 mM Tris/HCl pH 8.0, 50 mM NaCl, 500 mM imidazole in dH_2O.
- Histrap elution buffer pH 9.0: 50 mM Tris/HCl pH 8.0, 50 mM NaCl, 500 mM imidazole in dH_2O.. Final pH was adjusted to 9.0 with 10 N NaOH.
- 10 x SDS running buffer: 250 mM Tris, 2.0 M Glycine, 1.0 % SDS in dH_2O.
- 2 x SDS sample buffer: 20 % Glycerol, 10% ß-Mercaptoethanol, 6 % SDS, 0.125 M Tris, 10 % (w/v) Bromphenol Blue in dH_2O. Final pH was adjusted to 6.8 with 1 M HCl.
- 5 x SDS sample buffer: 50 % Glycerol, 25 % ß-Mercaptoethanol, 15% SDS, 0.31 M Tris, 25 % (w/v) Bromphenol Blue in dH_2O. Final pH was adjusted to 6.8 with 1 M HCl.

- 4 x Lower gel solution: 1.5 M Tris, 0.4 % SDS in dH_2O. Final pH was adjusted to 8.8 with HCl.
- 4 x Upper gel solution: 0.5 M Tris, 0.4 % SDS in dH_2O. Final pH was adjusted to 6.8 with HCl.
- 10 x PBS: 14 mM KH_2PO_4, 27 mM KCl, 43 mM Na_2HPO_4, 1.37 M NaCl in dH_2O.
- 1 x PBST: 1.4 mM KH_2PO_4, 2.7 mM KCl, 4.3 mM Na_2HPO_4, 137 mM NaCl, 0.1 % Tween20 in dH_2O.
- Blocking solution: 2 mg/ml I-Block™ (Tropix®) in 1 x PBST.
- Transfer buffer: 25 mM Tris, 192 mM glycine, 20 % CH_3OH in dH_2O.
- 50 x TAE buffer: 2 M Tris, 1 M glacial acetic acid, 50 mM EDTA in dH_2O. Final pH was adjusted to 8.0 with HCl.
- Coomassie staining solution: 0.4 % coomassie, 40 % C_2H_5OH in dH_2O.
- Destaining solution: 40 % CH_3OH, 8 % CH_3COOH in dH_2O.

3.2 Plasmids

The plasmids pGEM-13Zf(+) HRV1A (figure 3.1 C), pET3d HRV2 $2A^{pro}$ and pBlueScript II KS(-) (figure 3.1 A) were kindly provided by Martina Aumayr. The pMA-T vector carrying HRV4 $2A^{pro}$ was purchased from Invitrogen® (see figure 3.1 B).

A

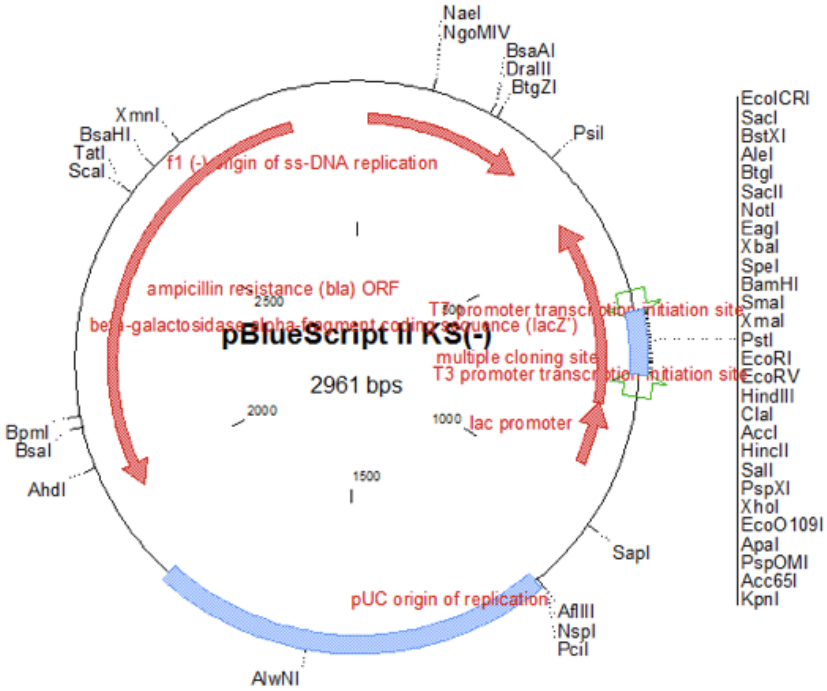
NaeI
NgoMIV
BsaAI
DraIII
BtgZI
PsiI
XmnI
BsaHI
TatI
ScaI
f1 (-) origin of ss-DNA replication
ampicillin resistance (bla) ORF
beta-galactosidase alpha-fragment coding sequence (lacZ')
pBlueScript II KS(-)
2961 bps
T3 promoter transcription initiation site
multiple cloning site
T3 promoter transcription initiation site
lac promoter
EcoICRI
SacI
BstXI
AleI
BtgI
SacII
NotI
EagI
XbaI
SpeI
BamHI
SmaI
XmaI
PstI
EcoRI
EcoRV
HindIII
ClaI
AccI
HincII
SalI
PspXI
XhoI
EcoO109I
ApaI
PspOMI
Acc65I
KpnI
BpmI
BsaI
AhdI
SapI
pUC origin of replication
AflIII
NspI
PciI
AlwNI

B

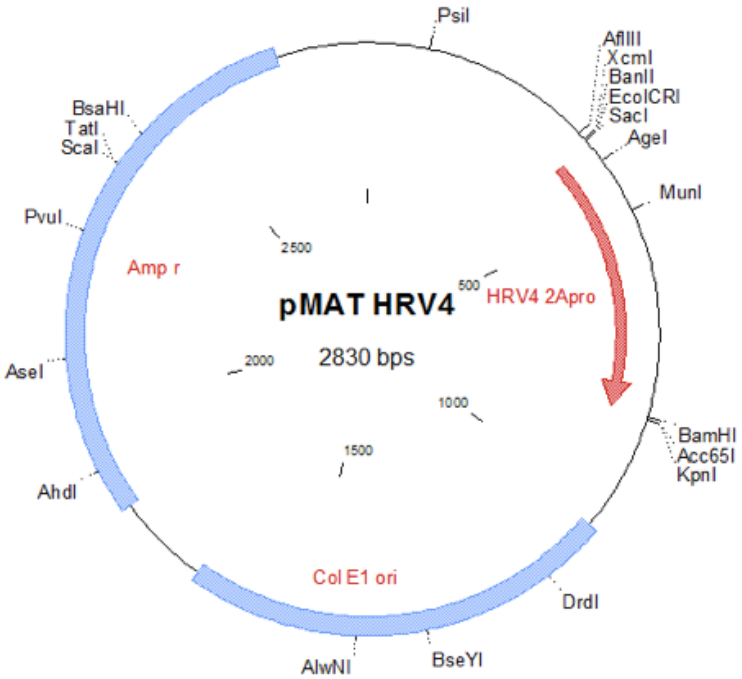
PsiI
AflIII
XcmI
BanII
EcoICRI
SacI
AgeI
MunI
BsaHI
TatI
ScaI
PvuI
Amp r
pMAT HRV4
2830 bps
HRV4 2Apro
AseI
AhdI
BamHI
Acc65I
KpnI
Col E1 ori
DrdI
AlwNI
BseYI

C

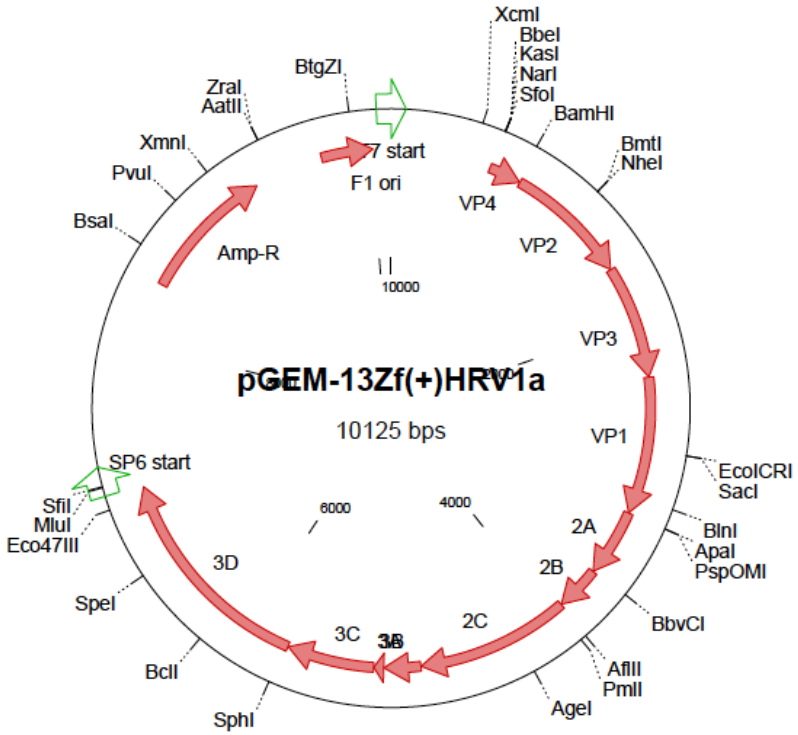
pGEM-13Zf(+)HRV1a
10125 bps
F1 ori
T7 start
SP6 start
Amp-R
VP4
VP2
VP3
VP1
2A
2B
2C
3C
3D
XcmI
BbeI
KasI
NarI
SfoI
BamHI
BmtI
NheI
EcoICRI
SacI
BlnI
ApaI
PspOMI
BbvCI
AflII
PmlI
AgeI
SphI
BclI
SpeI
SfiI
MluI
Eco47III
BsaI
PvuI
XmnI
ZraI
AatII
BtgZI
10000
6000
4000

D

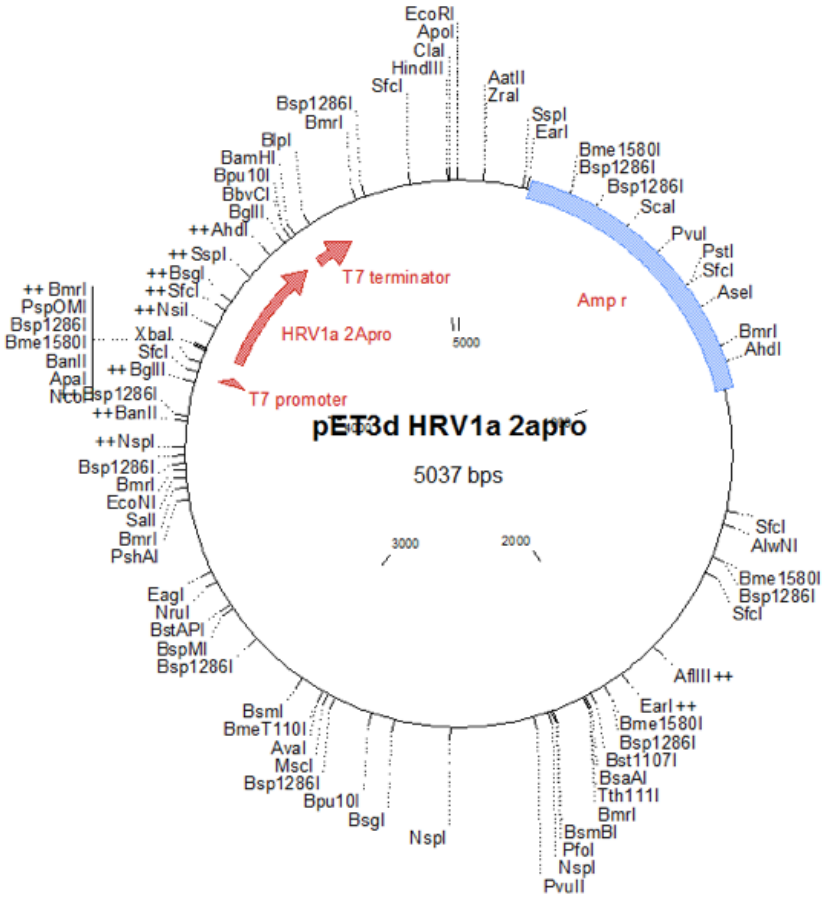
pET3d HRV1a 2apro
5037 bps
T7 terminator
HRV1a 2Apro
T7 promoter
Amp r
EcoRI
ApoI
ClaI
HindIII
SfcI
AatII
ZraI
SspI
EarI
Bme1580I
Bsp1286I
Bsp1286I
ScaI
PvuI
PstI
SfcI
AseI
BmrI
AhdI
SfcI
AlwNI
Bme1580I
Bsp1286I
SfcI
AflIII++
EarI++
Bme1580I
Bsp1286I
Bst1107I
BsaAI
Tth111I
BmrI
BsmBI
PfoI
NspI
PvuII
NspI
BsgI
Bpu10I
Bsp1286I
MscI
AvaI
BmeT110I
BsmI
EagI
NruI
BstAPI
BspMI
Bsp1286I
PshAI
BmrI
SalI
EcoNI
BmrI
Bsp1286I
++NspI
++BanII
Bsp1286I
NcoI
ApaI
BanII
Bme1580I
PspOMI
++BmrI
++BglII
SfcI
XbaI
++NsiI
++SfcI
++BsgI
++SspI
++AhdI
BglII
BbvCI
Bpu10I
BamHI
BlpI
Bsp1286I
BmrI
5000
3000
2000

E

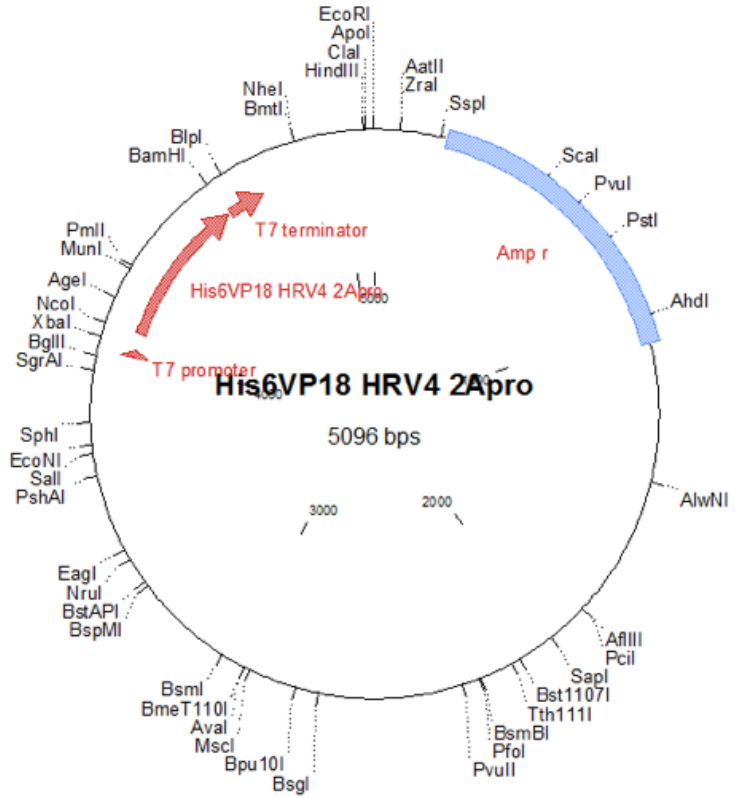

F

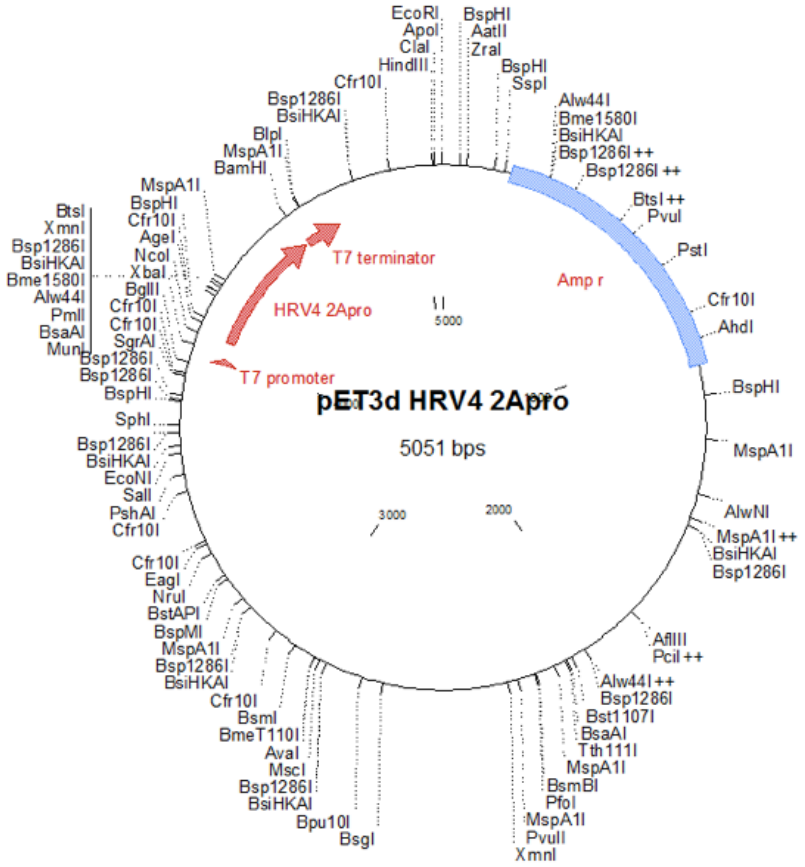

Figure 3.1 (A) The plasmid map of pBlueScript II KS(-). (B) The plasmid map of pMA-T vector containing HRV4 2A^{pro} (Invitrogen®). (C) The plasmid map of pGEM-13Zf(+) HRV1A. (D) The plasmid map of pET3d HRV1A 2A^{pro}. (E) The plasmid map of pET3d HRV4 His6VP18 2A^{pro}. (F) The plasmid map pET3d HRV4 2A^{pro}. *Eco*RV, *Nco*I and *BamH*I restriction sites and significant features are visualized by the CloneManager software.

Table 3.1 The list of primers that were used in this project.

Name	Sequence 5'-3'	Strand
TIM2175	ATAGCCATGGGGCCCAGTGATCTATATGTGCATGTAGG	sense
TIM2176	TATCGGATCCTATTATTGTTCCTCAGCACAGTGAAATTGTCTAAGATC	antisense
TIM2177	CATGTGAACCTGGTGATGCTGGTGGAAAACTTCTTTG	sense
TIM2178	CAAAGAAGTTTTCCACCAGCATCACCAGGTTCACATG	antisense
TIM2179	GTTGATGCACGTGCACATGGTAGCGAAACCG	sense
TIM2180	CGGTTTCGCTACCATGTGCACGTGCATCAAC	antisense
TIM2181	CCCATGGGGTTAGGTCCGCGT	sense
TIM2204	CTTTGTTAGCAGCCGGATCCATTAC	antisense
TIM2183	CCGGGTGATTCTGGTGGTATTCTGCGTTG	sense
TIM2184	CAACGCAGAATACCACCAGAATCACCCGG	antisense
TIM2203	GATATACCATGGGGCATCACCATCACCATCACACCAGAGAAAGCATC AACACCTACGGGTTAGGTCCGC	sense
TIM2282	CCGGGTGATGCTGGTGGTATTCTGCGTTG	sense
TIM2283	CAACGCAGAATACCACCAGCATCACCCGG	antisense

3.3 DNA methods

3.3.1 Transformation

Competent cells were thawed on ice for 15' and subsequently transformed with ~100 μg DNA. Transformed cells were incubated on ice for another 15 minutes. As the next step, bacterial cells were exposed to heat shock at 42°C for 45'' during which DNA uptake occurs. After the 2' incubation on ice, 300 μl of LB medium was added to the competent cells without any antibiotics and incubated at 37°C for minimum 30 minutes. Following the incubation, cells were plated out on the antibiotic containing agar plates in a sterile environment. Cells were left to grow colonies overnight at 37°C.

3.3.2 Chemically competent cells

A pinch of chemical competent cells of any strain (from the purchased glycerol stock) was put into 3-5 ml 2 x TY medium and grown overnight at 37°C at 220 rpm. Next day 100 ml of 2 x TY medium was inoculated with overnight culture (OD_{600} 0.1). Cells were grown until an OD_{600} between 0.45-0.55 was reached and directly put on ice for 15'. Then cells were harvested at 2500 rpm for 15 minutes at 4°C. Pellet was resuspended in 33 ml of RF1 solution and incubated on ice for 15'. Second

harvesting step was performed as described above. Then pellets were resuspended in 8 ml RF2. Chemically competent cells were aliquoted in 200 μl volumes and snap frozen in liquid nitrogen for longer storage at -80°C .

3.3.3 Agarose gel electrophoresis

DNA sample was mixed with 10 x loading dye and loaded on a 1 % agarose gel prepared in 1 x TAE buffer. Gels were run at 120V for 30' in 0.5 x TAE buffer.

3.3.4 Minipreparation (wizard® plus SV miniprepS DNA purification system) (Birnboim and Doly 1979)

In order to isolate a single-copy of plasmid from plated colonies, competent TOP10 (NEB) cells were transformed with DNA. From this transformation, overnight cultures of single colonies were prepared in 5 ml LB + ampicillin (Sigma, 100 mg/ml). Overnight cultures carrying single genotype of plasmids were harvested (3-5 ml) at 5000 rpm for 10'. Pellets were resuspended in 250 μl resuspension buffer thoroughly until there were no cell clumps. Collected cells were lysed with 250 μl of cell lysis buffer and tubes were inverted several times. For protein catalysis 10 μl alkaline proteinase was added and tubes were inverted several times. The mixture was incubated for 5' at room temperature. Genomic DNA was precipitated by the addition of 350 μl of neutralization buffer. Tubes were mixed through inverting several times. Cell lysates were cleared out with centrifugation at 13200 rpm for 10'. Circular plasmid DNA bearing clear supernatant was transferred into spin columns. Once the column had been equilibrated with the plasmid DNA, it was spun down at 13200 rpm for 2' enabling binding to the column. Later, the column was washed 2 x with 750 μl and 250 μl washing solution, respectively and centrifuged at 13200 rpm for 2'. The remaining ethanol was removed from the column with further centrifugation (if necessary). DNA was eluted in a fresh 1.5 ml Eppendorf tube with 30 μl nuclease-free water (incubated for at least 5'), stored at -20°C for longer periods.

3.3.5 Midipreparation

In order to obtain larger scale of single-copy DNA for cloning approaches, plasmid DNA was isolated from the transformed competent TOP10 (NEB) cells with Nucleobond AX plasmid Midi Kit (Macherey-Nagel). The protocol of manufacturer was followed.

3.3.6 Gradient PCR

Table 3.2 Gradient PCR reaction composition.

Ingredients	Amount per 50 μl reaction
Template DNA	500 μg (~10 μg/μl)
dNTPs	5 μl (250 μM)
Forward primer	1 μl (0.66 μM)
Reverse primer	1 μl (0.66 μM)
Q5 Reaction Buffer (5 x)	10 μl
Q5 High Fidelity Polymerase (added at last)	0.5 μl (20 u/ml)
dH_20	variable to be filled until the end volume

Every ingredient was mixed in 0.5 ml Eppendorf tubes by vortexing (see table 3.2). The polymerase was added last and reactions were mixed by pipetting up and down. Reaction tubes were placed into the master cycler gradient (Eppendorf) according to gradient temperatures set by the machine: middle section corresponding to 55°C and 10°C lower at very left, 10°C higher at very right section. Then gradient PCR program was initiated (see table 3.3).

Table 3.3 Gradient PCR program

Initial denaturation at 95°C	30''
30 cycle for the following steps:	
1. Denaturation in cycle at 95°C	10''
2. Annealing at 55°C ± 10°C	30''
3. Elongation at 72°C	4'30''
Final elongation at 72°C	10'
Store at 4°	∞

3.3.7 Digestion of the DNA with restriction enzymes

Either ~100 ng of DNA or 50 μl of PCR reaction was mixed with 10 x CutSmart® Buffer (NEB) and mixed well by vortexing (see table 3.4). Restriction reactions were performed at 37°C with 1 μl of the restriction enzyme, which was mixed by pipetting up and down. When DNA was completely restricted, enzyme activity was tested on a 1 % agarose gel together with the non-digested negative control.

Table 3.4 Restriction reaction conditions and restriction sites. Cuts are indicated with * symbol. DpnI cuts from the methylated adenine represented in bold.

Enzymes	Incubation conditions	Restriction sequence
DpnI (NEB)	5 h at 37°C	5'...G**A***TC...3' 3'...CT***A**G...5'
EcoRV (NEB)	2 h at 37°C	5'...GAT*ATC...3' 3'...CTA*TAG...5'
BamHI (NEB)	2 h at 37°C	5'...G*GATCC...3' 3'...CCTAG*G...5'
NcoI (NEB)	2 h at 37°C	5'...C*CATGG...3' 3'...GGTAC*C...5'

3.3.8 DNA extraction from agarose gel or PCR clean up (wizard® SV gel and PCR clean-up sysyem, Promega)

The DNA fragment of interest, which is intercalated with ethidium bromide, was visualized under UV light and excised with a clean scalpel. The excised gel was weighed in an eppendorf tube. Membrane binding solution (MBS) was mixed with the excised agarose gel or PCR reaction in 1:1 ratio (i.e. for 100 mg gel 100 μl MBS is used or 50 μl PCR reaction is mixed with 50 μl of MBS) and heated up to 65°C until the gel is completely dissolved (vortex if necessary). The mixture was loaded on a spin column, incubated for 1' and then spun down at 13200 rpm for 1'. The column was washed with 750 μl and 200 μl washing solution, respectively and centrifuged at 13200 rpm for 2'. The remaining ethanol was removed from the column with further centrifugation if necessary. DNA was eluted in a fresh 1.5 ml eppendorf tube with 30 μl nuclease-free water (incubated for at least 5'), stored at -20°C for longer periods.

3.3.9 Phosphorylation of PCR product (NEB)

In order to phosphorylate a PCR-amplified fragment, 50 μl of the PCR reaction was mixed with 6 μl of 100 mM ATP, 6.3 μl of 10 x T4 polynucleotide kinase (PNK) buffer and mixed by vortexing. Phosphorylation was initiated with the addition of 1 μl T4 PNK, and the enzyme was mixed by pipetting up and down. Following incubation at 37°C for 1 hour, the reaction was heat shocked at 90°C for 1' and as a final step incubated at 37°C for 10'. DNA was cleaned-up with PCR Clean-up kit (Promega) after the phosphorylation reaction was completed.

3.3.10 Dephosphorylation of cut vector (NEB)

Any given amount of the cut vector was mixed with 10 x CutSmart® buffer and mixed well by vortexing. Dephoshorylation was performed with 1 μl calf intestinal alkaline phosphatase (CIP) and reaction was mixed by pipetting up and down. The reaction volume was added up with dH_2O and incubated at 37°C for 1-2 hours. After the dephosphorylation, reaction is cleaned-up with PCR Clean-up kit (Promega).

3.3.11 Ligation (NEB)

Phosphorylated blunt end PCR products or restricted inserts were ligated into dephosphorylated vector. Reactions were either incubated at 4°C overnight or at room temperature for 1 h (see table 3.5).

Table 3.5 Ingredients of a ligation reaction. A, B, C are representing examples for different ratios of insert and vector. D and E are representing the control reactions.

	A	B	C	D (ctrl)	E (ctrl)
Phosphorylated insert	300 ng (15 ng/μl)	600 ng (30 ng/μl)	300 ng (15 ng/μl)	x	300 ng (15 ng/μl)
Dephosphorylated vector	100 ng (5 ng/μl)	100 ng (5 ng/μl)	50 ng (2.5 ng/μl)	100 ng (5 ng/μl)	x
T4 buffer (10 x)	2 μl	2 μl	2 μl	2 μl	2 μl
T4 ligase (20 x 10^3 u/ml)	1 μl	1 μl	1 μl	1 μl	1 μl
dH_2O	variable	variable	variable	variable	variable
End Volume	20 μl	20 μl	20 μl	20 μl	20 μl

3.4 Protein Methods

3.4.1 SDS-PAGE

Protein samples were mixed with either 5 x or 2 x SDS sample buffer and denaturized at 95°C for 5' prior to loading on 17.5% gels. Self prepared gels (see table 3.6) were run at 300 V for 30' in 1 x SDS running buffer (from a stock solution of 10 x), stained with coomassie staining solution and destained with H_2O or destaining solution.

Table 3.6 SDS-PAGE gel ingredients. APS: ammoniumperoxidisulfate. TEMED: N,N,N',N'-tetramethyl-ethane-1,2-diamine.

Per one 17.5 % gel:	Separation Gel	Stacking Gel
30 % acrylamid/bis solution (29:1)	2 ml	0.334 ml
4 x lower gel solution	1 ml	x
4 x upper gel solution	x	0.5 ml
dH_2O	1 ml	1.134 ml
APS	0.05 ml	0.02 ml
TEMED	0.005 ml	0.002 ml

3.4.2 Western Blot

All histidine-tagged proteins were detected through western blotting and visualized with horseradish peroxidase reaction. Primary antibody with α-HisTag (mouse) which was obtained from GE Healthcare and secondary antibody α-mouse (rabbit) from Jackson Immuno Research Laboratories were used. The SDS-PAGE gel was put in a sandwich chamber in transfer buffer where it is blotted on a nitrocellulose membrane (Millipore). Sandwich was supported with Whatman papers and sponges. Blotting was performed at 4°C in transfer buffer for either 1 h at 400 mA or overnight at 40 mA. After the blotting, the membrane was incubated with blocking solution for 20' under gentle shaking. Then, 3.3 μl of primary antibody was diluted in blocking solution (1:3000) and the membrane was rolled for 1 h. The membrane was washed 5 times with 5 ml 1 x PBST with 5' incubations. Secondary antibody was diluted in 1 x PBST (1:10000). After incubation for 1 h with the secondary antibody, membrane was washed again as described above. The membrane was treated with SuperSignal Western Blot Enhancer Kit (Thermo Scientific) for initiating the reporter reaction. Secondary antibody, which is attached to the His-tagged proteins via primary antibody, is coupled to the horseradish peroxidase. Taking the advantage of an immobilized enzyme in the presence of its substrate (i.e. Luminol), the reaction signal can easily be detected as a photon emission on the film. The substrate was mixed on the membrane following the protocol from manufacturer. The film was developed in a dark room using AGFA Curix600.

3.4.3 Overnight culture preparation

Colonies were picked from plates that were transformed with a plasmid coding the corresponding protein, and put in 100 ml LB medium with ampicillin (Sigma, 100 mg/ml), grown overnight at 37°C, 200 rpm.

3.4.4 Protein expression

Expressions were performed in 2 liters of fresh medium with ampicillin (Sigma, 100 mg/ml) and were inoculated with overnight cultures (OD_{600} = 0.1). Cells were grown at 37°C at 175 rpm until an OD_{600} of 0.6 - 0.8 was reached. Cells were then induced with IPTG (Discovery Fine Chemicals) and expressions were performed for variable hours per each protein (see table 3.7). Expression was terminated by harvesting the cells at 5-6000 rpm for 15' at 4°C and pellets were resuspended in buffer A or buffer A without DTT which was used in case of an initial HisTrap purification step and then frozen at -80°C. Each protein was purified following different methodologies and conditions due to their different isoelectric points (see table 3.8, 3.9 and 3.10).

3.4.5 Cell lysis

Thawed cells were mixed with 200 μg DNaseI (per 3L pellet) prior to lysis. Homogenization with french press was performed at 4°C with air pressure in between 10000 - 15000 psi in the Emulsiflex-C3 homogenizer (Avestin) machine. Sonication was performed on ice with 3 times 30'' bursts with 10 %, continued with 40 % with same power, followed finally by 1 time 30'' burst with 100 %, at 73/D power. This approach was repeated as described when needed. Lysed cells were spun down at 18000 rpm for 30' at 4°C. Supernatant bearing the soluble proteins was always filtered through 0.45 μm filters before loading onto purification columns.

3.4.6 Ammonium sulfate precipitation

Increasing concentrations of salt enhances the surface tension of water. This tension generates hydrophobic interactions between water and certain proteins thereby enabling protein-specific purification with different salt concentrations, namely salting out (Wingfield 2001). HRV1A 2A proteinases were salted out with 2-step incubation at 4°C temperature. First 20 % concentration of saturated $(NH_4)_2SO_4$ solution was added drop-by-drop to homogenized cell lysates and incubated for 3 h with continuous stirring. At this step non-specific proteins were precipitated through spinning down at 18000 rpm for 30'. Supernatant at a concentration of 20% was then treated with additional ammonium sulfate drop wise until 40 %. After overnight incubation with continuous stirring, the precipitated protein-of-interest was spun down at 18000 rpm for 30'. To remove excess $(NH_4)_2SO_4$, the supernatant was dialyzed against buffer A.

3.4.7 Histrap 5 ml affinity chromatography

HisTrap column (GE Healthcare) was washed with 5 column volumes (CV) of dH_2O. Following the manual load of 10 ml $NiCl_2$ in a syringe through the 10 ml pre-washed loop, Ni-bound sepharose column was washed with Histrap equilibration buffer for 5 CV. Sample was then loaded via the 50 ml super-loop and flow-through was collected. Then the sample bound to the column was washed with equilibration buffer for 5 CV and wash-through was collected. His-tagged proteins were eluted from the column with Histrap elution buffer with increasing concentrations of imidazole as competing agent.

All purifications were analyzed on a 17.5 % SDS-PAGE gel. Scanned gels (Canon) were simply cut and resized in Word. All buffers and solutions used on columns were filtered through 0.22 μm filters.

3.4.8 Mono Q HR 10/100 anion exchange chromatography

MonoQ HR 10/100 (GE Healthcare) anion exchange chromatography column was first washed with with 5 CV of dH_2O. Then it was washed with 1 CV of MonoQ elution buffer. Following the equilibration with 5 CV of buffer A, sample was loaded to the column using super-loop. Flow-through during sample load was collected. After binding onto the column, wash-through was collected while washing with 1.25 CV of buffer A. Negatively charged proteins which are bound on positively charged column resin were collected with a gradient of 50 mM to 1M of NaCl as competing agent.

3.4.9 Preparative size exclusion chromatography with HiLoad® 26/60 Superdex® 75 prep grade or HiLoad® 16/60 Superdex® 75 prep grade

Maximum of 5 ml sample was loaded onto variable sized gel filtration columns according to preparation volume and the molecular weight of the protein. All single protein purifications were performed with a HiLoad® Superdex® 75 prep grade column which was equilibrated with either Hepes buffer or buffer A at pH 9.0.

3.4.10 Concentration of the proteins

Since the loaded sample volume differs in each step of purification, proteins were concentrated in Centriprep® 10K centrifugal filters which eliminates proteins that are smaller than 10 kDa from the solution. After the gel filtration all proteins were concentrated in Amicon® Ultra 10K centrifugal filters for enabling in higher concentrations for later analytical usage purposes. All concentration steps were

conducted at 4000 rpm 4°C using an Eppendorf 5810 R tabletop centrifuge. Protein density was measured afterwards with nanodrop spectrophotometer ND-1000 (Peqlab Biotechnologie GmbH).

3.4.11 Dialysis of the proteins

All dialysis steps were performed at 4°C using a SnakeSkin® Dialysis Tubing (Thermo Scientific) with 7,000 Da molecular weight cut-off. Pooled fractions were collected into the tubing while securing the bag with clips and put in assay buffer in a dilution of at least 1:70 with an exchange of fresh buffer every 30', twice.

3.5 Biochemical and biophysical methods

3.5.1 *in vitro* cleavage assays

To understand the cleavage performance of active 2A proteinases (from HRV1A and HRV4), experiments were performed with the recombinant substrates eIF4E and $eIF4GII_{551-745}$. Active proteinases (1, 10, 20, 40 ng) were incubated with either 1 μg of $eIF4GII_{551-745}$ or with 1 μg of eIF4E/$eIF4GII_{551-745}$ for 90 minutes at 37°C. Aliquots were taken at time points 0, 10, 20, 30, 60 and 90 minutes and reactions were stopped by adding 5 x sample buffer following denaturation at 95°C for 5 minutes. Different cleavage patterns from two different genetic groups were analyzed on a 17.5 % SDS-PAGE gels. Scanned gels (Canon) were simply cut and resized in Word.

3.5.2 Analytical size exclusion chromatography

Binding studies of the 2A proteinases with eIF4E and $eIF4GII_{551-745}$ were analyzed at 4°C on a HiLoad® 16/60 Superdex® 200 pg (GE Healthcare) column, with an internal standard aprotinin (6.5 kDa). Except for the internal standard (1 mg) all other proteins were loaded at ~0.5 mg and complexes were always incubated either 10 minutes or overnight with a gentle shaking at 4°C. Incubations were always terminated by centrifugation at 13200 rpm at 4°C for 10'. Next, the assay buffer and internal standard were added to the proteins, respectively. Sample was loaded onto column in 1 ml total volume through a 2 ml loop. All proteins and complexes were eluted with 1 ml/min flow rate and monitored at 280 nm UV light. Aliquots from elution fractions were mixed with 5 x SDS sample buffer and denaturated at 95°C for 5 minutes prior to SDS-PAGE.

3.5.3 Static light scattering (SLS)

Determination of the exact molecular weight and the oligomeric state of HRV1A $2A^{pro}$ C106A, eIF4E and $eIF4GII_{551-745}$ static light scattering measurements were performed at room temperature by

loading 100 μg of sample onto 10/300 Superdex® 200 prep grade column (pre equilibrated in Hepes buffer), which is connected to miniDAWN Trista light scattering instrument (Wyatt Technology, Santa Barbara, CA). Data analysis was done using the software ASTRA from the manufacturer.

3.5.4 Studying protein-protein interactions using isothermal titration calorimetry (ITC)

All experiments were done with MicroCal microcalormeter in Hepes buffer without DTT filtered through 0.22 μm filter. All proteins were dialyzed against this buffer. After equilibration of the sample cell at 25°C, experiments started with an initial delay of 60 - 300 seconds. For the binary interactions of eIF4E/HRV1A $2A^{pro}$ or $eIF4GII_{551-745}$/HRV1A $2A^{pro}$, the following injection style was used. Initial injection was started with 0.5 μl titrant, then remaining 20 injections were conducted with 2 μl of titrant with an interval of 180 seconds into a continuously stirring (750 rpm) sample cell. Titrant concentration (in 100 μl) was always 10 x higher than the sample cell concentration (in 200 μl), 650 μM to 65 μM respectively. For the ternary interactions in between the eIF4E/$eIF4GII_{551-745}$ complex (cell) and HRV1A $2A^{pro}$ (titrant), a different injection style was preferred. Initial 5 injections were performed with 0.5 μl of the titrant, subsequently 2 μl for 10 injections and finally 1 μl for the remaining 5 injections. The interval of injections was again 180 seconds. Titrant concentration was 500 μM and injected into a continuously stirring (750 rpm) sample cell in a concentration (in 200 μl) of 50 μM. Data was analyzed with the Origin software from MicroCal.

4 RESULTS

4.1 Cloning of HRV1A 2A^{pro}

The pET3d vector was used to ligate in HRV1A 2A^{pro} construct in between *Nco*I and *BamH*I restriction sites. The vector contains an ampicillin resistance for bacterial colony screening during expression with ampicillin. The gene-of-interest (viral 2A^{pro}) is transcribed in the bacteria from the T7 promoter by T7 RNA polymerase. There is a T7 terminator downstream of the 2A^{pro} coding region. Gene expressions were modulated via induction of *lacI* regulator gene with IPTG, which is an inducer of the *lac* operon in *Escherichia coli*. To introduce the above restriction sites to the 2A^{pro} sequence via gradient PCR, the HRV1A 2A^{pro} fragment was amplified from pGEM-13Zf(+) HRV1A (see figure 3.1 C) and modified by PCR through introducing *Nco*I and *BamH*I restriction sites with primers TIM2175, TIM2176. The PCR amplified product was cloned into (EcoRV cut) pBlueScript II KS(-) vector with blunt ends. Correct clones were determined via DNA sequencing of minipreparations. The HRV1A 2A^{pro} was cut with *NcoI* and *BamHI* restriction sites and ligated into (*NcoI* and *BamHI* cut) pET3d vector with sticky ends (see figure 3.1 D). The replacement of the active Cys106 codon with that for Ala to inactivate the expressed proteinase, was performed with gradient PCR with primers TIM2177, TIM2178 (see Table 3.1).

4.2 Expression and purification

Table 4.1 shows the isoelectric points and working pH of the buffers alongside with the calculated molecular weights of each protein expressed in this work. Table 4.2 lists the expression conditions of the proteins. Table 4.3 gives the methods followed to purify each protein, whereas table 4.4 marks the purification/elution points corresponding to given method.

Table 4.1 Different isoelectric points, molecular weights and working pH conditions of the proteins.

	Isoelectric point	Working buffer pH	M_w (kDa) (calculated)
eIF4E	5.65	7.4 - 8.0	28.8
eIF4GII$_{551-745}$	6.25	7.4 - 8.0	22.5
HRV1A 2A^{pro}	5.47	7.4 - 8.0	16.4
HRV4 His$_6$VP1$_8$ 2A^{pro}	7.16	9.0	18.2

Table 4.2 Expression conditions of each protein. *Expression medium Terrific Broth (TB) was mixed with phosphate buffer. **$ZnCl_2$ was added to strengthen the chymotrypsin-like fold of the $2A^{pro}$, which is fixed with tetra-coordinated zinc ions (Sommergruber et al., 1994b, Petersen et al., 1999)

	expression medium	IPTG	$ZnCl_2$**	expression hours	expression temperature	bacterial cell line
eIF4E	TB*	0.6 mM	x	overnight	18°C	T7 express (NEB)
$eIF4GII_{551-745}$	LB	0.6 mM	x	5 h	37°C	BL21 (DE3) (NEB)
HRV1A $2A^{pro}$ C106A	LB	0.15 mM	0.1 mM	overnight	18°C	SoluBL21 (Genvantis)
HRV1A $2A^{pro}$ active	LB	0.15 mM	0.1 mM	4 h	30°C	SoluBL21 (Genvantis)
HRV4 His_6VP1_8 $2A^{pro}$ C110S	LB	0.15 mM	0.1 mM	5 h	30°C	SoluBL21 (Genvantis)
HRV4 His_6VP1_8 $2A^{pro}$ C110A	LB	0.15 mM	0.1 mM	4 h	30°C	SoluBL21 (Genvantis)
HRV4 His_6VP1_8 $2A^{pro}$ act.	LB	0.15 mM	0.1 mM	4 h	30°C	SoluBL21 (Genvantis)

Table 4.3 Different methodologies to purify each protein.

		purification steps			
	cell lysis	1st step	2nd step	3rd step	storage buffer
eIF4E	french press	affinity chromatography	anion exchange chromatography	size exclusion chromatography	Hepes buffer
$eIF4GII_{551-745}$	sonication	affinity chromatography	size exclusion chromatography	x	Hepes buffer
HRV1A $2A^{pro}$ C106A	french press	$(NH_4)_2SO_4$ precipitation	anion exchange chromatography	size exclusion chromatography	Hepes buffer
HRV1A $2A^{pro}$ active	french press	$(NH_4)_2SO_4$ precipitation	anion exchange chromatography	size exclusion chromatography	Hepes buffer
HRV4 His_6VP1_8 $2A^{pro}$ C110S	french press	affinity chromatography	size exclusion chromatography	x	buffer A pH 9.0
HRV4 His_6VP1_8 $2A^{pro}$ C110A	french press	$(NH_4)_2SO_4$ precipitation	affinity chromatography	x	buffer A pH 9.0
HRV4 His_6VP1_8 $2A^{pro}$ active	french press	affinity chromatography	size exclusion chromatography	x	buffer A p.H 9.0

Table 4.4 Elution conditions of each protein in a purification specific manner.

		eIF4E	HRV1A $2A^{pro}$		$eIF4GII_{551-745}$	HRV4 His_6VP1_8 $2A^{pro}$		
			active	C106A		active	C110S	C110A
$(NH_4)_2SO_4$ precipitation	$(NH_4)_2SO_4$	x	40 %	40 %	x	40 %	x	20 %
Affinity chr.	Imidazole	~ 170 mM	x	x	115 - 380 mM	x	140 - 190 mM	140 – 164 mM
Anion exchange chr.	NaCl	~ 335 mM	350 mM	335 – 410 mM	x	x	x	x
Size exclusion chr. (26/60 S75)	retention volume	153 ml	195 ml	197 ml	137 ml	218 ml	226 ml	x

4.3 Expression and purification of HRV1A 2A^{pro}

4.3.1. HRV1A 2A^{pro} C106A and HRV1A 2A^{pro} active

Both active and inactive (C106A) constructs of the HRV1A 2A^{pro} were expressed in soluBL21 strain of *E.coli*, which enhances toxic and soluble protein expression. The optimized bacterial expression of recombinant proteins is a protein dependent phenomenon. Moreover, heterologous protein overproduction from bacterial cultures often result in aggregates which stick in inclusion bodies. Therefore, we needed optimizations for each of the proteins we expressed. Some suggestions are to reduce the IPTG concentration, and lower the expression temperature (San-Miguel et al., 2013). We tried an expression at 18°C and prolonged the expression time to overnight, since the protein synthesis rates are lower at this temperatures compared to the human biological environment (guidelines from Expression Technologies Inc.). First, we did the expression with two different IPTG concentrations; 0.25 mM and 0.6 mM (data not shown). Further purification steps did not yield enough protein from these amounts (data not shown); therefore, we decided to lower the IPTG concentration further to 0.15 mM, which resulted in a higher overexpression of HRV1A 2A^{pro} C106A (figure 4.2 A)

Temperature and expression period are one the most important parameters while improving the expression yield. Since the active HRV1A 2A^{pro} expression is unpleasant for bacterial cells due to its toxicity, lower temperatures than 37°C are recommended. Many proteins are highly active at 37°C, thus we tried expression attempts at 18°C and 25°C overnight. Unfortunately, the expression rate was too poor to continue for purification (see figure 4.3 A). Later, we tried expressing the active HRV1A 2A^{pro} for 5 hours at 30°C with 0.15 mM IPTG. Even though the expression time was considerably shorter, the corresponding band to viral proteinase was stronger (see figure 4.3 B).

Finally having found the optimal conditions for each inactive and active constructs of HRV1A 2A^{pro} (see table 4.2), expressions were performed following the protocol explained in materials and methods. The sequential purification methods for HRV1A 2A^{pro} and C106A mutant are explained in table 4.3.

HRV1A 2A^{pro}

M G P S D L Y V H V G N L I Y R N L H L F N S E M H D S I L I S Y S S D L I I Y R T N T I G
D D Y I P N C N C T E A T Y Y C R H K N R Y Y P I K V T P H D W Y E I Q E S E Y Y P K H
I Q Y N L L I G E G P C E P G D C G G K L L C R H G V I G I I T A G G E G H V A F I D L R
Q F H C A E E Q Stop

R/K: 10, E/D: 18, pI: 5.47

Figure 4.1 The positively and negatively charged amino acid residues at the working pH and the pI values of HRV1A 2A^{pro}.

The amino acid sequence of HRV1A $2A^{pro}$ C106A (see figure 4.1) is underlined with double line for positive charge carrying residues, and with single line for negative charge carrying residues at the working pH 8.0. We could use the MonoQ column due to net negative charge of the protein at the working pH (8.0). The HRV1A $2A^{pro}$ C106A was eluted at around 335 – 410 mM NaCl from the anion exchange MonoQ column (see table 4.4). This tells us about the high expression level since the elution continues for a longer while as the gradient increases (see figure 4.2 B). On the other hand, active HRV1A $2A^{pro}$ was eluted at exactly 350 mM concentration which is rather a small peak (see figure 4.3 C). The fractions from anion exchange chromatography were directly examined on 17.5 % SDS-PAGE gels and appropriate fractions were pooled together and concentrated for a further size exclusion purification step. Both inactive HRV1A $2A^{pro}$ (figure 4.2 C) and active HRV1A $2A^{pro}$ (figure 4.3 D) constructs were eluted at around 196 ml retention volume from SEC column as very sharp peaks. Since the active viral proteinase is toxic for bacterial cells it yielded ~ 20 times less than C106A construct. Inactive proteinase which was expressed from 6 liters of liquid culture yielded ~ 20 mg of protein (yield: 3.33 mg/L, figure 4.2 D). In contrast, ~ 2 mg of protein was purified from 12 liters of active HRV1A $2A^{pro}$ expression (yield: 0.17 mg/L, figure 4.3 E). Purification results of HRV1A $2A^{pro}$ and the C106A mutant are shown below.

A

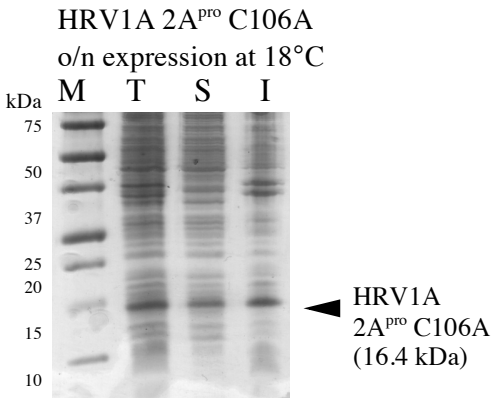

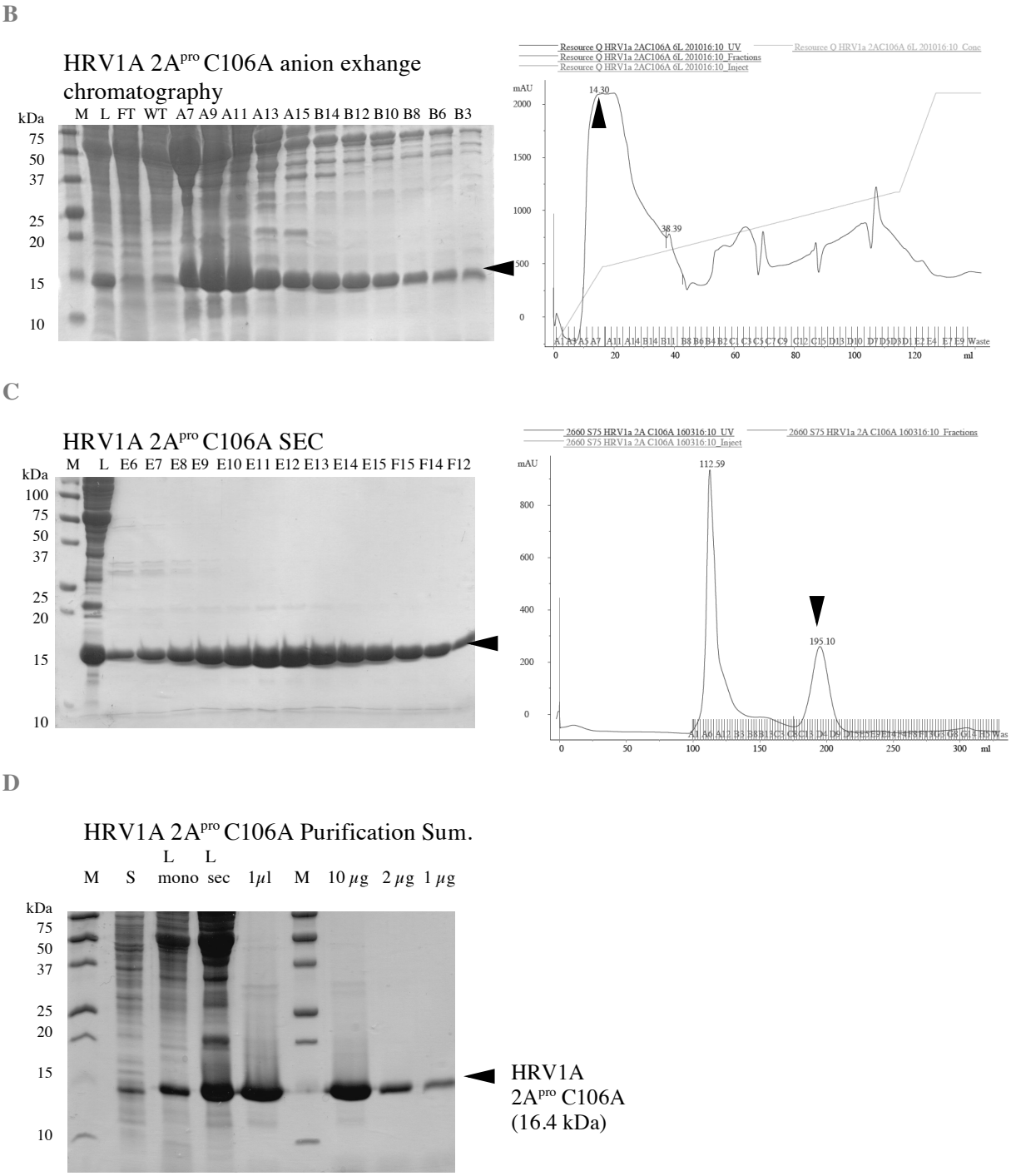

Figure 4.2 Purification of HRV1A 2A^{pro} C106A (A) Total-soluble-insoluble proteins from the expression lysates examined on 17.5 % SDS-PAGE gel. **M:** marker (4 μl) **T:** total (1 μl) **S:** soluble (1 μl) **I:** insoluble (1 μl) (B) 17.5 % SDS-PAGE gel of anion exchange chromatography and the chromatogram **M:** marker (2.5 μl) **L:** load (3 μl) **FT:** flow-through (8 μl) **WT:** wash-through (8μl). Elution of the 2A^{pro} at 335–410 mM NaCl is indicated with an arrow. (C) %17.5 SDS-PAGE gel of SEC and the chromatogram **M:** marker (2.5 μl) **L:** load (3 μl). Pure 2A^{pro} UV peak at 195 ml is indicated with an arrow. 8 μl from fractions corresponding to indicated peaks were mixed with 2 μl 5 x Sample Buffer (8 μl) (D) 17.5 % SDS-PAGE gel of purification summary **M:** marker (4 μl) **S:** soluble cell lysate (1 μl) **L MonoQ:** Loaded sample onto anion exchange column (MonoQ) (3 μl) **L SEC:** Loaded sample onto SEC column (3 μl) **1 μl:** 1 μl of the pure and concentrated sample mixed with 7 μl dH_2O and 2 μl 5 x SDS sample buffer (10μl) **10 μg, 2μg, 1μg:**

10, 2, and 1 μg of the concentrated sample was filled with dH_2O until 8 μl and then mixed with 2 μl 5 x SDS sample buffer (10 μl)

A

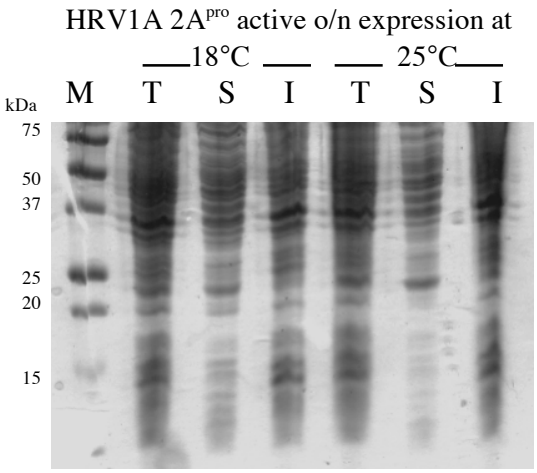

B

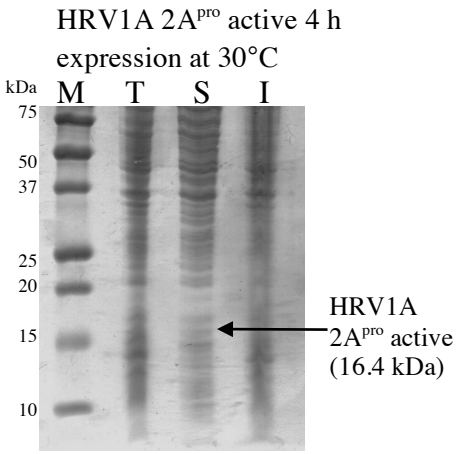

C

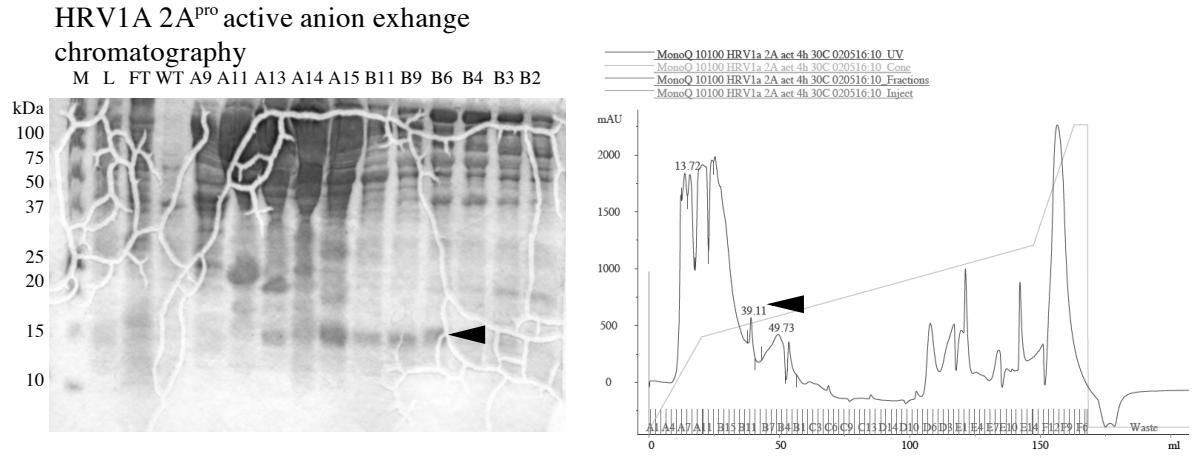

D

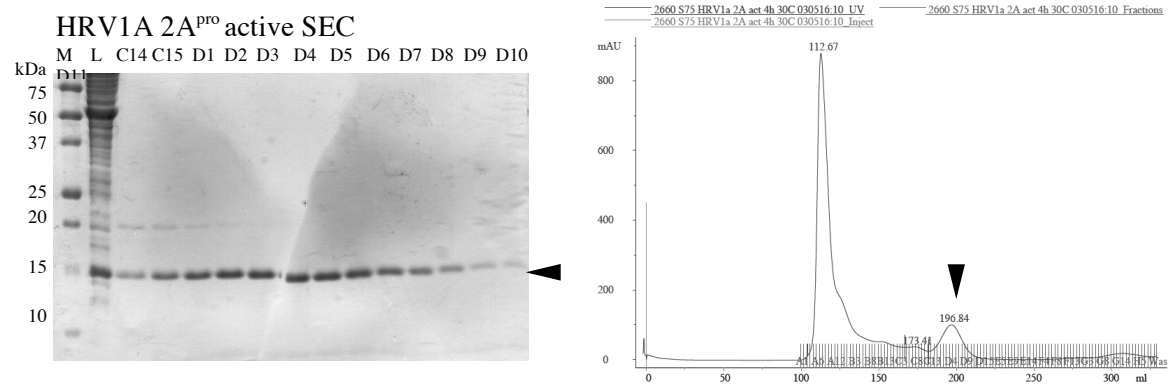

E

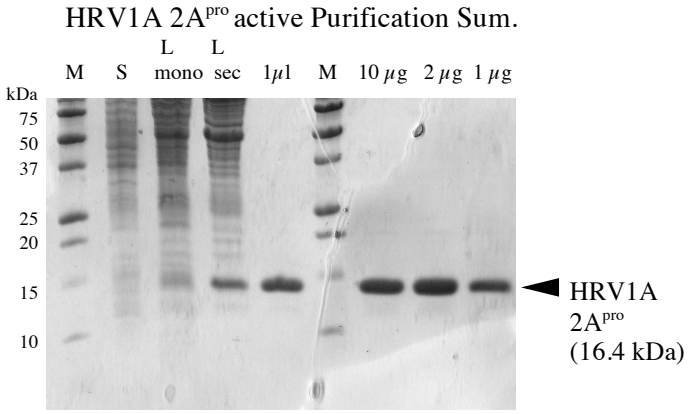

Figure 4.3 Purification of HRV1A 2A^{pro} active (A) Total-soluble-insoluble proteins from the expression lysates examined on 17.5 % SDS-PAGE gel. **M:** marker (4 μl) **T:** total (1 μl) **S:** soluble (1 μl) **I:** insoluble (1 μl) (B) 17.5 % SDS-PAGE gel of anion exchange chromatography and the chromatogram **M:** marker (2.5 μl) **L:** load (3 μl) **FT:** flow-through (8 μl) **WT:** wash-through (8μl). Elution of the 2A^{pro} at 350 mM NaCl is indicated with an arrow. (C) %17.5 SDS-PAGE gel of SEC and the chromatogram **M:** marker (2.5 μl) **L:** load (3 μl). Pure 2A^{pro} UV peak at 196 ml is indicated with an arrow. 8 μl from fractions corresponding to indicated peaks were mixed with 2 μl 5 x Sample Buffer (8 μl) (D) 17.5 % SDS-PAGE gel of purification summary **M:** marker (4 μl) **S:** soluble cell lysate (1 μl) **L MonoQ:** Loaded sample onto anion exchange column (MonoQ) (3 μl) **L SEC:** Loaded sample onto SEC column (3 μl) **1 μl:** 1 μl of the pure and concentrated sample mixed with 7 μl dH_2O and 2 μl 5 x SDS sample buffer (10μl) **10 μg, 2μg, 1μg:** 10, 2, and 1 μg of the concentrated sample was filled with dH_2O until 8 μl and then mixed with 2 μl 5 x SDS sample buffer (10 μl)

Further the identity of HRV1A 2A^{pro} (only the inactive proteinase) was confirmed via mass spectrometry (MS) with a nearly full sequence coverage. For all MS analyses, proteinases were digested with trypsin. Trypsin cleaves at the C-terminal of some K and R (see figure 4.4) residues depending on the adjacent amino acids. Table 4.5 shows MS results below.

Table 4.5 Mass spectrometry results of HRV1A 2A^{pro} C106A.

	Sequence Coverage (%)	MS/MS count (# of peptide spectrum matches)	Intensity (summed peptide intensities)	Peptides (number)	Molecular weight (kDa)
HRV1A 2A^{pro} C106A	90.9	423	2.7 x 10^7	68	16.43

HRV1A 2A^{pro} C106A

M G P S D L Y V H V G N L I Y R N L H L F N S E M H D S I L I S Y S S D L I I Y R T N T I G

D D Y I P N C N C T E A T Y Y C R H K N R Y Y P I K V T P H D W Y E I Q E S E Y Y P K H

I Q Y N L L I G E G P C E P G D A G G K L L C R H G V I G I I T A G G E G H V A F I D L R

Q F H C A E E Q Stop

Figure 4.4 The cleavage sites of trypsin enzyme within the HRV1A 2A^{pro} C106A sequence.

4.4 Cloning of HRV4 2A^{pro}

Genetic group B picornaviral proteinases are not well-characterized and hard to find in the soluble fraction of *E.coli* cell lysates. To investigate the structure and function of HRV4 2A^{pro} and its binding dynamics with eIF4GII$_{551-745}$ & eIF4E, we tried different approaches to express the proteinase. The proteinase coding region (NCBI protein ID:ABF51184.1 2A^{pro} coding sequence residues 854-1000) was synthesized chemically in pMAT plasmid from Invitrogen (see figure 3.1 B). The pET3d vector contains an ampicillin resistance gene that was used for screening the bacterial clones, a T7 promoter that allows *in vitro* transcription by T7 RNA polymerase, and a T7 terminator. The NcoI and BamHI sites are present at the 5'- and 3'-ends of the coding sequence of the gene-of-interest (viral 2A^{pro} coding gene). Therefore, these restriction sites were introduced to the 2A^{pro} gene via gradient PCR, using primers TIM2181, TIM2204 (see table 3.1 for primer list). The HRV4 2A^{pro} was cloned from pMAT into pET3d via *NcoI* and *BamHI* restriction sites (see figure 3.1 F). The inactivation of the proteinase was first performed by mutating nucleophilic Cys into Ser via primers TIM2183 and TIM2184, namely the C110S.

To mimick the idea from a CVB4 2A^{pro} construct which was expressed with 8 amino acid residues from VP1 by David Neubauer (Dissertation, 2013), we also wished to clone the HRV4 2A^{pro} alongside with 8 amino acid residues from the C-terminal of VP1 capsid protein coding region. Moreover, we wished to include a polyhistidine tag upstream to the VP1 residues at the N-terminal of construct to ease the purification, namely the HRV4 His$_6$VP1$_8$ 2A^{pro} (see figure 4.5). The His$_6$VP1$_8$ HRV4 2A^{pro} construct was designed with the primers TIM2203, TIM2204 and performed through a gradient PCR. This construct was then cloned into pET3d vector with *NcoI* and *BamHI* sites (see figure 3.1 E). Both HRV4 His$_6$VP1$_8$ 2A^{pro} C110S and C110A inactive proteinases were obtained by gradient PCR. The C110S inactivation was performed with the primers TIM2183 and TIM2184. Later, the still slightly nucleophilic Ser was mutated into Ala with the TIM 2282 & TIM 2283 primer set, namely the C110A.

These two constructs HRV4 His$_6$VP1$_8$ 2A^{pro} and the untagged HRV4 2A^{pro}, both in pET3d expression vectors, were used to compare expression efficiencies. This approach was followed to

make the protein more soluble. Inactivated 2A^{pro} were obtained for kinetic measurements by disabling substrate cleavage.

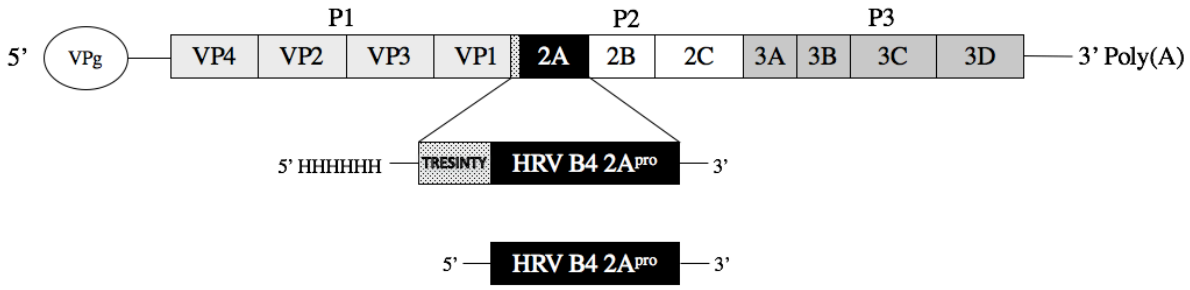

Figure 4.5 Schematic (+)ssRNA genome of HRV4, the recombinant tagged 2A^{pro} construct, and the non-tagged HRV4 2A^{pro} are shown in the figure.

The chemically synthesized HRV4 2A^{pro} coding gene in pMAT vector was ordered with the *NcoI* and *BamHI* restriction sites at the N- and C-termini (3'-*NcoI*$_{386}$ – 5'-*BamHI*$_{837}$) (see table 4.6). Unfortunately, the second ***NcoI*** restriction site in the middle of the 2A^{pro} coding sequence (**mid-*NcoI*$_{528}$**), was missed during cloning (figure 4.6). The table 4.6 shows digestion products from the original pMAT plasmid which was cut with *NcoI* and *BamHI*. As there are 2 *NcoI* and 1 *BamHI* sites in the original plasmid, there were 3 digestion products after the restriction reaction (figure 4.7 lanes: ctrl, 8, 9). On the other hand, after the PCR mutagenesis, a correct clone must have only 2 digestion products (see table 4.7) (figure 4.7 lanes: 6, 7, 10, 11). A silent mutation was made with gradient PCR for the second *NcoI* site was performed with primers TIM2181 and TIM2204 at the **mid-*NcoI*$_{528}$** site. This mutation simplified the cloning of the fragment into pET3d vector with single cutter *Nco*I/*BamH*I enzymes. The correct clone was determined after sequencing the DNA mini preparations. The PCR amplified construct missing the **mid-*NcoI*$_{528}$** site (clone number 11) was restricted with *Nco*I and *BamH*I (e.g. 450 bp insert from figure 4.7 lanes 6, 7, 10 or 11) and ligated into the pET3d plasmid.

Table 4.6 Three digestion products of HRV4 2A^{pro} containing original pMAT vector that is cut with *NcoI* and *BamHI* restriction enzymes. The second ***NcoI*** site (coordinate 528) that is located in the middle of the sequence is indicated in bold.

#	Ends	Coordinates	Length
1	*BamHI-NcoI*	837-386	2380 bp
2	***NcoI*-*BamHI***	**529**-836	308 bp
3	*NcoI*-***NcoI***	387-**528**	142 bp

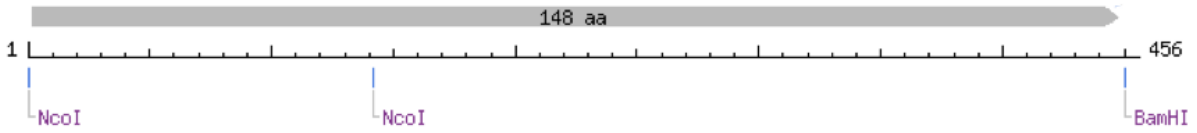

Figure 4.6 HRV4 $2A^{pro}$ coding 456 nucleotides are simply shown as gray line. The figure shows that $2A^{pro}$ coding sequence has *NcoI* restriction sites at the nucleotide residues 1 and 143. The *BamHI* restriction site is positioned at residue 451. (Picture made by using NEBcutter V2.0)

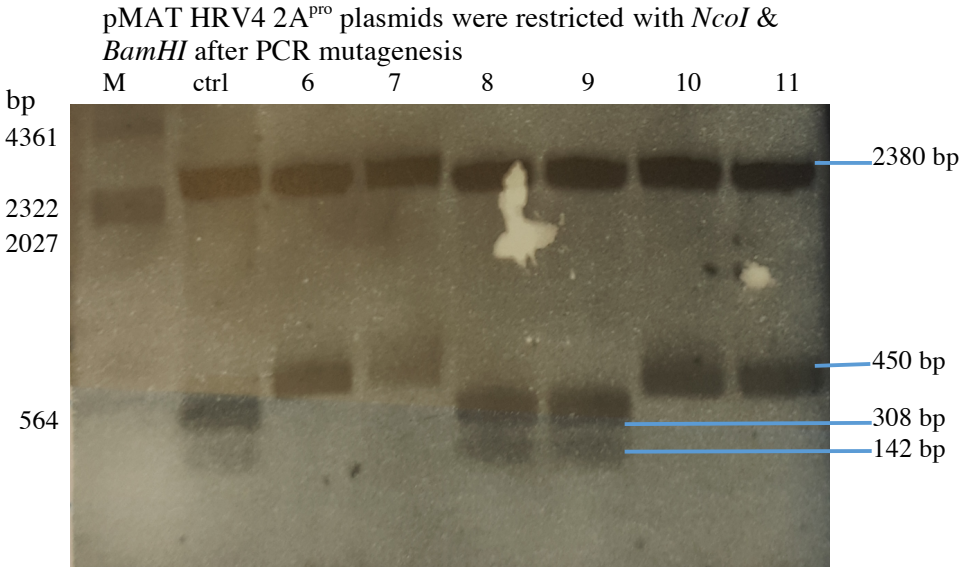

Figure 4.7 The silent mutation at the second *NcoI* site was conducted with gradient PCR. After the PCR, all clones were checked for the mutation. DNA was simply digested using *NcoI* and *BamHI* enzymes, and reaction was loaded on a 1 % agarose gel. The clones which still have the second *NcoI* site gave 3 digestion products (see table). M: marker (20 μl λ-*HindIII* DNA marker), ctrl: original pMAT plasmid with 2 *NcoI* and 1 *BamHI* sites. 6-11: plasmid DNA obtained after PCR mutagenisis. Clones 6, 7, 10 and 11 had only two fragments and were sent for sequencing.

Table 4.7 The HRV4 $2A^{pro}$ containing pMAT vector which is bearing a silent mutation at the second *NcoI* site gives 2 digestion products when cut with *NcoI* and *BamHI* restriction enzymes.

#	Ends	Coordinates	Length
1	*BamHI-NcoI*	837-386	2380 bp
2	*NcoI-BamHI*	387-836	450 bp

4.5 Expressions and purifications of HRV4 $2A^{pro}$

All HRV4 $2A^{pro}$ (clone 11 in figure 4.7 was ligated into pET3d) expressions were conducted using pET3d expression vector, in soluBL21 cell line of *E.coli*. The active proteinase expression was challenging due to aggregation tendencies of the protein (see figure 4.10 A lane: I). HRV4 His_6VP1_8 $2A^{pro}$ C110S and HRV4 $2A^{pro}$ C110S mutants were expressed and compared for yield (see table 4.2).

We expected the VP1 residues to enhance the solubility of the proteinase, as explained above (see chapter 4.2). We concluded that HRV4 His_6VP1_8 $2A^{pro}$ C110S was expressed at a higher level and therefore continued with it (see figure 4.8). Expression and purification results are detailed below (see also table 4.3).

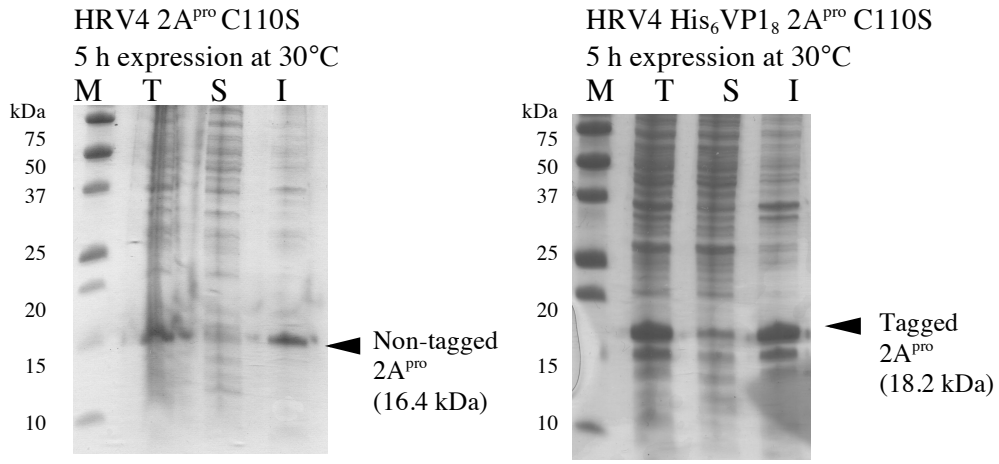

Figure 4.8 Total-soluble-insoluble proteins from the expression lysates were examined on 17.5 % SDS-PAGE gels for 2 different HRV4 $2A^{pro}$ constructs under the same expression conditions and in the same cell lines (soluBL21). Enhanced expression of soluble $2A^{pro}$ upon poly histidine tagged VP1/2A junction construct design is visible. **M:** marker (4 μl) **T:** total cell lysate (1 μl) **S:** soluble cell lysate (1 μl) **I:** insoluble cell lysate (1 μl).

We observed that HRV4 His_6VP1_8 $2A^{pro}$ C110S was still slightly active, as evidence by the second band appearing right underneath of the the overexpressed protein (see figure 4.8). The serine substituted cysteine position still carries a minor nucleophilic character; therefore, the proteinase appeared to be cleaving itself from the VP1 residues. To avoid this nucleophilic reaction, we decided to generate another mutation with an alanine substitution at this position. Both C110S and C110A substituted inactive HRV4 2A proteinases as well as the active version, all as His_6VP1_8 jointed $2A^{pro}$ constructs, were expressed in soluBL21 strain of *E.coli*. The expressions were performed as described above for HRV1A $2A^{pro}$ with changes only in the expression conditions. The induction time was shortened to 5 hours while the induction temperature was increased to 30°C after attempts to express overnight failed (data not shown). The same concentration of IPTG [0.15 mM] and $ZnCl_2$ [100 μM] were added at induction (see table 4.4).

HRV4 $2A^{pro}$

M G L G P R F G G V H T G N I K I M N Y H L M T H E D N L R L L T P M P E R D L A I V D A R A H G S E T V P Q C S C T S G V Y Y S R Y Y N K Y Y P V V C E K P T C V W I E G N N Y Y P S R Y Q Q G V M K G V G P A E P G D S G G I L R C V H G P I G L L T A G G C G F V C F A D I R M L E L F K A E Y Q Stop

R/K: 13, E/D: 13, pI: 6.94

HRV4 His_6VP1_8 $2A^{pro}$

M G H H H H H H T R E S I N T Y G L G P R F G G V H T G N I K I M N Y H L M T H E D N L R L L T P M P E R D L A I V D A R A H G S E T V P Q C S C T S G V Y Y S R Y Y N K Y Y P V V C E K P T C V W I E G N N Y Y P S R Y Q Q G V M K G V G P A E P G D C G G I L R C V H G P I G L L T A G G S G F V C F A D I R M L E L F K A E Y Q Stop

R/K: 14, E/D: 14, pI: 7.16

Figure 4.9 The positively and negatively charged amino acid residues at the working pH and the pI values of HRV1A $2A^{pro}$ from HRV4 $2A^{pro}$ and HRV4 His_6VP1_8 $2A^{pro}$ constructs.

Since the pI (isoelectric point) values between the HRV4 $2A^{pro}$ (also the $VP1_8His_6$ $2A^{pro}$) and HRV1A $2A^{pro}$ differed remarkably (compare tables 4.4 and 4.9), we adjusted the buffer pH (from 8.0 to 9.0). HRV4 His_6VP1_8 $2A^{pro}$ C110S was purified using the HisTrap affinity column and eluted in between 140 – 190 mM imidazole concentrations, where the single sharp peak was visible on the chromatogram (see figure 4.10 B). The HisTrap elution fractions of HRV4 His_6VP1_8 2A proteinase were rather pure. High concentrations of imidazole presence in the buffer usually triggers an aggregation in the case of leaked Ni^{2+} ions from the affinity column (Edsall et al., 1954). Therefore, corresponding HisTrap fractions were pooled together and dialyzed against buffer A pH 9.0. Size exclusion was performed on HiLoad® 2660 Superdex® S75 column in buffer A pH 9.0. Retention ml of HRV4 His_6VP1_8 $2A^{pro}$ C110S (theoretical molecular weight: 18.2 kDa) was measured as 226 ml (figure 4.10 C). However, HRV1A $2A^{pro}$ C106 was measured at 196 ml (theoretical molecular weight: 16.4 kDa). Hence, we could conclude that HRV4 $2A^{pro}$ was probably a monomer as it eluted later, even though its molecular mass was larger due to the tag. The protein could not be far concentrated after SEC, as it aggregated. The cleavage and binding experiments were conducted with slightly concentrated (0.62 mg/ml, figure 4.10 D) sample in buffer A pH 9.0. The purification results of HRV4 His_6VP1_8 $2A^{pro}$ C110S are shown below.

4.5.1 HRV4 His_6VP1_8 $2A^{pro}$ C110S

A

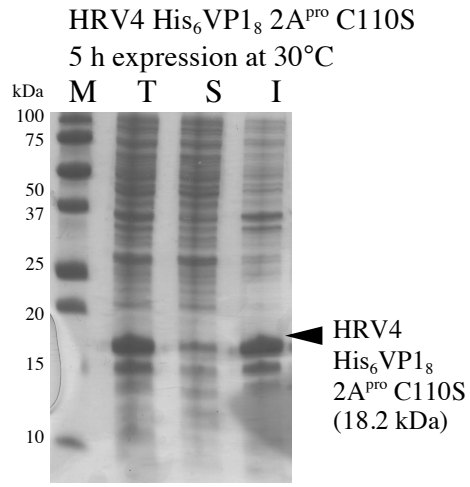

B

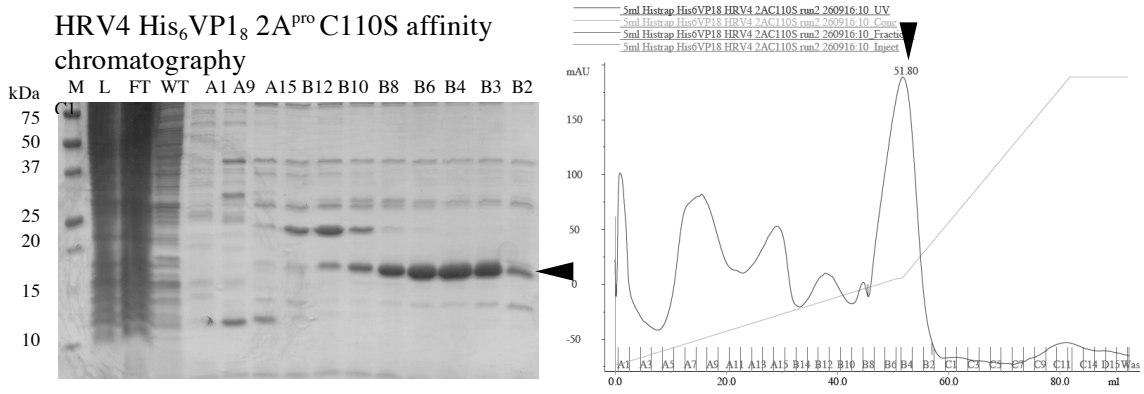

C

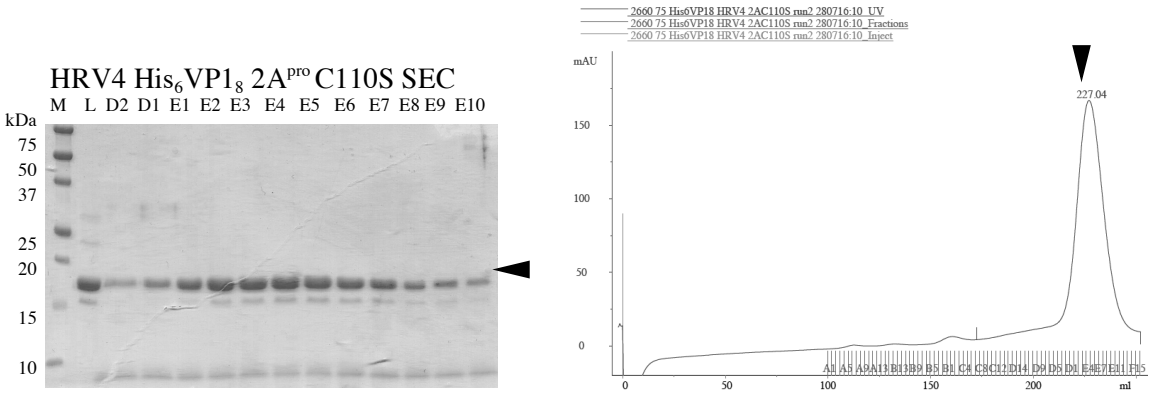

D

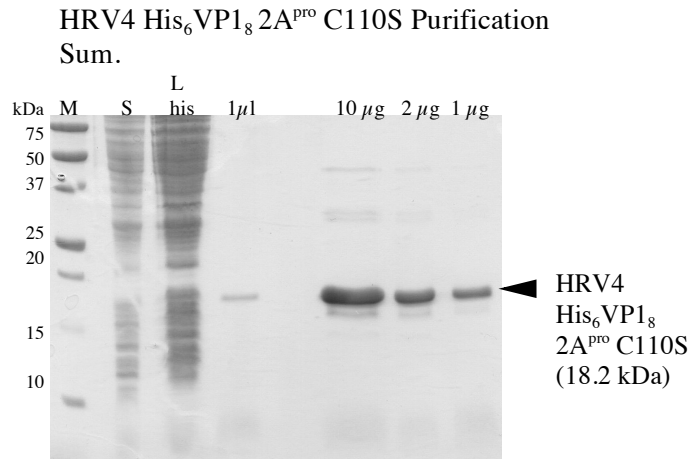

Figure 4.10 Purification of HRV4 His_6VP1_8 $2A^{pro}$ C110S (A) Total-soluble-insoluble proteins from the expression lysates were examined on 17.5 % SDS-PAGE gel. **M:** marker (4 μl) **T:** total (1 μl) **S:** soluble (1 μl) **I:** insoluble (1 μl). (B) 17.5 % SDS-PAGE gel of Histrap affinity chromatography and the chromatogram **M:** marker (2.5 μl) **L:** load (3 μl) **FT:** flow-through (8 μl) **WT:** wash-through (8μl). Elution of the $2A^{pro}$ at 140-190 mM imidazole is indicated with an arrow. (C) 17.5 % SDS-PAGE gel of SEC and the chromatogram **M:** marker (2.5 μl) **L:** load (3 μl). Pure $2A^{pro}$ UV peak at 227 ml is indicated with an arrow. 8 μl from fractions corresponding to indicated peaks were mixed with 2 μl 5 x Sample Buffer (8 μl). (D) 17.5 % SDS-PAGE gel of purification summary **M:** marker (4 μl) **S:** soluble cell lysate (1 μl) **L His:** Loaded sample onto affinity column (HisTrap) (3 μl) **1 μl:** 1 μl of the pure sample mixed with 7 μl dH_2O and 2 μl 5 x SDS sample buffer (10μl) **5 μg:** 5 μg of the sample was filled with dH_2O until 16 μl and then mixed with 4 μl 5 x SDS sample buffer (20 μl) **2 μg, 1 μg:** 2 μg and 1 μg of the sample were filled with dH_2O until 8 μl and mixed with 2 μl 5 x SDS sample buffer (10 μl).

The HRV4 His_6VP1_8 $2A^{pro}$ C110S identity was confirmed by MS with a nearly full sequence coverage. The results are given below in table 4.8 and the trypsin cleavage of the proteinase is shown in figure 4.11.

Table 4.8 Mass spectrometry results of HRV4 His_6VP1_8 $2A^{pro}$ C110S mutant.

	Sequence Coverage (%)	MS/MS count (# of peptide spectrum matches)	Intensity (summed peptide intensities)	Peptides (number)	Molecular weight (kDa)
HRV4 His_6VP1_8 $2A^{pro}$ C110S	94.4	486	5.5×10^{10}	17	18.09

HRV4 His_6VP1_8 $2A^{pro}$ C110S

M G H H H H H H T R E S I N T Y G L G P R F G G V H T G N I K I M N Y H L M T H E D N L
R L L T P M P E R D L A I V D A R A H G S E T V P Q C S C T S G V Y Y S R Y Y N K Y Y P
V V C E K P T C V W I E G N N Y Y P S R Y Q Q G V M K G V G P A E P G D S G G I L R C
V H G P I G L L T A G G S G F V C F A D I R M L E L F K A E Y Q Stop

Figure 4.11 The cleavage sites of trypsin enzyme are highlighted within the HRV4 His_6VP1_8 $2A^{pro}$ C110S sequence.

4.5.2 HRV4 His_6VP1_8 $2A^{pro}$ C110A

The HRV4 His_6VP1_8 $2A^{pro}$ C110A was used to establish a purification protocol for active HRV4 His_6VP1_8 $2A^{pro}$ (see chapter 4.3.3). The C110A mutant was expressed in soluBL21 strain of *E.coli* (see table 4.2), as explained above for HRV4 His_6VP1_8 $2A^{pro}$ C110S (see figure 4.12 A). The soluble cell lysate was treated with ammonium sulfate as described previously for HRV1A $2A^{pro}$ (see also table 4.3 and table 4.4). We kept both the 20 % and 40 % $(NH_4)_2SO_4$ containing samples and dialyzed them both against buffer A pH 9.0 to remove the excess ammonium sulfate. First, HRV4 His_6VP1_8 $2A^{pro}$ C110A which was salted out with 40 % $(NH_4)_2SO_4$ was loaded on anion exchange column and elution fractions were checked via SDS-PAGE and western blot. Unfortunately, only a minor amount of the proteinase was collected in wash-through, which we confirmed via western blot (see figure 4.12 B). We decided not to continue further with purification of this HRV4 His_6VP1_8 $2A^{pro}$ C110A sample.

Then, we loaded HRV4 His_6VP1_8 $2A^{pro}$ C110A sample which was salted out in 20 % of $(NH_4)_2SO_4$ onto the anion exchange column (see figure 4.12 C). The protein was again collected in flow-through and wash-through yet, western blot results indicated the amount of protein eluted was much larger. Probably the equal amount of negatively and positively charged amino acid residues at pH 9.0 was the reason for sample not binding onto positively charged resin (see figure 4.12 B & C).

After analyzing the SDS-PAGE and western blot, we understood that 20 % of $(NH_4)_2SO_4$ was enough to salt out HRV4 His_6VP1_8 $2A^{pro}$ C110A (see figure 4.12 C) The western blots show almost all HRV4 His_6VP1_8 $2A^{pro}$ C110A were already precipitated in the first step (20 %) of $(NH_4)_2SO_4$ precipitation (data not shown). Collected proteins from flow-through and wash-through (figure 4.12 C) were loaded onto HisTrap column. HRV4 His_6VP1_8 $2A^{pro}$ C110A was eluted quite pure from the affinity column at 140-164 mM imidazole, and subsequently slightly concentrated until 1.26 mg/ml (see figure 4.12 E). The yield was 2.4 mg of protein from 6 liters of expression (0.4 mg/L). Purification results of HRV4 His_6VP1_8 $2A^{pro}$ C110A are shown below.

A

HRV4 His_6VP1_8 $2A^{pro}$ C110A
4 h expression at 30°C

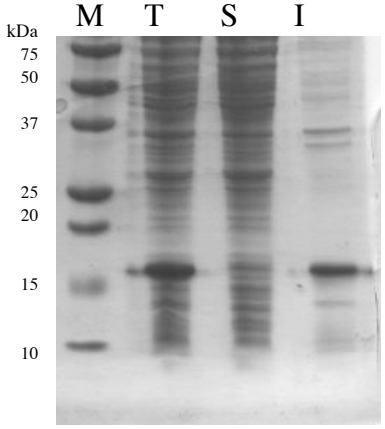

HRV4
His_6VP1_8 $2A^{pro}$
C110A
(18.2 kDa)

B

HRV4 His_6VP1_8 $2A^{pro}$ C110A anion exchange chromatography (salted out with 40 %)

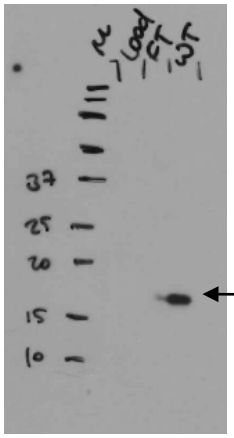

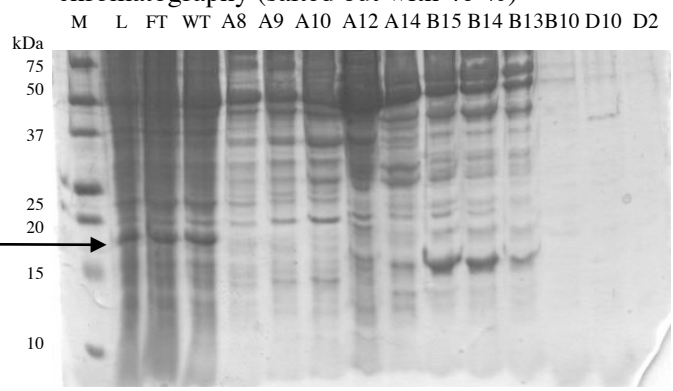

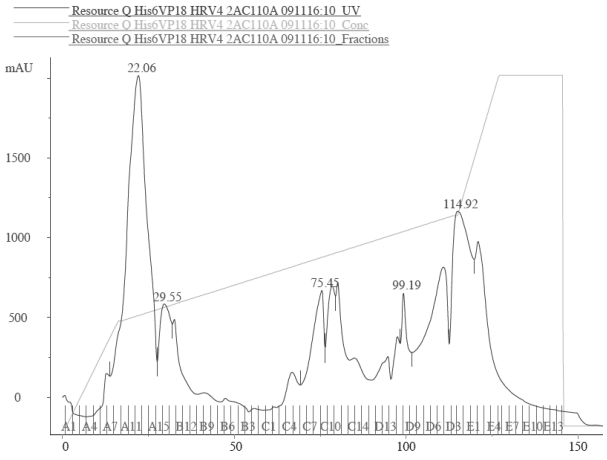

C

HRV4 His_6VP1_8 $2A^{pro}$ C110A anion exchange chromatography (salted out with 20 %)

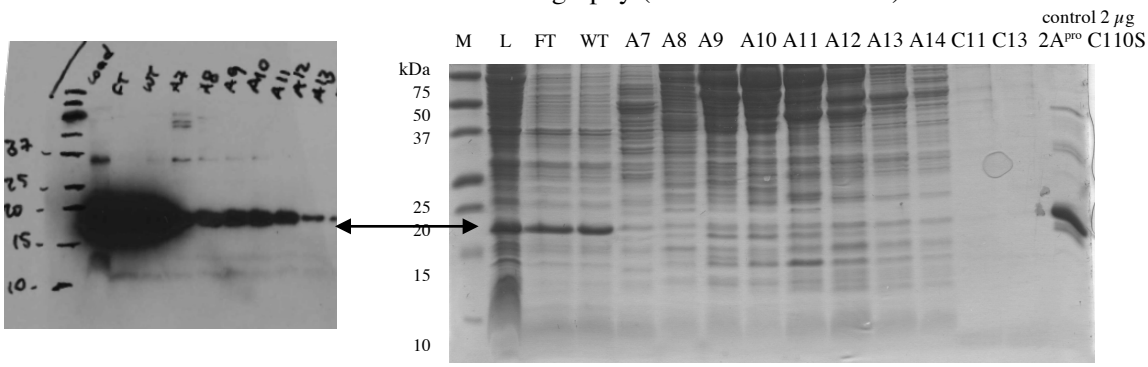

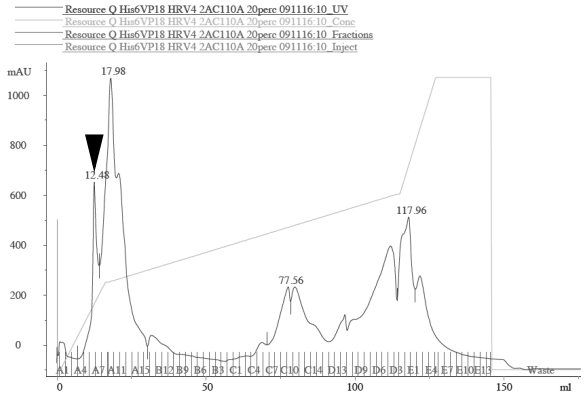

D

HRV4 His_6VP1_8 $2A^{pro}$ C110A affinity chromatography (FT & WT were pooled together from anion exchange chromatography)

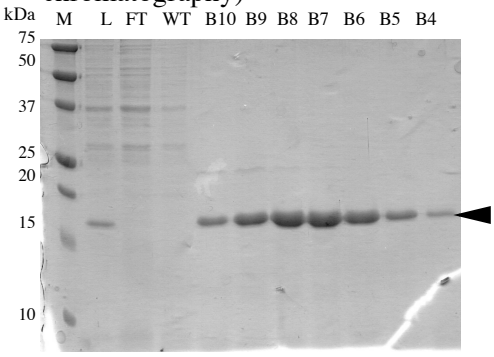

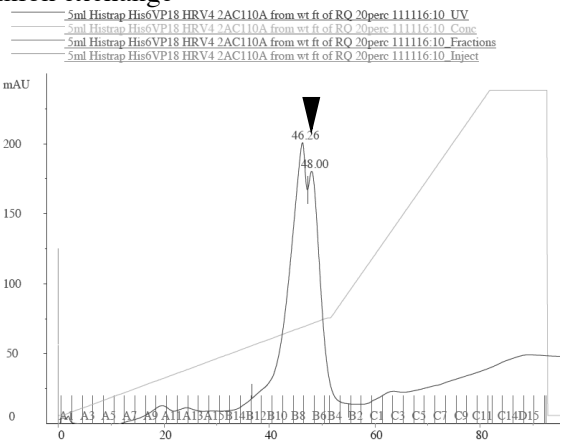

E

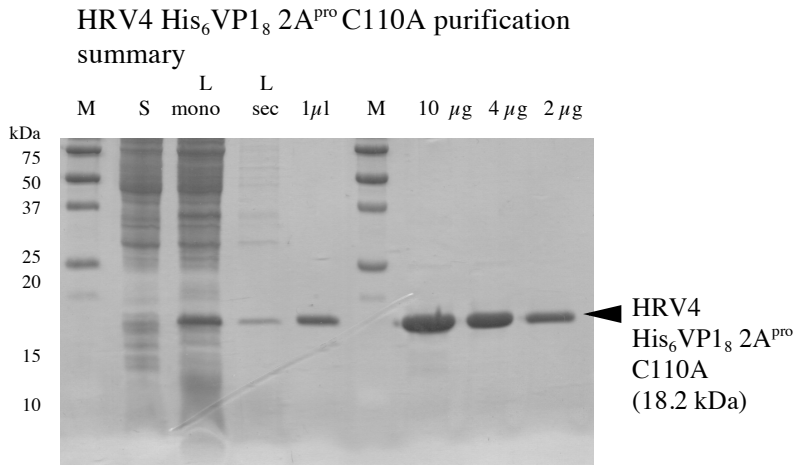

Figure 4.12 Purification of HRV4 His6VP18 $2A^{pro}$ C110A (A) Total-soluble-insoluble proteins from the expression lysates examined on 17.5 % SDS-PAGE gel. **M:** marker (4 μl) **T:** total (1 μl) **S:** soluble (1 μl) **I:** insoluble (1 μl). (B) 17.5 % SDS-PAGE gel of anion exchange chromatography, western blot and the chromatogram from the 40 % $NH_4(SO_4)_2$-salted-out HRV4 His_6VP1_8 $2A^{pro}$ **M:** marker (2.5 μl) **L:** load (3 μl) **FT:** flow-through (8 μl) **WT:** wash-through (8μl). The protein was not bound onto column hence it was collected in FT and WT. (C) 17.5 % SDS-PAGE gel of anion exchange chromatography, western blot and the chromatogram from the 20 % $NH_4(SO_4)_2$-salted-out HRV4 His_6VP1_8 $2A^{pro}$ **M:** marker (2.5 μl) **L:** load (3 μl) **FT:** flow-through (8 μl) **WT:** wash-through (8μl). The protein slightly bound onto column. The WT fraction was kept. (D) 17.5 % SDS-PAGE gel of Histrap affinity chromatography and the chromatogram **M:** marker (2.5 μl) **L:** load (3 μl). Pure $2A^{pro}$ UV peak at 140-164 mM imidazole is indicated with an arrow. 8 μl from fractions corresponding to indicated peaks were mixed with 2 μl 5 x Sample Buffer (8 μl) (E) 17.5 % SDS-PAGE gel of purification summary **M:** marker (4 μl) **S:** soluble cell lysate (1 μl) **L MonoQ:** Loaded sample onto anion exchange column (MonoQ) (3 μl) **L His:** Loaded sample onto affinity column (HisTrap) (3 μl) **1 μl:** 1 μl of the pure sample mixed with 7 μl dH_2O and 2 μl 5 x SDS sample buffer (10μl) **5 μg:** 5 μg of the sample was filled with dH_2O until 16 μl and then mixed with 4 μl 5 x SDS sample buffer (20 μl) **2 μg, 1 μg:** 2 μg and 1 μg of the sample were filled with dH_2O until 8 μl and mixed with 2 μl 5 x SDS sample buffer (10 μl).

The HRV4 His_6VP1_8 $2A^{pro}$ C110A identity was confirmed by MS with an almost complete sequence coverage. However, the peptide length parameter that was used during analyses excluded two peptides with 6 a.a. (C-terminal MLELFK) and 5 a.a. (N-terminal GLGPR) long (see figure 4.13). Later, the C-terminal MLELFK was manually found in the chromatogram. The N-terminal GLGPR was detected in a precursor single charged form and was not fragmented. Therefore, these two peptides were not included in the % calculations. The results are given below in table 4.9.

Table 4.9 Mass spectrometry results of HRV4 His_6VP1_8 $2A^{pro}$ C110A.

	Sequence Coverage (%)	MS/MS count (# of peptide spectrum matches)	Intensity (summed peptide intensities)	Peptides (number)
HRV4 His_6VP1_8 $2A^{pro}$ C110S	88.3	48	8.4×10^{10}	17

HRV4 His_6VP1_8 $2A^{pro}$ C110A

M G H H H H H H T R E S I N T Y G L G P R F G G V H T G N I K I M N Y H L M T H E D N L
R L L T P M P E R D L A I V D A R A H G S E T V P Q C S C T S G V Y Y S R Y Y N K Y Y P
V V C E K P T C V W I E G N N Y Y P S R Y Q Q G V M K G V G P A E P G D A G G I L R C
V H G P I G L L T A G G S G F V C F A D I R M L E L F K A E Y Q Stop

Figure 4.13 The cleavage sites of trypsin enzyme are highlighted within the HRV4 His_6VP1_8 $2A^{pro}$ C110A sequence.

4.5.3 HRV4 His_6VP1_8 $2A^{pro}$ active

Unfortunately, the active HRV4 His_6VP1_8 $2A^{pro}$ could not be purified from histidine affinity column. As the catalytic cysteine was present, the proteinase cleaves itself from the N- terminal VP1 junction and loses its hexahistidine tag. We tried different approaches for purification of this protein (see table 4.3). In order to purify HRV4 His_6VP1_8 $2A^{pro}$ active without using the Histrap affinity column, we aimed to perform ammonium sulfate precipitation followed by anion exchange chromatography. The anion exchange column could not purify the protein. Nevertheless, we tried the following purification approach. The active proteinase was expressed as explained above for C110A mutant (see chapter 4.3.2) (see figure 4.14 A). Later, it was salted out with 40 % $(NH_4)_2SO_4$ and dialyzed in buffer A pH 9.0 as described previously. Then, it was loaded on anion exchange column to elute with an increasing NaCl gradient. Yet, the proteinase was collected at flow-through and was-through, without binding onto column (see figure 4.14 B). Then, we decided to load 10 ml of the wash-through onto size exclusion column. Luckily, the unspecific proteins were removed and the active HRV4 His_6VP1_8 2A proteinase was eluted as a single peak at 218 ml retention volume (see figure 4.14 C). Finally, HRV4 His_6VP1_8 $2A^{pro}$ active was slightly concentrated to 0.17 mg/ml (see figure 4.14 D). Total purified active proteinase amount was ~ 400 μg from 6 liters of expression medium. The calculated yield is 0.07 mg/L.

A

HRV4 His_6VP1_8 $2A^{pro}$ active 4 h expression at 30°C

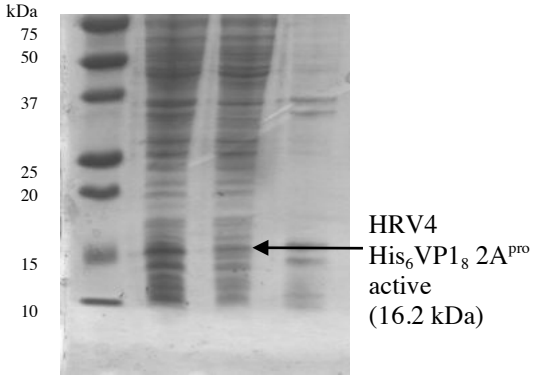

B

His_6VP1_8 HRV4 $2A^{pro}$ active anion exchange chromatography (salted out with 40 %)

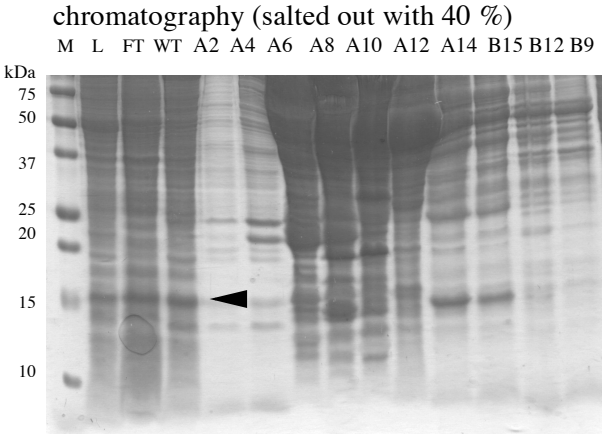

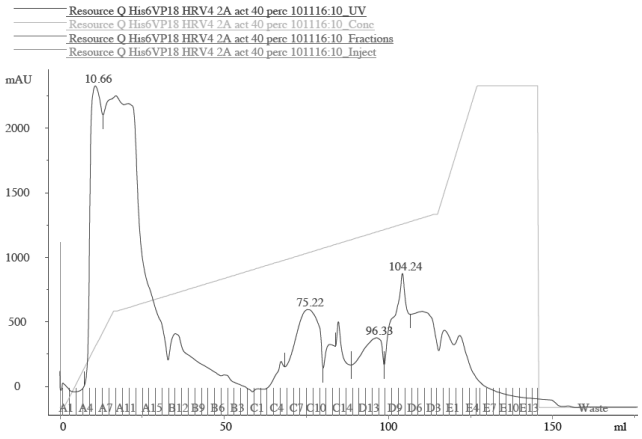

C

His_6VP1_8 HRV4 $2A^{pro}$ active SEC (salted out with 40 %)

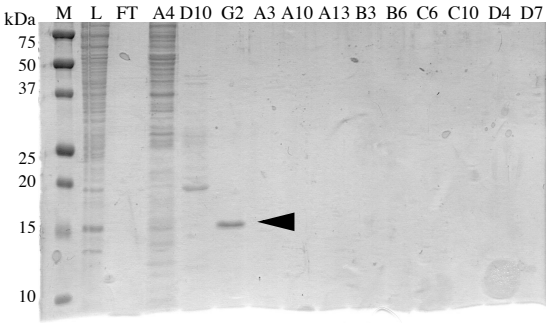

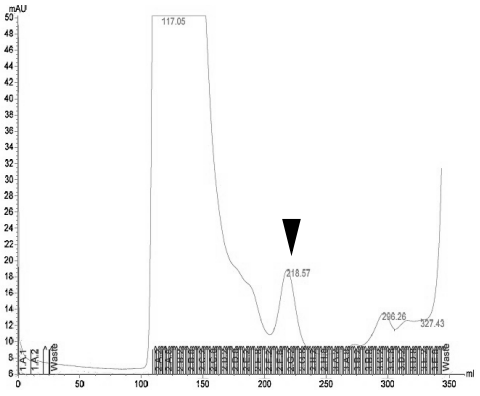

D

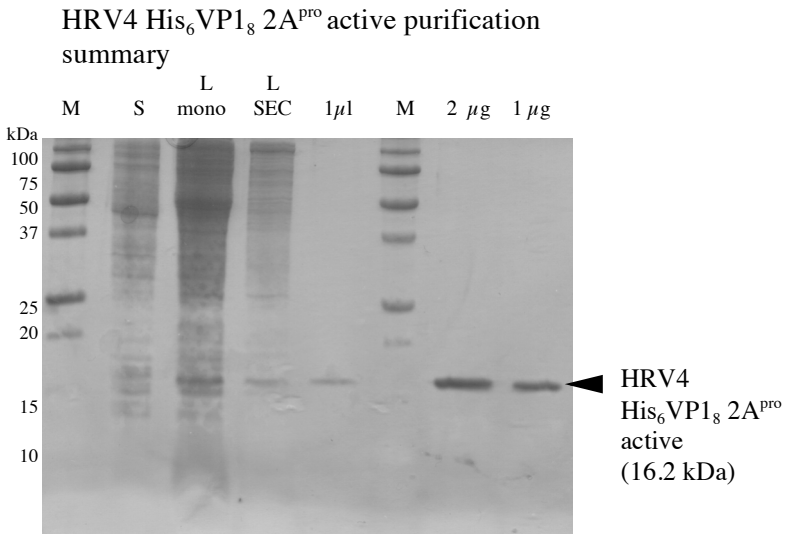

Figure 4.14 Purification of HRV4 His_6VP1_8 $2A^{pro}$ active (A) Total-soluble-insoluble proteins from the expression lysates were examined on 17.5 % SDS-PAGE gel. **M:** marker (4 μl) **T:** total (1 μl) **S:** soluble (1 μl) **I:** insoluble (1 μl). (B) 17.5 % SDS-PAGE gel of anion exchange chromatography and the chromatogram from the 40 %-$(NH_4)_2SO_4$-salted-out HRV4 His_6VP1_8 $2A^{pro}$ **M:** marker (2.5 μl) **L:** load (3 μl) **FT:** flow-through (8 μl) **WT:** wash-through (8μl). The protein was not bound onto column. Therefore, it was collected in FT and WT. The WT fraction was kept. (C) 17.5 % SDS-PAGE gel of SEC chromatography and the chromatogram **M:** marker (2.5 μl) **L:** load (3 μl) **FT:** flow-through (8 μl) **WT:** wash-through (8μl). Pure $2A^{pro}$ UV peak at 218 ml is indicated with an arrow **M:** marker (2.5 μl) **L:** load (3 μl). 8 μl from fractions corresponding to indicated peaks were mixed with 2 μl 5 x Sample Buffer (8 μl) (D) 17.5 % SDS-PAGE gel of purification summary **M:** marker (4 μl) **S:** soluble cell lysate (1 μl) **L mono:** Loaded sample onto anion exchange column (MonoQ) (3 μl) **L SEC:** Loaded sample onto SEC column (3 μl) **1 μl:** 1 μl of the pure sample mixed with 7 μl dH_2O and 2 μl 5 x SDS sample buffer (10μl) **5 μg:** 5 μg of the sample was filled with dH_2O until 16 μl and then mixed with 4 μl 5 x SDS sample buffer (20 μl) **2 μg, 1 μg:** 2 μg and 1 μg of the sample were filled with dH_2O until 8 μl and mixed with 2 μl 5 x SDS sample buffer (10 μl).

The HRV4 His_6VP1_8 $2A^{pro}$ was confirmed by MS with a good sequence coverage. Active proteinase self processing results in an N-terminal peptide MGHHHHHHTR. However, it was not found in the analysis, since highly charged His-tag corresponds to an undetectable m/z value. Unfortunately, results showed that the wild-type active proteinase was contaminated with C110A mutant. The peptide signals within the nucleophilic $\mathbf{Cys_{110}}$ region was present for both the active (GVGPAEPGD$\mathbf{C_{110}}$GGILR) and the inactive (GVGPAEPGD$\mathbf{A_{110}}$GGILR) (see figure 4.15). When the corresponding peak areas were compared, the contamination ratio was calculated at 30:1. This situation is considered for the cleavage experiments that were conducted with this proteinase. The results are given below in table 4.6.

Table 4.10 Mass spectrometry results of HRV4 His_6VP1_8 $2A^{pro}$.

	Sequence Coverage (%)	MS/MS count (# of peptide spectrum matches)	Intensity (summed peptide intensities)	Intensity of active site-covering peptide
HRV4 His_6VP1_8 $2A^{pro}$	87.1	398	4.4×10^{10}	4.70×10^{7}
HRV4 His_6VP1_8 $2A^{pro}$ C110A (contaminant)	87.1	8	3.9×10^{8}	1.45×10^{9}

HRV4 His_6VP1_8 $2A^{pro}$

M G H H H H H H T R E S I N T Y G L G P R F G G V H T G N I K I M N Y H L M T H E D N L R L L T P M P E R D L A I V D A R A H G S E T V P Q C S C T S G V Y Y S R Y Y N K Y Y P V V C E K P T C V W I E G N N Y Y P S R Y Q Q G V M K G V G P A E P G D C G G I L R C V H G P I G L L T A G G S G F V C F A D I R M L E L F K A E Y Q Stop

Figure 4.15 The cleavage sites of trypsin enzyme are highlighted within the HRV4 His_6VP1_8 $2A^{pro}$ sequence. Underlined sequence was compared for intensities for the contamination.

4.6 Interaction studies with eIF4E/$eIF4G_{551-745}$

4.6.1 Cleavage assay with HRV1A $2A^{pro}$

Picornaviral $2A^{pro}$ cleave many host cell proteins, such as eukaryotic initiation factor 4G (eIF4GI and eIF4GII). The assay was performed by following the protocol for HRV2 $2A^{pro}$ cleavage (Aumayr et al., 2015). A short and well expressed $eIF4GII_{551-745}$ construct was kindly provided by Martina Aumayr (residues in between 551-745 covering eIF4E binding site and the $2A^{pro}$ cleavage site). The purified $eIF4GII_{551-745}$ and full length purified murine eIF4E were used to perform cleavage assays.

Proteolytically active HRV1A $2A^{pro}$ with Cys at position 106 was used in the cleavage assays to understand the enzyme activity. *In vitro* cleavage experiments were performed at 37°C for 90 minutes and analyzed on 17.5 % SDS-PAGE gels (see figure 4.16). Experiments clearly show the enhanced cleavage of the $eIF4GII_{551-745}$ in the presence of eIF4E (figure 4.16 B). Naturally, N-terminal and C-terminal cleavage products and the additionally further cleaved N-terminal cleavage product could be seen when more $2A^{pro}$ was used (figure 4.16 A). Almost immediate complete cleavage of $eIF4GII_{551-745}$ was observed when 50 ng of $2A^{pro}$ was incubated with both of the substrates (figure 4.16 A). Half of the $eIF4GII_{551-745}$ (5.3 μM) was cleaved after an incubation for 30' with 10 ng proteinase (76 nM) (figure 4.10 B). No cleavage product was visible when substrates were incubated with 5 ng proteinase (38 nM), and no 50 % cleavage of $eIF4GII_{551-745}$ was reached within 90 minutes, not even in the presence of eIF4E

(figure 4.16 C). When 1 ng $2A^{pro}$ was used, no cleavage was observed (figure 4.16 D). In the absence of eIF4E, less dramatic $eIF4GII_{551-745}$ (5.3 μM) cleavage could only be seen after 30' when using 50 ng proteinase (380 nM) (see Figure 4.16 A).

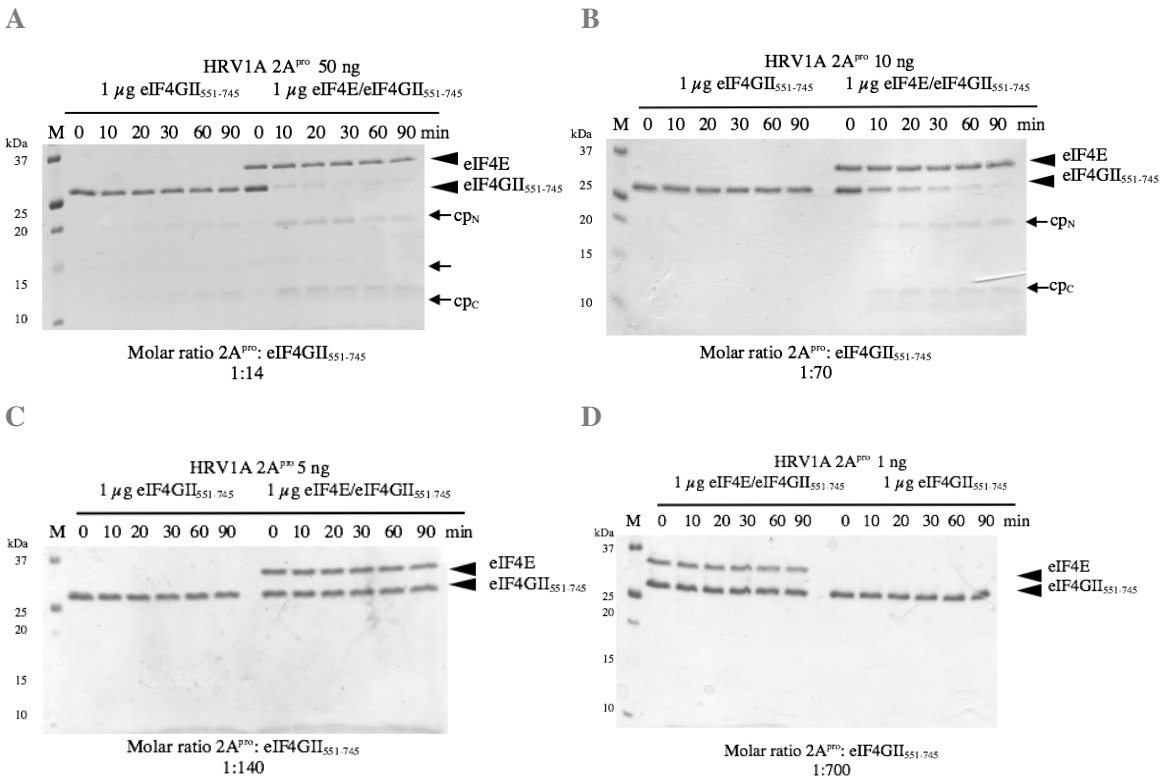

Figure 4.16 *in vitro* cleavage of $eIF4GII_{551-745}$ and eIF4E by HRV1A $2A^{pro}$. 50 ng, 10 ng, 5 ng, 1 ng of the proteinase incubated with 1 μg of $eIF4GII_{551-745}$ and 1 μg eIF4E/$eIF4GII_{551-745}$ in figures A, B, C and D, respectively.

4.6.2 Binding studies with HRV1A $2A^{pro}$ C106A using analytical SEC

Cleavage assays raised the question why eIF4E presence enhances the $eIF4GII_{551-745}$ cleavage. Hence, we wanted to investigate the formation of binary complexes between HRV1A $2A^{pro}$/eIF4E, HRV1A $2A^{pro}$/$eIF4GII_{551-745}$, and finally the ternary complex between HRV1A $2A^{pro}$/eIF4E/$eIF4GII_{551-745}$.

Binding studies were conducted using inactive HRV1A $2A^{pro}$ bearing an alanine substitution at the catalytic site. Proteins were, either singly or in complexes, loaded onto HiLoad® 16/60 Superdex® 200 prep grade column with an internal standard aprotinin (6.5 kDa). First, single proteins were run with aprotinin. The complexes were always incubated overnight and for 10' for comparison (see chapter 3.5.2 for detailed analytical SEC method). All experiments were run in 1 ml/min flow rate with Hepes buffer. Overlays of the single proteins, binary complexes and the ternary complex were adjusted based on the internal standard and are explained in figure 4.17 A. eIF4E can be seen at 89 ml retention volume, indicated as green curve. HRV1A $2A^{pro}$ was eluted at 96 ml retention volume (blue curve). When HRV1A $2A^{pro}$ C106 was incubated with eIF4E, the $2A^{pro}$ peak was decreased and a shifted peak

appeared at 86 ml retention volume (gray curve), the stable binary complex (see figure 4.17 B lane: 1). The single eIF4GII$_{551-745}$ peak (orange curve) was eluted at 79 ml retention volume.

After the incubation of eIF4E/eIF4GII$_{551-745}$ translation initiation factors, a stable binary complex formed (see figure 4.17 C lane: 1). This complex formation, as published in Amumayr et al. 2015, was eluted from the column at 76 ml (light green curve) (figure 4.17 A). However, when alone eIF4GII$_{551-745}$ was incubated with inactive HRV1A 2A^{pro}, no complex formation was observed from the chromatograms. The incubation of HRV1A 2A^{pro} with eIF4GII$_{551-745}$ is indicated as brown curve; we see two individual protein peaks at almost same retention volumes. When the SDS-PAGE gel was analyzed, the peak at 78 ml retention volume was found to be only eIF4GII$_{551-745}$ alone (data not shown). When HRV1A 2A^{pro} was incubated with initiation factors, a ternary complex peak was formed at 65 ml retention volume (pink curve). Single protein peak heights were decreased when forming the ternary complex. Analysis of the ternary complex peak on SDS-PAGE gel showed that all three proteins were present (see figure 4.17 D lanes: 1, 2).

A

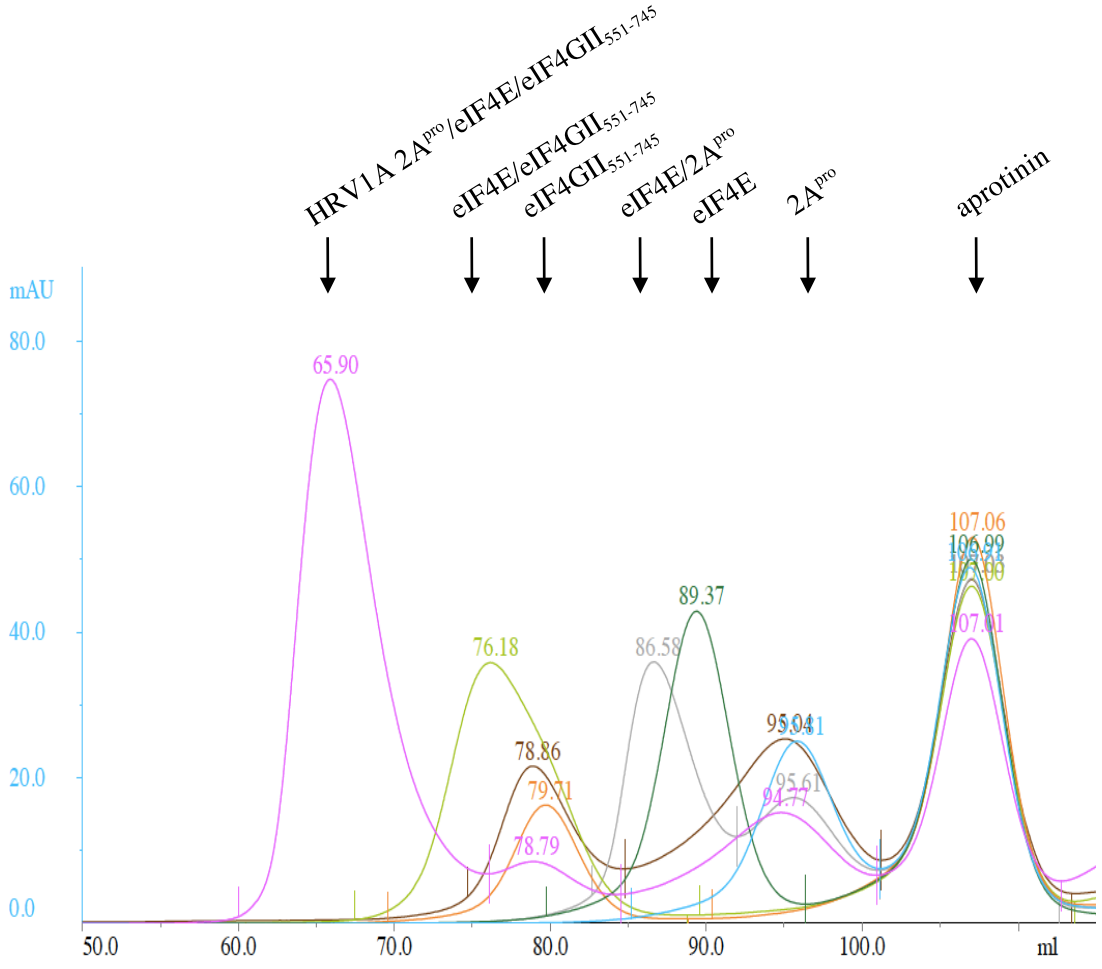

B

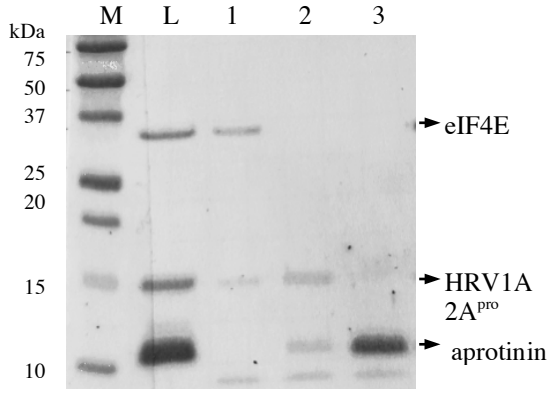

HRV1A 2A^{pro} C106A binding studies binary complex with eIF4E

C

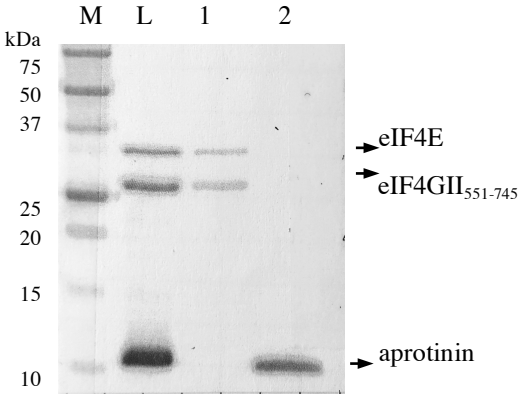

Binding studies binary complex of eIF4E/eIF4GII$_{551-745}$

D

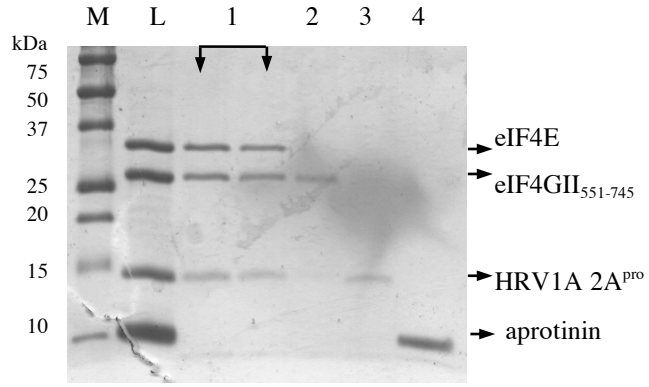

HRV1A 2A^{pro} C106A binding studies ternary complex

Figure 4.17 Individual proteins and complexes were loaded onto HiLoad® 16/60 Superdex® 200 pg column together with an internal standard aprotinin (6.5 kDa). For complex formation, 0.5 mg of each individual protein were incubated together at 4°C overnight under gentle shaking. Prior to loading onto column 1 mg of aprotinin and assay buffer were added in 1 ml total volume. (A) Superimposed chromatograms are distinctive by colors: eIF4GII$_{551-745}$ orange, eIF4E green, HRV1A 2A^{pro} C106A blue. Color code for the binary complexes: eIF4E/eIF4GII$_{551-745}$ light green, HRV1A 2A^{pro}/eIF4E gray, HRV1A 2A^{pro}/eIF4GII$_{551-745}$ brown. Ternary complex composed of HRV1A 2A^{pro}/eIF4E/eIF4GII$_{551-745}$ chromatogram is showed in pink. (B) Overnight incubated HRV1A 2A^{pro} C106A and eIF4E were analyzed on 17.5 % SDS-PAGE gel. **M:** marker (4 μl) **L:** load (3 μl) **1:** HRV1A 2A^{pro} C106A and eIF4E binary complex (8μl) **2:** HRV1A 2A^{pro} C106A came together with aprotinin (8 μl) **3:** aprotinin (8μl)) (C) Overnight incubated eIF4E and eIF4GII$_{551-745}$ were analyzed on 17.5 % SDS-PAGE gel. **M:** marker (4 μl) **L:** load (3 μl) **1:** eIF4E/eIF4GII$_{551-745}$ binary complex (8μl) **2:** aprotinin (8μl)) (D) Overnight incubated HRV1A 2A^{pro} C106A, eIF4E, and eIF4GII$_{551-745}$ were analyzed on 17.5 % SDS-PAGE gel. **M:** marker (4 μl) **L:** load (3 μl) **1:** ternary complex of 2A^{pro}/eIF4E/eIF4GII$_{551-745}$ (8μl) in two lanes from the middle and the end of the peak **2:** excess eIF4GII$_{551-745}$ (8 μl) **3:** excess HRV1A 2A^{pro} C106A (8 μl) **4:** aprotinin (8μl)). 8 μl from fractions corresponding to indicated peaks were mixed with 2 μl 5 x Sample Buffer (8 μl).

4.6.3 Cleavage assay with HRV4 His_6VP1_8 $2A^{pro}$ active

Cleavage assays were performed as described above for HRV1A $2A^{pro}$. Active HRV4 His_6VP1_8 $2A^{pro}$ with Cys at position 110 was used in the cleavage assays to examine the enzyme activity. *In vitro* cleavage experiments were performed at 37°C for 90 minutes and analyzed on 17.5 % SDS-PAGE gels. Experiments were conducted with 10 ng, 70 ng and 100 ng of the active proteinase among with either 1 μg of $eIF4GII_{551\text{-}745}$ (5.3 μM) or 1 μg of each $eIF4GII_{551\text{-}745}$ and eIF4E. However, MS results from this proteinase revealed a contamination with the C110A inactive mutant at a ~30:1 rate (see chapter 4.5.3). This bias does not misinterpret the results dramatically; therefore, we can still present them. At the end of 90 minutes, no cleavage was observed at any concentration. Cleavage assays using 770 nM (100 ng), 540 nM (70 ng), and 77 nM (10 ng) $2A^{pro}$ are shown below in figures 4.18 A, B, and C, respectively.

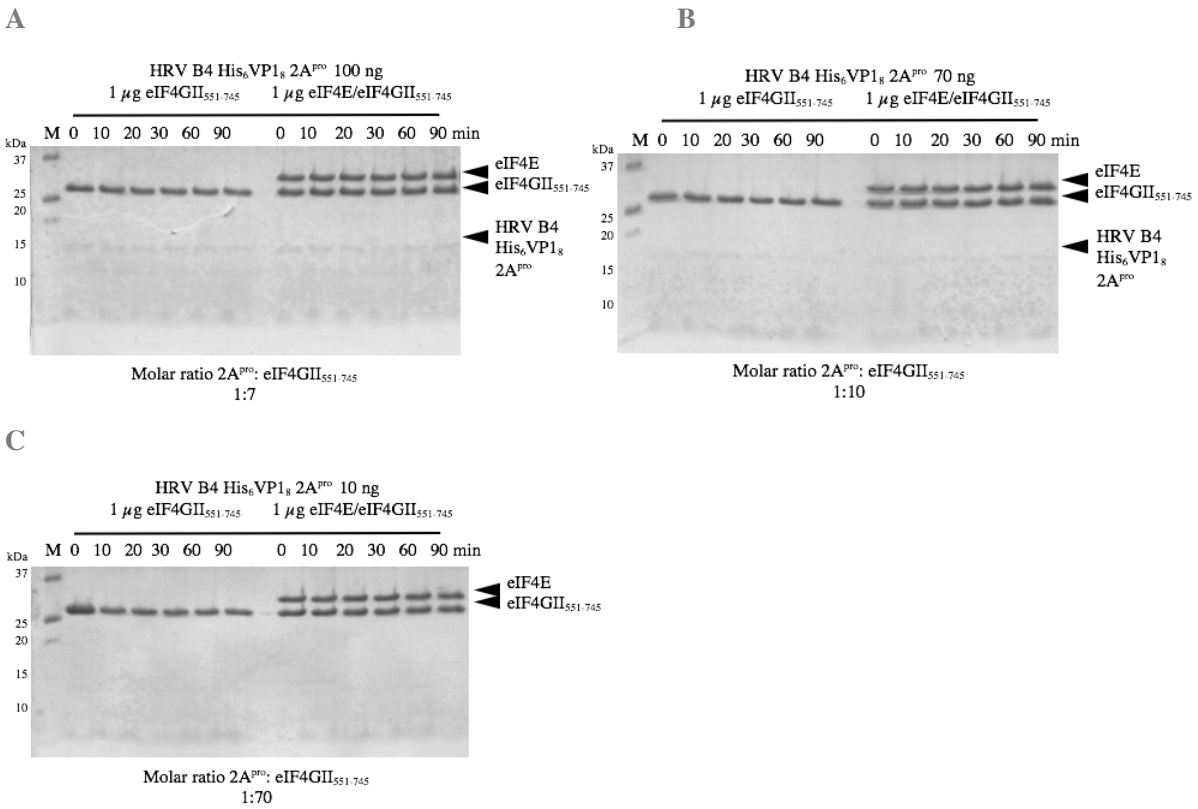

Figure 4.18 *in vitro* cleavage of $eIF4GII_{551\text{-}745}$ and eIF4E by HRV4 His_6VP1_8 $2A^{pro}$. 100 ng, 70 ng, and 10 ng of the proteinase incubated with 1 μg of $eIF4GII_{551\text{-}745}$ and 1 μg eIF4E/$eIF4GII_{551\text{-}745}$ in figures A, B, and C, respectively.

4.6.4 HRV4 His_6VP1_8 $2A^{pro}$ C110S to translation initiation factors

HRV4 His_6VP1_8 $2A^{pro}$ C110S is stable at pH 9.0; therefore, we conducted both the preparative as well the analytical SEC in tris containing buffers (buffer A) at pH 9.0. Therefore, all proteins ($2A^{pro}$, eIF4E, $eIF4GII_{551\text{-}745}$) were dialyzed in assay buffer and the experimental approach was performed as described above, using the same internal standard. Under these circumstances, the binding studies were

of course not directly comparable with HRV1A $2A^{pro}$ C106A which was performed in Hepes buffer pH 7.4. However, we repeated the HRV1A experiments in buffer A pH 9.0 to have a better comparison.

According to our findings, HRV4 proteinase was unable to form a complex with either eIF4E or with eIF4E/$eIF4GII_{551-745}$, when proteins were incubated overnight in buffer A pH 9.0. When eIF4E and $2A^{pro}$ incubation (gray curve) was overlaid with the eIF4E-only chromatogram (green curve), we observed that eIF4E peak at 86 ml was not shifted upon the addition of $2A^{pro}$ (see figure 4.19 A). SDS-PAGE showed that eIF4E and HRV4 His_6VP1_8 $2A^{pro}$ were eluted separately (see figure 4.19 B lanes: 1, 2). In the same way, we observed no ternary complex formation (pink curve) when all three proteins were incubated overnight. The SDS-PAGE designated that the peak at 73 ml comes from the binary complex formation between eIF4E and $eIF4GII_{551-745}$ (figure 4.19 C lane: 1). For this reason, we tested the ternary complex formation with HRV1A $2A^{pro}$ in buffer A pH 9.0, which was formed (see chapter 4.4.2). We saw that ternary complex formation with HRV1A 2A was not disturbed by buffer alteration (see figure 4.19 D lane: 1). Thus, we demonstrated that solely the buffer was responsible for the failure of complex formation. Moreover, we conducted another experiment where HRV4 His_6VP1_8 $2A^{pro}$ C110S was incubated with eIF4E/$eIF4GII_{551-745}$ overnight in Hepes buffer at pH 7.4 (data not shown). After the centrifugation prior loading onto column, there was a remarkably big pellet which might have occurred because of the low solubility features of HRV4 His_6VP1_8 $2A^{pro}$ at a pH very close to its isoelectric point. Yet, we could still observe individual $2A^{pro}$ peak, eIF4E/$eIF4GII_{551-745}$ binary complex peak, and internal standard peak distinctly without a ternary complex formation.

A

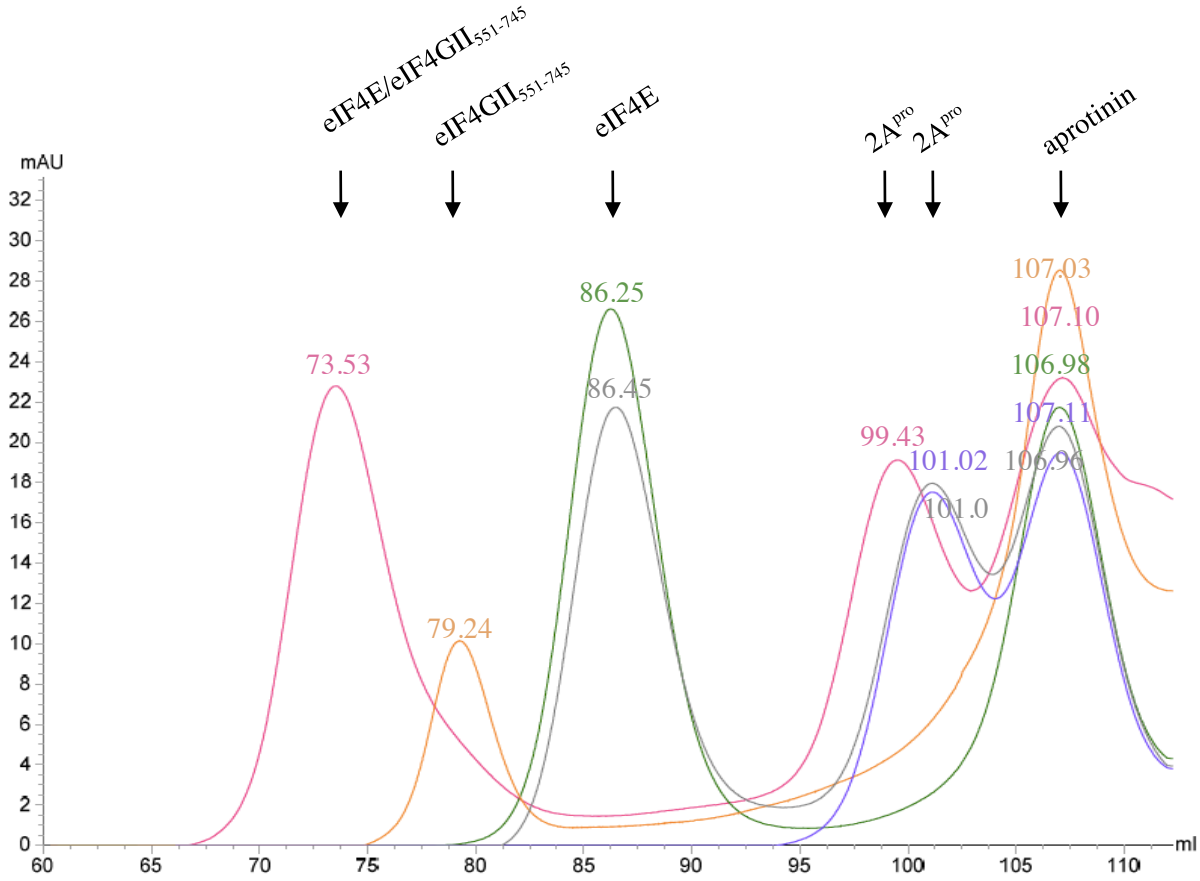

B

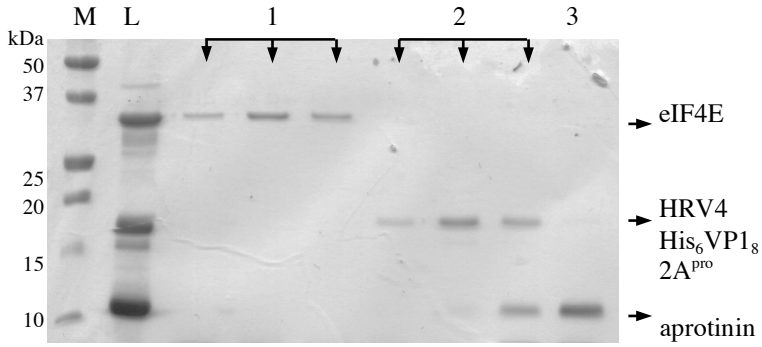

HRV4 His_6VP1_8 $2A^{pro}$ C110S binding studies Binary incubation with eIF4E

C

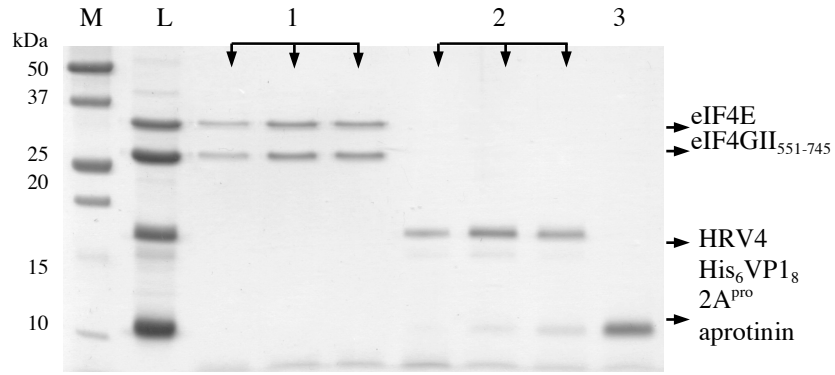

HRV4 His_6VP1_8 $2A^{pro}$ C110S binding studies ternary incubation with eIF4E and $eIF4GII_{551-745}$

D

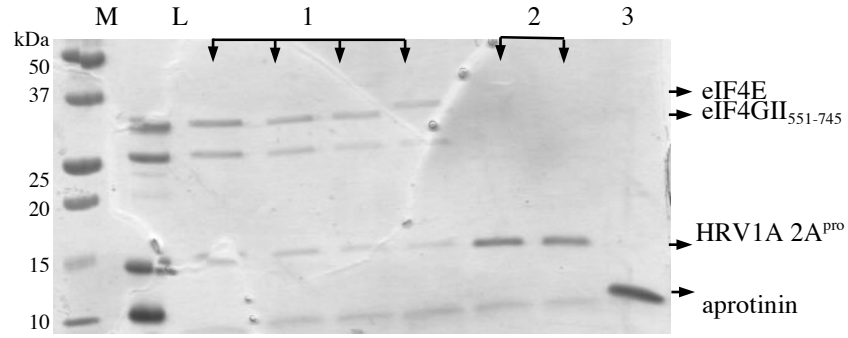

HRV1A $2A^{pro}$ C106A binding studies ternary complex with eIF4E and $eIF4GII_{551-745}$ in buffer A pH 9.0

Figure 4.19 Individual proteins and complexes were loaded onto HiLoad® 16/60 Superdex® 200 pg column together with an internal standard aprotinin (6.5 kDa). For complex formation, 0.5 mg of each individual protein were incubated together at 4°C overnight under gentle shaking. Prior to loading onto column 1 mg of aprotinin and assay buffer were added in 1 ml total volume. (A) Superimposed chromatograms are distinctive by colors: $eIF4GII_{551-745}$ orange, eIF4E green, HRV4 His_6VP1_8 $2A^{pro}$ C110S purple. Color code for the binary incubation of HRV4 His_6VP1_8 $2A^{pro}$/eIF4E gray, and ternary incubation of HRV4 His_6VP1_8 $2A^{pro}$/eIF4E/$eIF4GII_{551-745}$ pink. There are multiple lanes loaded from the same peak to analyze the peak through the fractions. (B) Overnight incubated HRV4 His_6VP1_8 $2A^{pro}$ and eIF4E were analyzed on 17.5 % SDS-PAGE gel. **M:** marker (4 μl) **L:** load (3 μl) **1:** eIF4E eluted alone (8μl) **2:** HRV4 His_6VP1_8 $2A^{pro}$ (8 μl) **3:** aprotinin (8μl) (C) Overnight incubated HRV4 His_6VP1_8 $2A^{pro}$, eIF4E and $eIF4GII_{551-745}$ were analyzed on 17.5 % SDS-PAGE gel. **M:** marker (4 μl) **L:** load (3 μl) **1:** eIF4E/$eIF4GII_{551-745}$ binary complex (8μl) **2:** HRV4 His_6VP1_8 $2A^{pro}$ **3:** aprotinin (8μl) (D) Overnight incubated HRV1A $2A^{pro}$ C106 A, eIF4E, and $eIF4GII_{551-745}$ in buffer A pH 9.0 were analyzed on 17.5 % SDS-PAGE gel. **M:** marker (4 μl) **L:** load (3 μl) **1:** ternary complex of $2A^{pro}$/eIF4E/$eIF4GII_{551-745}$ (8μl) **2:** excess HRV1A $2A^{pro}$ C106A (8 μl), 3: aprotinin (8μl). 8 μl from fractions corresponding to indicated peaks were mixed with 2 μl 5 x Sample Buffer (8 μl).

4.6.5 Measuring the molecular masses of individual proteins and oligomeric states of the binary/ternary complexes using SLS

This technique gives the average molecular mass of a protein in a solution by measuring the intensity of scattered light. The proteins are eluted from a 10/300 Superdex® 200 prep grade column with 0.75 ml/min flow rate and measured by the miniDAWN Trista light scattering instrument. The SEC-MALLS (size exclusion-multi angle light scattering) experiments elucidated the molecular masses of the individual proteins, and the oligomeric states of complexes formed with HRV1A $2A^{pro}$ and its substrates.

First, single proteins and then the (overnight) incubated binary/ternary complexes were measured. HRV1A $2A^{pro}$ was determined to be a dimer depending on the result of 32 kDa (see table 4.7), whereas eIF4E and $eIF4GII_{551-745}$ were measured to be in a monomeric state. The binary complex between eIF4E and HRV1A $2A^{pro}$, was measured as 36 kDa, whereas it should be 45 kDa by calculation. When the $eIF4GII_{551-745}$ and HRV1A $2A^{pro}$ were incubated overnight and measured using SLS, we obtained molecular mass measurements between 36 kDa and 38 kDa for 10' and overnight incubation, respectively. When molecular masses of individual proteins summed, we would expect 39 kDa. Yet, we do not observe a complex formation either from binding studies (see figure 4.17 A), or from SLS chromatogram data (data not shown). Hence, it is suspicious whether there is any interaction between $eIF4GII_{551-745}$ and HRV1A $2A^{pro}$. The most remarking result was the oligomeric state of ternary complex. We found a molecular mass of 133 kDa for the complex, whereas a 1:1:1 formation would have resulted in 67 kDa. We concluded that this was a result of higher order state of binding.

Finally, HRV4 His_6VP1_8 $2A^{pro}$ was measured individually using SLS and it was found as a monomer.

Table 4.11 SLS results indicating exact molecular masses of the indicated proteins, binary, and ternary complexes. The percentage values indicate the error range of the measurement.

individual proteins	M_w measured with SLS (kDa)	M_w (kDa) theoretical
eIF4E	30.05 (2%)	28.8
$eIF4GII_{551-745}$	25.05 (0.9%)	22.5
HRV1A $2A^{pro}$	32.23 (1%)	16.4
HRV4 His_6VP1_8 $2A^{pro}$	21.02 (1%)	18.2

complexes	M_w measured with SLS (kDa)		M_w (kDa) theoretical
	10' incubation	overnight incubation	
HRV1A $2A^{pro}$ + eIF4E	37 (1%)	36 (1%)	45.2
HRV1A $2A^{pro}$ + $eIF4GII_{551-745}$	36.34 (1%)	38 (1%)	38.9
HRV1A $2A^{pro}$ + eIF4E + $eIF4GII_{551-745}$	143.3 (0.3%)	133.3 (0.8%)	67.7
eIF4E + $eIF4GII_{551-745}$	55.6 (0.5 %)	55.6 (1%)	51.3

4.6.6 Thermodynamics of the binary/ternary complexes using ITC

Thermodynamics help us to understand the relationship between energy and heat by following the rules of Carnot and Kelvin. Every chemical reaction can be described by using the parameters such as heat release, entropy and Gibbs free energy. In light of this information, we wanted to describe the binary and ternary complex formation reactions. Enthalpy change, entropy change, stoichiometry, and association constant of the reaction were measured by ITC. Disassociation constants were calculated from the formula [$1/K_a$]. Free Gibbs energies can also be calculated from the formula [$\Delta G=\Delta H-T.\Delta S$]. ITC measurements were performed to analyze interactions between the inactive HRV1A $2A^{pro}$ and its binding partners eIF4E and $eIF4GII_{551-745}$ (only one out of triplicates is shown). The HRV1A $2A^{pro}$ was in the stirring syringe (titrant) and titrated drop wise into a cell with either one of the binding partners or both of them. Data indicates that HRV1A $2A^{pro}$/eIF4E interaction is a spontaneous reaction ($\Delta G < 0$) with a dissociation constant of 7 μM (see table 4.8). This result is in line with the analytical SEC

experiments. SLS data for ten-minute and overnight incubations of eIF4E and HRV1A $2A^{pro}$ indicated 1:1 complex with a dissembled HRV1A $2A^{pro}$ dimer. In addition, the stoichiometry measured by ITC indicated every ~ 0.5 molecule from the titrant ($2A^{pro}$) was binding to 1 molecule from the cell (eIF4E). An explanation can be that HRV1A $2A^{pro}$ dissociates from its dimer composition and disassembles in order to bind to eIF4E. Interestingly, when HRV1A $2A^{pro}$ titrated into a cell with $eIF4GII_{551-745}$ the dissociation constant was measured 12 μM with a relatively high standard deviation. This deviation can be explained as a very unstable and faint interaction, in line with analytical SEC experiments. However, the calculated free Gibbs energy from this reaction indicated a spontaneous interaction. The stoichiometry of the $2A^{pro}$/$eIF4GII_{551-745}$ interaction was not very clear from the ITC measurements due to high standard deviation rate. Unfortunately, a sigmoid curve could not be obtained (see figure 4.20 B) even after many trials. Finally, the ternary complex formation reaction was measured using ITC. These measurements were challenging because of the permutation of interactions between three proteins. In order to overcome this problem, we fist tried to elute an overnight-formed stable eIF4E/$eIF4GII_{551-745}$ binary complex from the SEC columns and to use it in the cell of the ITC machine. Second, the initial 5 injections were performed with 0.5 μl of $2A^{pro}$, subsequently 2 μl for 10 injections and finally 1 μl for the remaining 5 injections. This helped to obtain a better sigmoid-like curve with the initial saturation (see figure 4.20 C). $eIF4GII_{551-745}$ forms a rather tight ternary complex with HRV1A $2A^{pro}$ in the presence of eIF4E, with a dissociation constant of 1 μM. Data shows clearly the tightest binding is when all three proteins are present to form a ternary complex and it is again spontaneous ($\Delta G < 0$). The stoichiometry of this reaction could not be explained well from ITC measurements when compared to SLS data; however, it was measured ~ 1:1 ratio in between the titrant ($2A^{pro}$) and the cell (binary complex of eIF4E/$eIF4GII_{551-745}$).

Table 4.12 Thermodynamic interactions of HRV1A $2A^{pro}$ upon complex formation with eIF4E and $eIF4GII_{551-745}$. Data measured using isothermal titration calorimetry (ITC). Experiments were repeated several times in order to calculate the mean values and standard deviations (n=3).

(titrant + cell)	K_d (μM)	ΔS (cal.mol^{-1}.deg^{-1})	ΔH (cal.mol^{-1})	ΔG	N (stoichiometry)
$2A^{pro}$ + eIF4E	6.71 ± 0.92	-62 ± 6.99	-25556 ± 2023	-29816	0.36 ± 0.07
$2A^{pro}$ + $eIF4GII_{551-745}$	11.77 ± 11.9	2.59 ± 0.92	-6166 ± 440	-29034	1.24 ± 0.16
$2A^{pro}$ + eIF4E/$eIF4GII_{551-745}$	0.95 ± 0.42	8.41 ± 3.17	-5752 ± 647	-34512	1.22 ± 0.06

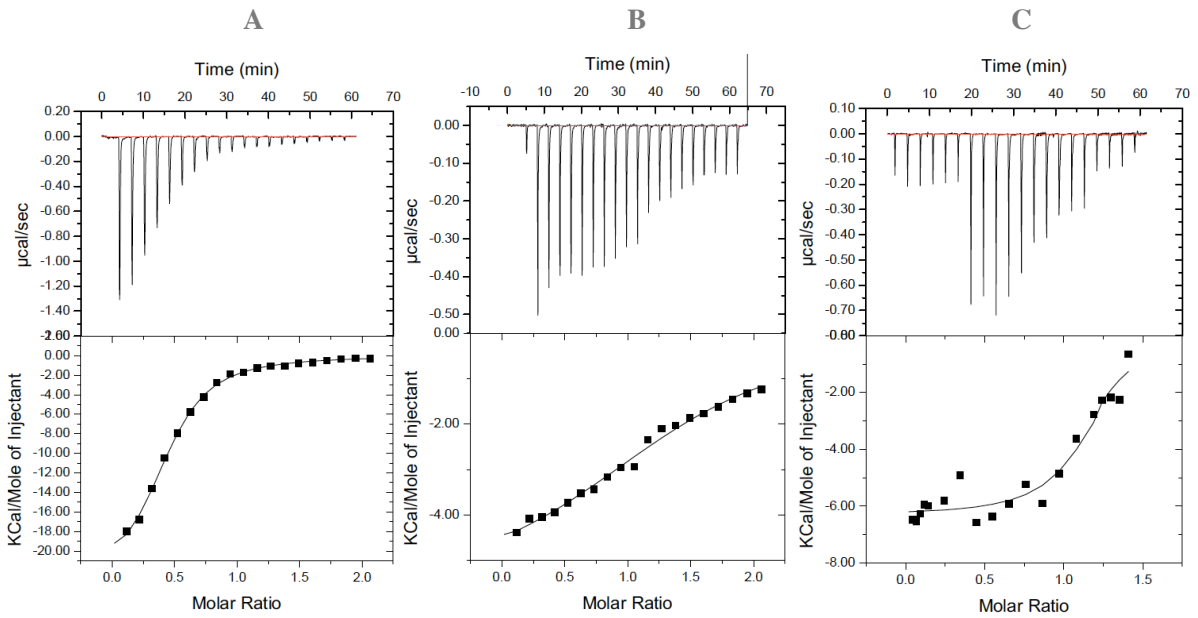

Figure 4.20 Thermodynamics of the protein complexes with HRV1A 2A proteinase. Isothermal titration calorimetry graphs of $2A^{pro}$/eIF4E, $2A^{pro}$/eIF4GII$_{551-745}$, $2A^{pro}$/eIF4E/eIF4GII$_{551-745}$ are shown in figures A, B and C respectively.

5 DISCUSSION

Human rhinovirus infections are to blame for more than 50 % of cold-like illnesses all around the globe. It is the most common cause of upper respiratory tract infections (URI) and billions of dollars are spent on medication annually (Fendrick et al., 2003). Moreover, severe bronchiolitis in infants and children, asthma development, and exacerbations of chronic pulmonary disease are linked with HRV infections. At present, PCR-based methods are used to detect these respiratory viruses (Pappas et al., 2008). There are more than 150 serotypes of HRV (http://www.picornaviridae.com/) and high sequence variability within antigenic sites hinder a common vaccine development for all serotypes (Jacobs et al, 2013). However, recent studies focus on synthesizing compounds that target non-structural viral proteins. Ruprintrivir (Agouron Pharmaceuticals, Inc.), an anti-viral drug in phase II, targets the $3C^{pro}$ and inhibits its activity in experimentally-induced HRV-infected volunteers (Hayden et al., 2003). The substrate specificity (see chapter 1.4.3) of HRV proteinases differ greatly; nevertheless, there are conserved sequences among the cleavage sites. For example, GlyP1' is identical among all picornaviral 2A proteinases and definitely required for cleavage. Moreover, ThrP2 is highly conserved within both *cis* and *trans* substrates. The hydrogen bond between ThrP2 and Ser83 seems to be critical for maintaining the structure of HRV2 $2A^{pro}$. The importance of S1 site was established by Petersen et al. for substrate binding. Access to this narrow pocket is limited by a consensus Leu19 residue (Petersen et al., 1999). Anti-viral drug development should make use of the substrate specificity of $2A^{pro}$ and the consensus residues involved in substrate cleavage.

This work investigates the $2A^{pro}$ from different genetic groups (genetic group A: HRV1A and genetic group B: HRV4) (see figure 5.1, 5.2). In this study, HRV1A $2A^{pro}$ and HRV4 $2A^{pro}$ were compared for their structural properties and substrate interactions. There are well-studied representatives of each genetic group, which were investigated structurally or for their substrate specificity. Therefore, we compared also our data to the previous works about the pioneer examples.

HRV2 $2A^{pro}$, the representative of genetic group A, is well-studied for host translation shut off *in vitro*. However, mutational analyses to elucidate the substrate specificity of $2A^{pro}$ were investigated in cell culture using HRV1A subtype, a close relative to HRV2 with 86.3 % amino acid sequence identity (Martina Aumayr, 2012 Masterarbeit & Neubauer et al., 2013).

The *in vitro* substrate-proteinase interactions had not been investigated extensively with HRV1A $2A^{pro}$, unlike HRV2 $2A^{pro}$ (Aumayr et al., 2015). We wanted to answer whether such close relatives would share similar structural properties as well. Therefore, here I will discuss the comparison based on the published results of HRV2 $2A^{pro}$.

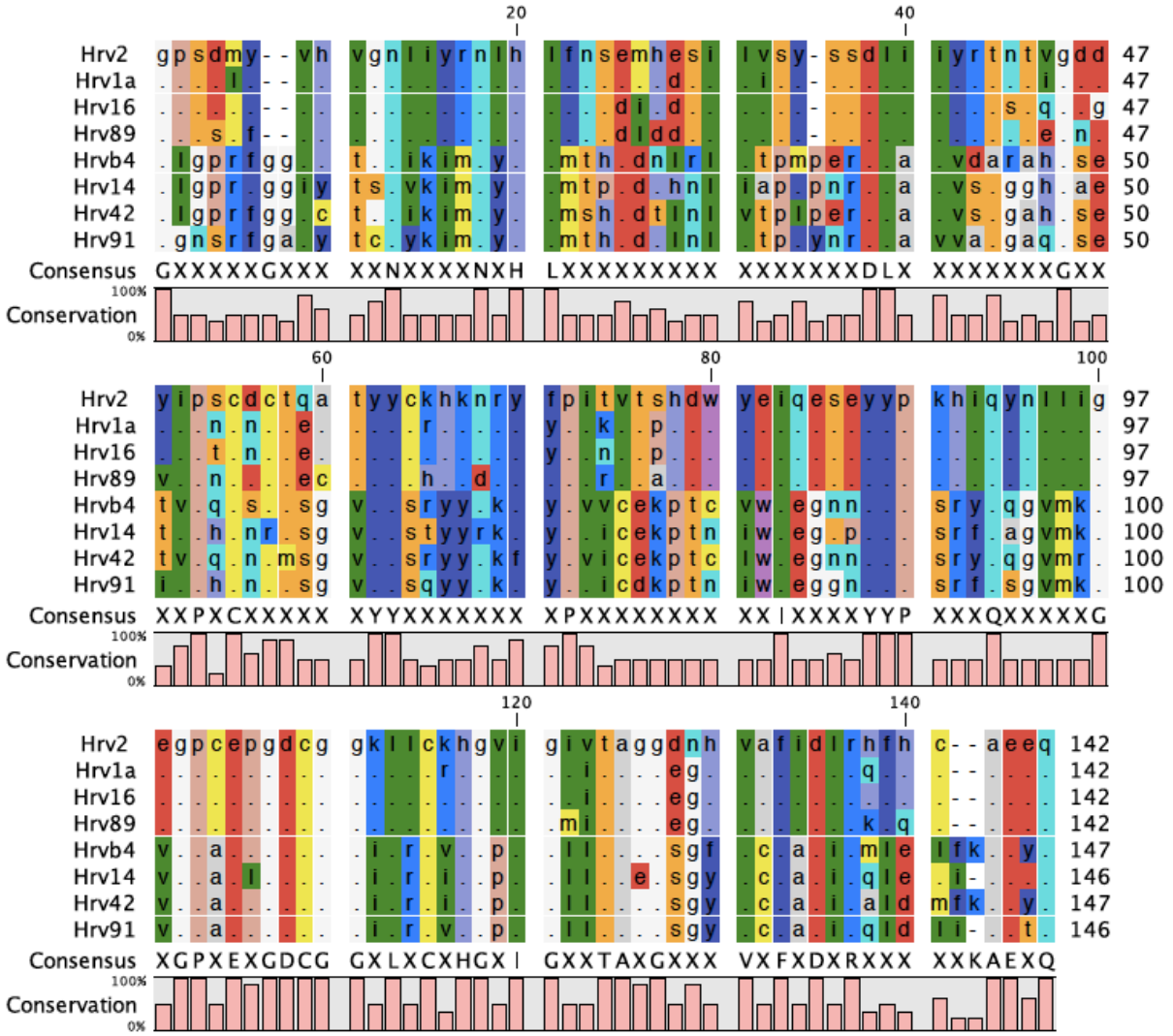

Figure 5.1 The $2A^{pro}$ amino acid sequence alignment of HRV genetic group A and B (4 viruses per group). HRV2, HRV1A, HRV16, HRV89 belong to the genetic group A. HRV4, HRV14, HRV42, HRV91 belong to the genetic group B. The catalytic triad consisting of His_{20}, Asp_{38}, Cys_{109} are conserved among proteinases from different species (with ± residue numbers). Dots indicate identical amino acid residues on corresponding column. Consensus residue limit was set to 100%; therefore, all residues are marked as 'X' (variable) unless they are 100% conserved. The length difference of sequences is compensated using dashes. The bars underneath alignment indicate conservation of the given residue. The right column of numbers indicates the sequence length. Alignment was made by using CLC Genomics Workbench 9. (NCBI accession codes HRV89: ACK37440.1, HRV16: AAA69862.1, HRV1A: AKF02546.1, HRV2: CAA26181.1, HRV4: ABF51184.1, HRV14: NP_041009.1, HRV42: ACK37386.1, HRV91: ACK37424.1)

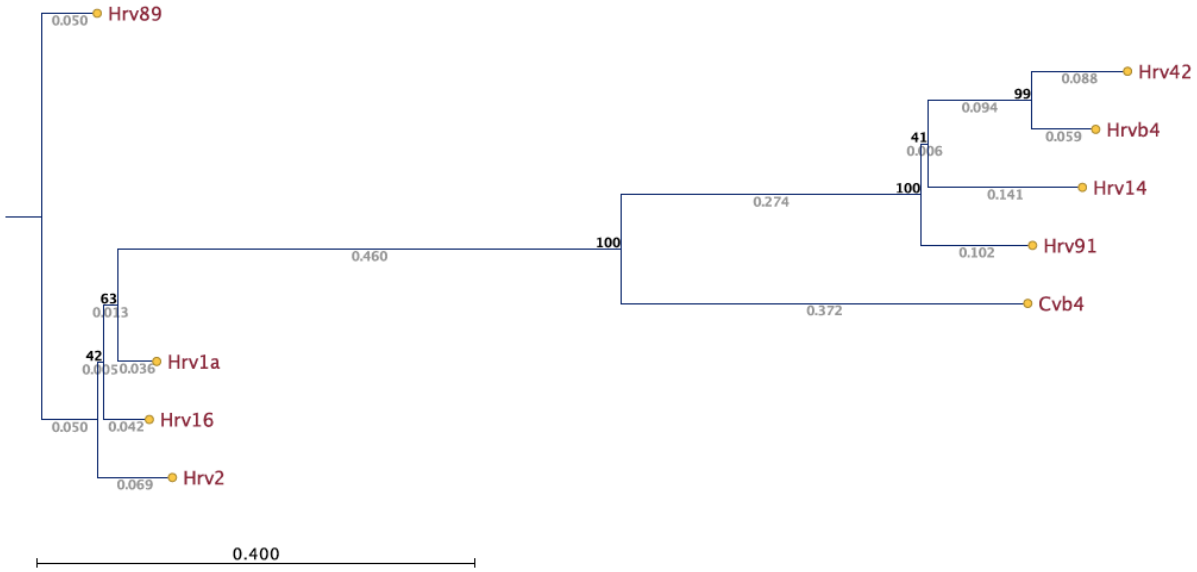

Figure 5.2 The maximum likelihood phylogenetic tree of the $2A^{pro}$ from human rhinovirus genetic group A (HRV1A, HRV2, HRV16, HRV89), genetic group B (HRV4, HRV14, HRV42, HRV91), and enterovirus CVB4. The $2A^{pro}$ from genetic group A viruses are remarkably distant to the group B. On the other hand, the genetic group B rhinovirus $2A^{pro}$ is a closer relative to enterovirus member CVB4 $2A^{pro}$ than group A of the same family. The branch length values (gray) represent amino acid substitutions per site. The bootstrap values (black, in percentage) indicate a measure of support for each node where 100 indicates maximal support. The black bar underneath is a scale of genetic divergence. Figure made by using CLC Genomics Workbench 9.

HRV1A $2A^{pro}$ was expressed in *E.coli* in soluBL21(DE3) strain, a special strain for enhanced expression of soluble and toxic proteins. Cells were induced with 0.15 mM IPTG and 100 μM $ZnCl_2$ was added simultaneously (to enhance the structural maintenance, see chapter 1.4.2). The expression temperature was set to 18°C and the cells incubated overnight. HRV1A $2A^{pro}$ expressions yielded 3.33 $mg/L_{expression}$ purified protein. The published expression and purification protocol for HRV2 $2A^{pro}$ was rather different (Liebig et al., 1993). The BL21(DE3)pLysE (*E.coli*) cells were inoculated with HRV $2A^{pro}$-coding plasmids that were induced with 0.3 mM IPTG and incubated for 5 h at 34°C.

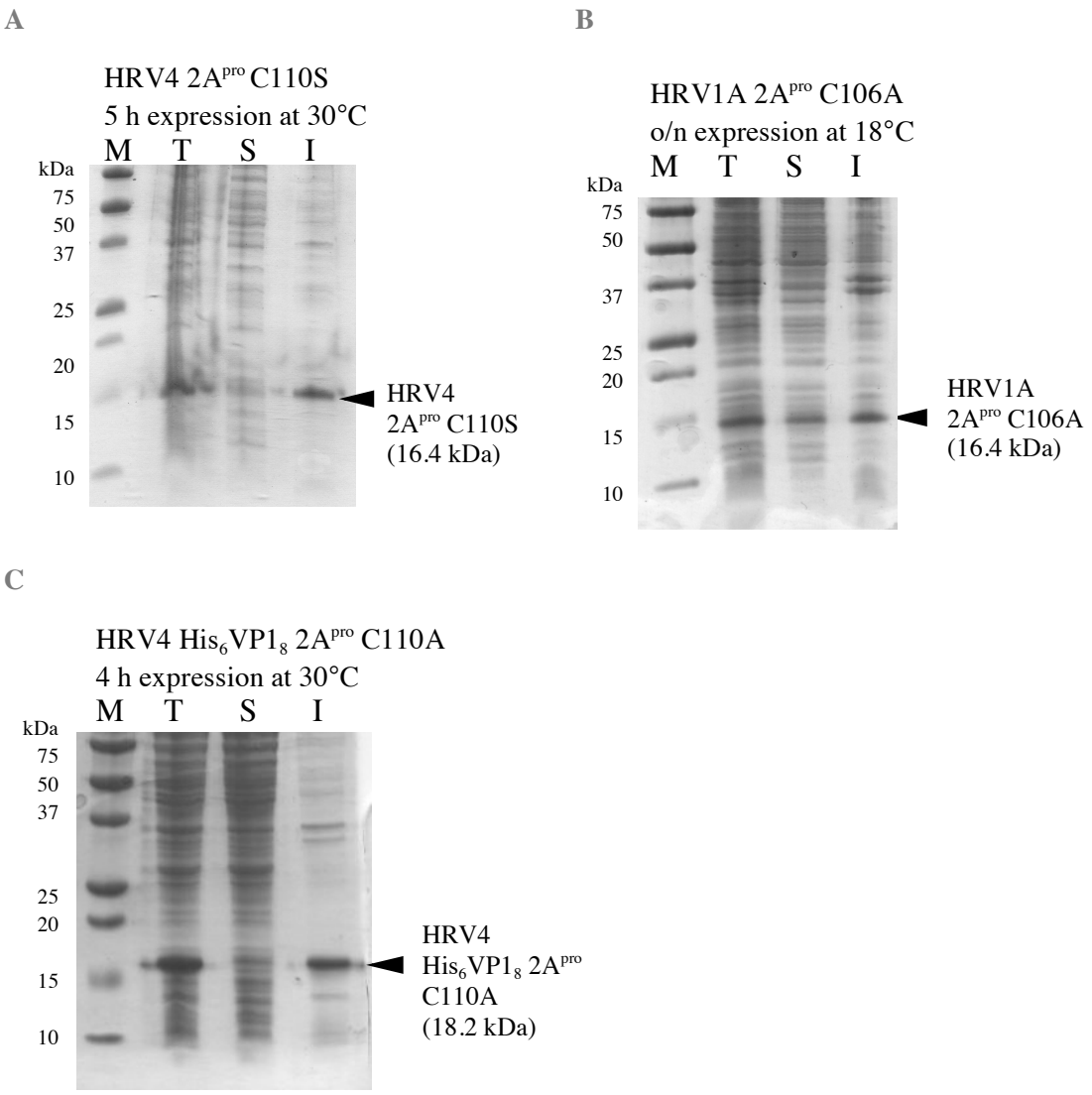

Figure 5.3 Expression-level comparison of (A) HRV4 $2A^{pro}$ C110S, (B) HRV1A $2A^{pro}$ C106A, and (C) HRV4 His_6VP1_8 $2A^{pro}$ C110A.

Expression of recombinant HRV4 $2A^{pro}$ was rather challenging. The IPTG and $ZnCl_2$ concentrations were used the same within all $2A^{pro}$ expressions. In addition, all proteinases were expressed in soluBL21(DE3) cell line of *E.coli*. The HRV1A $2A^{pro}$ was successfully expressed overnight at 18°C and could be seen in the soluble cell lysate (lane S: 1 μl loaded) in figure 5.3 B. Unfortunately, the HRV4 $2A^{pro}$ remained mostly in the insoluble fraction (see figure 5.3 A, lane I: 1 μl loaded). After many modifications on expression-temperature and -duration that failed (data not shown), we decided to clone a different DNA construct of HRV4 $2A^{pro}$ with specific modifications (see chapter 4.4). We introduced an N-terminal hexahistidine tag upstream to the 8 amino acid residues from the carboxyl terminus of VP1 capsid protein. These exact N-terminal extensions were used before by David Neubauer (Dissertation, 2013) to express CVB4 $2A^{pro}$ and to set crystals with it. The satisfying expression levels and solubility inspired us to mimic this idea. Here we establish an expression protocol

for HRV4 His_6VP1_8 $2A^{pro}$. Figure 5.3 C shows the enhanced expression level upon the N-terminal extension in HRV4 $2A^{pro}$. Although the conditions differ, HRV4 His_6VP1_8 $2A^{pro}$ C110A is expressed at higher levels in total (lane T: 1 μl loaded) than HRV1A $2A^{pro}$ C106A (figure 5.3 B, lane T: 1μl loaded). Unfortunately, a higher percentage of the total expression is still insoluble (figure 5.3 C). HRV4 His_6VP1_8 $2A^{pro}$ C110A yielded 0.4 mg/$L_{expression}$ purified protein, which is almost 10 times less than HRV1A $2A^{pro}$ C106A production. However, this problem can possibly be improved in the future by engineering the protein-of-interest with fusion partner proteins (Costa et al., 2014).

Analytical size exclusion experiments with HiLoad® 16/60 Superdex® 200 prep grade column showed that HRV1A $2A^{pro}$ C106A is similar to HRV2 $2A^{pro}$ C106S. Aumayr et al. published stable ternary complex formation with $eIF4G_{551-745}$ and eIF4E at ~70 ml retention volume. We followed the same experimental procedure and showed that HRV1A $2A^{pro}$ C106A forms a stable ternary complex as well. This complex was found at 66 ml retention volume (see figure 4.17 A). Both proteinases form a binary complex with eIF4E at ~90 ml retention volume. The $eIF4GII_{551-745}$ alone is not capable of forming a complex with either of the proteinases. However, the $2A^{pro}$ peak was broadened in both serotypes when the proteinase was incubated overnight with $eIF4GII_{551-745}$, presumably due to sample dispersion.

As discussed previously in chapter 1.4.3, self-processing cleavage sites of HRV2 $2A^{pro}$ and HRV1A $2A^{pro}$ are identical within the region P4-P4' (see table 1.2). In addition, the $2A^{pro}$ share 88.7 % sequence homology. We also expected similar processing efficiencies towards $eIF4GII_{551-745}$. The C-terminal and N-terminal cleavage products of $eIF4GII_{551-745}$ (5.3 μM) are first observed with 10 ng (76 nM) HRV1A $2A^{pro}$ (see figure 4.16 B) in the presence of eIF4E (5.3 μM). The $eIF4GII_{551-745}$ cleavage was not reached within 90 minutes when incubated with 10 ng HRV1A $2A^{pro}$ in the absence of eIF4E. The active HRV2 $2A^{pro}$ processing profile is comparable and similar when HRV2 $2A^{pro}$ was incubated with both initiation factors (the same concentrations were used as in this thesis). HRV2 $2A^{pro}$ as well processes $eIF4GII_{551-745}$ with 10 ng (80 nM) and both the N- and C-terminal cleavage products are visible in the presence of eIF4E. The eIF4E support is crucial for $eIF4GII_{551-745}$ to bind the $2A^{pro}$ from both HRV1A and HRV2. However, the C-terminal cleavage product of $eIF4GII_{551-745}$ (in the absence of eIF4E) was observed after 60-90 minutes upon the processing by 10 ng HRV2 $2A^{pro}$, in contrast to HRV1A $2A^{pro}$. However, serotypes belonging to the same genetic group may behave differently. As an example, Vlasak and colleagues published the receptor recognition variation between HRV2 and HRV1A. They are both minor group viruses that recognize LDLR and were experimented against human and mouse homologues of their receptor. The results showed that HRV1A has a prevalence of binding to the mouse homologue, whereas HRV2 binds very well to the LDLR of both species (Vlasak et al., 2003).

Table 5.1 SLS results indicating exact molecular masses of the indicated proteins, binary, and ternary complexes. The percentage values indicate the error range of the measurement.

individual proteins	M_w measured with SLS (kDa)	M_w (kDa) theoretical
eIF4E	30.05 (2%)	28.8
$eIF4GII_{551-745}$	25.05 (0.9%)	22.5
HRV1A $2A^{pro}$	32.23 (1%)	16.4
HRV4 His_6VP1_8 $2A^{pro}$	21.02 (1%)	18.2

complexes	M_w measured with SLS (kDa)		M_w (kDa) theoretical
	10' incubation	overnight incubation	
HRV1A $2A^{pro}$ + eIF4E	37 (1%)	36 (1%)	45.2
HRV1A $2A^{pro}$ + $eIF4GII_{551-745}$	36.34 (1%)	38 (1%)	38.9
HRV1A $2A^{pro}$ + eIF4E + $eIF4GII_{551-745}$	143.3 (0.3%)	133.3 (0.8%)	67.7
eIF4E + $eIF4GII_{551-745}$	55.6 (0.5 %)	55.6 (1%)	51.3

The molecular masses of the single proteins and complexes were determined using SLS for HRV1A $2A^{pro}$ C106A. The results indicated that HRV1A $2A^{pro}$ C106A is a dimer, as is the HRV2 $2A^{pro}$ C106S, with a 32 kDa molecular mass (monomer is 16.4 kDa by calculation) (see table 5.1). The initiation factors (eIF4E and $eIF4GII_{551-745}$) were measured singly. The eIF4E has a measured mass of 30 kDa with an error range of 2 %, which fits to the calculated value (28.8 kDa). The $eIF4GII_{551-745}$ would have a mass of 22.5 kDa, which was measured as 25 kDa (0.9 %).

The initiation factors together form a complex, which was also shown with analytical SEC experiments (see figure 4.17 A), and the molecular mass of this complex was measured as 55 kDa using SLS. The calculated binary eIF4E/$eIF4GII_{551-745}$ complex would have a mass of 51 kDa.

The measured molecular mass of the HRV1A $2A^{pro}$/eIF4E heterodimer however does not fit to the calculated mass. Assuming the $2A^{pro}$ binds to eIF4E as a monomer, this complex would have a mass of 45.2 kDa. However, our findings indicated a molecular mass around 36 kDa (1 %). We assume that

an error might have occurred due to non-equivalent concentrations of eIF4E and HRV1A $2A^{pro}$ C106A. If there are any smaller proteins in the vicinity of the complex due to nonequivalent concentrations, this would result in measurements of those individual proteins. Therefore, the measured average mass would decrease, leading to errors. On the other hand, HRV2 $2A^{pro}$/eIF4E complex was measured as 38-40 kDa using SEC-MALLS, which is in the line with our findings (Aumayr et al, 2015).

There is no binary complex formation with $eIF4GII_{551-745}$/HRV2A $2A^{pro}$ C106S. Similarly, an overnight incubation of HRV1A $2A^{pro}$ C106A with $eIF4GII_{551-745}$ chromatogram of SEC showed in contrast that there is no complex formed; however, a broadened $2A^{pro}$ peak was observed (4.17 A). The SDS-PAGE analysis of SEC experiments clarified that $eIF4GII_{551-745}$ does not form a stable complex with HRV1A $2A^{pro}$ C106A when incubated alone (data not shown). If the $eIF4GII_{551-745}$ interaction with HRV1A $2A^{pro}$ has a slower off-rate constant (k_{off}) than the one with HRV2 $2A^{pro}$, this may cause the broadened HRV1A $2A^{pro}$ peak in analytical SEC experiments. However, the SLS measurements gave a molecular mass of 38 kDa for the overnight incubation of $eIF4GII_{551-745}$ with HRV1A $2A^{pro}$ C106A; this interaction would have a mass of 39 kDa by calculation. We conclude that the concurring measured & calculated M_w values for the binary interaction with $eIF4GII_{551-745}$ may as well reflect a slow k_{off}. More experiments should be conducted to fully understand this interaction.

The oligomeric state of the ternary complex with HRV2 $2A^{pro}$ is difficult to understand. The heterotrimeric complex (HRV2 $2A^{pro}$/eIF4E/$eIF4GII_{551-745}$) would have a mass of 68 kDa by calculation. This calculation is based on the assumption that the dissociated $2A^{pro}$ monomer would interact with one molecule of each initiation factor. However, the SEC-MALLS results propose a complex with 104-106 kDa molecular mass for HRV2 $2A^{pro}$ (Aumayr et al., 2015). Interestingly, ternary complex formation with HRV1A $2A^{pro}$ C106A was measured as 133 kDa. Possibly, the complex is not formed in a 1:1:1 stoichiometry and there is a higher oligomeric state. One assumption is that two ternary complexes (2 times 1:1:1 is 136 kDa by calculation) can interact with each other and can therefore have twice the mass of one complex.

The most remarkable measurement is monomeric HRV4 His_6VP1_8 $2A^{pro}$ C110A confirmation by SLS. In contrast to its relatives from genetic group A, HRV4 His_6VP1_8 C110A was measured as a monomer with 21 kDa molecular mass (18.2 kDa by calculation). Baxter et al. published the crystal structure resemblance between coxsackievirus (CV) B4 $2A^{pro}$ and HRV2 $2A^{pro}$. Although the low level of sequence homology (40 %), these two proteinases fold similarly and both contain a Zn ion for structural stability. The CVB4 $2A^{pro}$ is a monomer with 19 kDa molecular mass (Baxter et al., 2006) unlike HRV1A $2A^{pro}$ (see figure 5.4 C). Here, we establish that the genetic group B element HRV4 His_6VP1_8 $2A^{pro}$ resembles CVB4 $2A^{pro}$ by the means of the oligomeric state (see figure 5.2, 5.4 B) more than the same genus member HRV1A $2A^{pro}$.

A

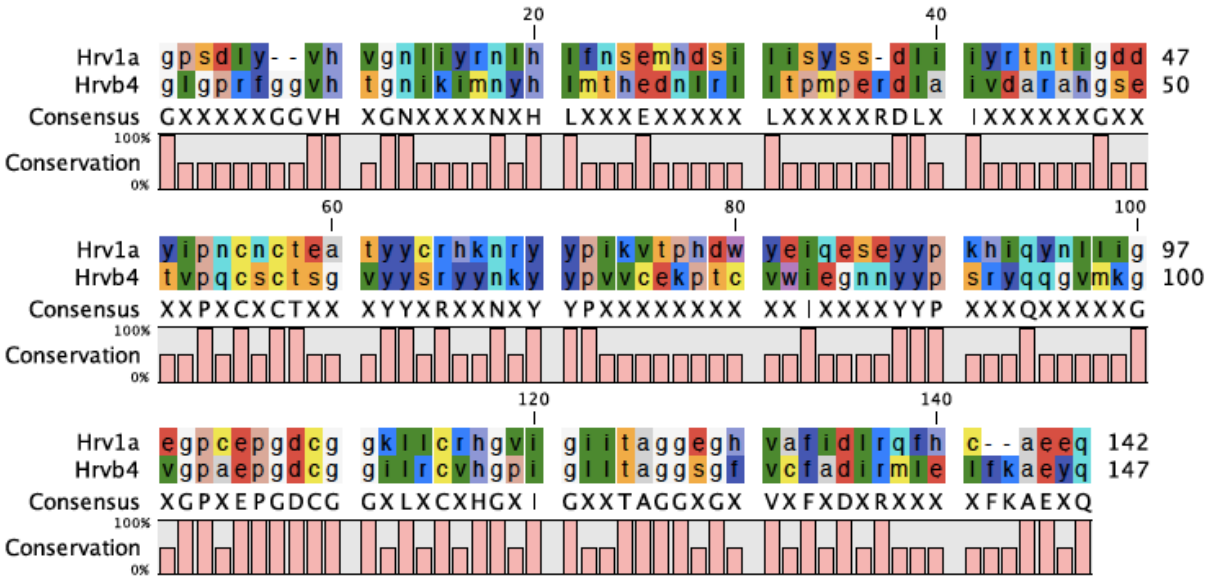
20
40
Hrv1a gpsdly--vh vgnliyrnlh lfnsemhdsi lisyss-dli iyrtntigdd 47
Hrvb4 glgprfggvh tgnikimnyh lmthednlrl ltpmperdla ivdarahgse 50
Consensus GXXXXXGGVH XGNXXXXNXH LXXXEXXXXX LXXXXXRDLX IXXXXXXGXX
100%
Conservation
0%
60
80
100
Hrv1a yipncnctea tyycrhknry ypikvtphdw yeiqeseyyp khiqynlIig 97
Hrvb4 tvpqcsctsg vyysryynky ypvvcekptc vwiegnnyyp sryqqgvmkg 100
Consensus XXPXCXCTXX XYYXRXXNXY YPXXXXXXXX XXIXXXXYYP XXXQXXXXXG
100%
Conservation
0%
120
140
Hrv1a egpcepgdcg gkllcrhgvi giitaggegh vafidlrqfh c--aeeq 142
Hrvb4 vgpaepgdcg gilrcvhgpi gllitaggsgf vcfadirmle lfkaeyq 147
Consensus XGPXEPGDCG GXLXCXHGXI GXXTAGGXGX VXFXDXRXXX XFKAEXQ
100%
Conservation
0%

B

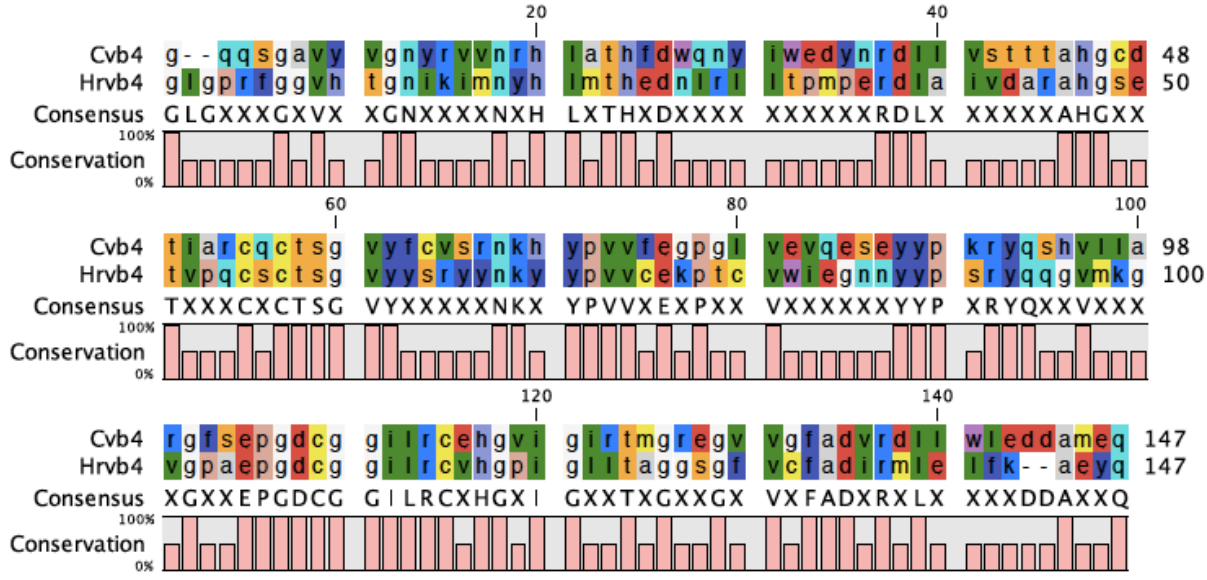
20
40
Cvb4 g--qqsgavy vgnyrvvnrh latHfdwqny iwedynrdll vsttta hgcd 48
Hrvb4 glgprfggvh tgnikimnyh lmthednlrl ltpmperdla ivdarahgse 50
Consensus GLGXXXGXVX XGNXXXXNXH LXTHXDXXXX XXXXXXRDLX XXXXXAHGXX
100%
Conservation
0%
60
80
100
Cvb4 tiarcqctsg vyfcvsrnkh ypvvfegpgl vevqeseyyp kryqshvlla 98
Hrvb4 tvpqcsctsg vyysryynky ypvvcekptc vwiegnnyyp sryqqgvmkg 100
Consensus TXXXCXCTSG VYXXXXXNKX YPVVXEXPXX VXXXXXXYYP XRYQXXVXXX
100%
Conservation
0%
120
140
Cvb4 rgfsepgdcg gilrcehgvi girtmgregv vgfadvrdll wleddameq 147
Hrvb4 vgpaepgdcg gilrcvhgpi gllitaggsgf vcfadirmle lfk--aeyq 147
Consensus XGXXEPGDCG GILRCXHGXI GXXTXGXXGX VXFADXRXLX XXXDDAXXQ
100%
Conservation
0%

C

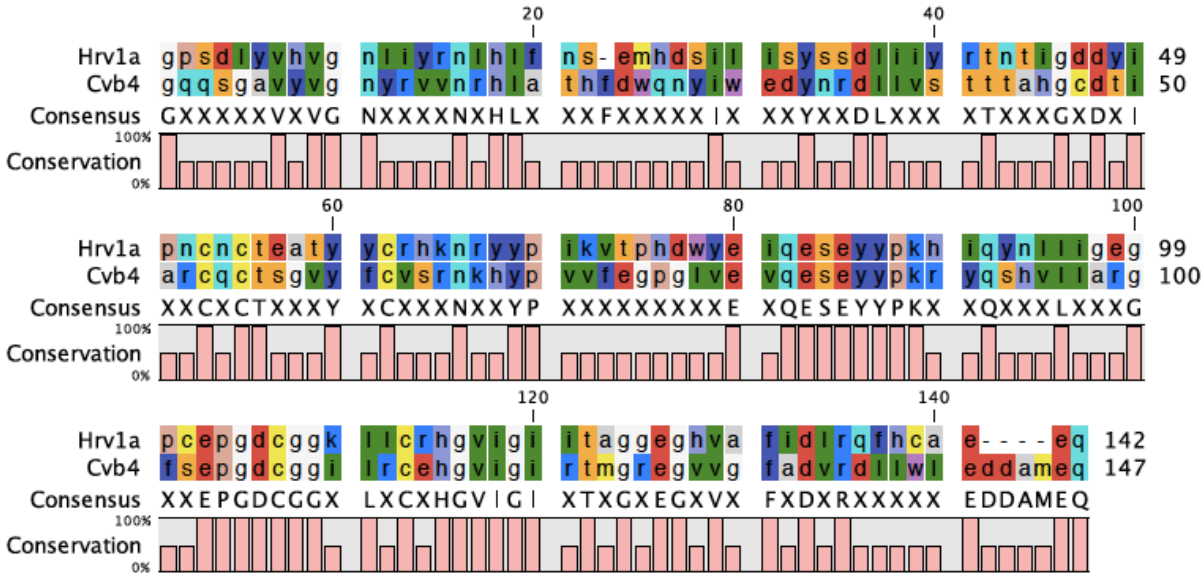

Figure 5.4 The amino acid sequence alignment of 2A^{pro} between rhinoviruses from different genetic groups (HRV1A 2A^{pro} and HRV4 2A^{pro}) is shown in figure A. The amino acid sequence alignment of 2A^{pro} between viruses from different genus (CVB4 2A^{pro} and HRV4 2A^{pro}) is shown in figure B. Figure C shows the amino acid sequence alignment of 2A^{pro} from HRV1A and CVB4. Consensus residue limit was set to majority; therefore, all residues are marked as 'X' (variable) unless they are identical for both sequences. The length difference of sequences is compensated using dashes. The bars underneath alignment indicate conservation of the given residue. The right column of numbers indicates the sequence length. Alignments were made by using CLC Genomics Workbench 9. (NCBI accession codes HRV1A: AKF02546.1, HRV4: ABF51184.1, CVB4: AAB33885.1)

Complex formation kinetics were investigated using a thermodynamic method, namely the isothermal titration calorimetry (ITC). Dissociation constants (K_D) were measured for binary/ternary complexes. The stable and rather tight ternary complex of HRV1A 2A^{pro} C106A/eIF4E/eIF4GII$_{551-745}$ has a K_D of 1 μM (see table 4.12, figure 4.20). This interaction was measured as 5 μM with the HRV2 2A^{pro} C106S by Aumayr et al.. The eIF4E forms a binary complex with a looser interaction (7 μM). A similar interaction with 12 μM K_D was published for HRV2 (Aumayr et al., 2015). eIF4E was found to have a tighter heterodimeric complex with HRV1A 2A^{pro} in comparison to the one with HRV2 2A^{pro}. We wanted to clarify whether eIF4GII$_{551-745}$ binds to 2A^{pro} at all and therefore measured this interaction using ITC. Results indicated a 12 μM K_D with a rather high (±12 μM) standard deviation. The SEC experiments confirmed that eIF4GII$_{551-745}$ and HRV1A 2A^{pro} C106A elute separately. Hence, we conclude that there is an interaction between eIF4GII$_{551-745}$ and the proteinase, yet it is not tight enough to form a complex. HRV2 2A^{pro} C106S interaction with eIF4GII$_{551-745}$ was measured previously with 75 ±12 μM dissociation constant (Aumayr et al., 2015). Interestingly, HRV2 2A^{pro} C106S has a looser interaction with eIF4GII$_{551-745}$, even though the active proteinase is more efficient at eIF4GII$_{551-745}$ cleavage (in the absence of eIF4E) when compared to HRV1A 2A^{pro}.

Intramolecular cleavage assay for HRV4 His_6VP1_8 $2A^{pro}$ was performed in the same way with HRV1A $2A^{pro}$; it therefore, is directly comparable. Our results show that genetic group A is very efficient in processing eIF4GII. However, we further wanted to investigate the *trans* substrate processing by HRV4 $2A^{pro}$. We tried an *in vitro* cleavage assay at 37°C with time course. We began with 77 nM HRV4 His_6VP1_8 $2A^{pro}$ incubation together with (5.3 μM) 1 μg $eIF4GII_{551-745}$ or 1 μg eIF4E/$eIF4GII_{551-745}$. The results showed that there was no cleavage after 90 minutes. We increased the $2A^{pro}$ concentration to 540 nM and later to 770 nM, but there were still no cleavage (see figure 4.18). Although we used 77-fold more $2A^{pro}$ by HRV4 experiments compared to HRV1A, we could not observe cleavage products of $eIF4GII_{551-745}$ within 90 minutes. Further, eIF4E assist did not change the result. On the other hand, *trans* processing of eIF4G by HRV4 was investigated by Watters et al., 2011. They used HeLa cell extracts as the eIF4G source. They detected the remaining eIF4G, and cleavage products of eIF4G after a 2 h incubation with recombinant picornaviral $2A^{pro}$ by using an Ab to the amino end of eIF4G. When HRV4 $2A^{pro}$ was incubated in HeLa cells for 2 h, 32 % remainder eIF4G was observed whereas the competitors from genetic group A (HRV89 and HRV16) efficiently cleaved >90 % of eIF4G by that time (Watters & Palmenberg, 2011). On the basis of these knowledge, we can not conclude an activity deficiency for our recombinant HRV4 His_6VP1_8 $2A^{pro}$. However, we can confirm that our findings fit to these results, since we found genetic group A more effective in cleavage assays than genetic group B as well. Moreover, our recombinant HRV4 His_6VP1_8 $2A^{pro}$ can be further tested with HeLa cell extracts. There may be other requirements for HRV4 $2A^{pro}$ to process eIF4GII, which of them may exist in HeLa cell extracts. Furthermore, poor recognition of eIF4GII isoform by another genetic group B rhinovirus (HRV14) was published by Gradi and colleagues (Gradi et al., 2003). They found that eIF4GI isoform cleavage was quicker than eIF4GII. Therefore, they concluded that eIF4GI cleavage site was better recognized. Table 5.2 focuses on the cleavage sites for both intramolecular and intermolecular processing by HRV4 $2A^{pro}$. The eIF4GI sequence coincides with the self-processing site at positions P7, P2 and P1'. Further, the LeuP4 is also similarly hydrophobic such as IleP4 by intramolecular cleavage site. In contrast, the eIF4GII sequence overlaps only at the position P1' with LeuP4. It will be intriguing to assay eIF4G fragments with HRV4 $2A^{pro}$ in the future. We conclude that there may be other parameters contribute to the eIF4G processing by HRV4 $2A^{pro}$ that to be further investigated.

Table 5.2 The cleavage sites on *cis* and *trans* substrates (eIF4GI and eIF4GII) of the $2A^{pro}$ from HRV4. Cleavage position between P1 and P1' is indicated with an arrow. P10-P1 amino acid sequences correspond to preceding protein. P1'-P10' amino acid sequences correspond to either $2A^{pro}$ or *trans* substrates eIF4GI/II. Conserved amino acid residues are indicated in bold. Sequences taken from NCBI. (HRV4: ABF51184.1, eIF4GI: NP_886553.3, eIF4GII: AAC02903.2)

	P10 P5 P1 ⬇ P1' P5' P10'
HRV4 $2A^{pro}$ (*cis*)	I K T **R** E S I N **T** Y **G** L G P R F G **G** V H
eIF4GI (*trans*)	N L G **R** T T **L** S **T** R **G** P P **R** G G **P** **G** G E
eIF4GII (*trans*)	G G R G V P **L** L N V **G** S R **R** S Q **P** **G** Q R

HRV1A $2A^{pro}$ is similar to HRV2 $2A^{pro}$ when measuring the interaction characteristics with initiation factors. Both $2A^{pro}$ form a stable binary complex with eIF4E, which was confirmed with binding studies. Moreover, K_D values indicated stable and rather tight complexes with either of the $2A^{pro}$. On the other hand, $2A^{pro}$/eIF4GII$_{551\text{-}745}$ complexes were detected neither on SDS-PAGE analysis nor on analytical SEC experiments for both serotypes. Both HRV1A $2A^{pro}$ and HRV2 $2A^{pro}$ do not form a complex with eIF4GII$_{551\text{-}745}$. However, we speculate that HRV1A $2A^{pro}$ has a slow k_{off} rate during this interaction; therefore, SLS measurements gave a molecular mass corresponds to a heterodimeric complex (table 5.1). HRV2 $2A^{pro}$ titration on eIF4GII$_{551\text{-}745}$ had a K_D value of 75 μM (Aumayr et al., 2015), which is higher than our findings for this interaction using HRV1A $2A^{pro}$ (12 μM). Our findings also showed showed that both $2A^{pro}$ consist of dimers, unlike HRV4 $2A^{pro}$.

We found impressive results from the binding studies with HRV4 His_6VP1_8 $2A^{pro}$. The binding studies were conducted as explained above for HRV1A $2A^{pro}$ C106A except for the assay buffer. HRV1A $2A^{pro}$ studies were measured in Hepes buffer (pH 7.4), whereas buffer A (pH 9.0) was used for HRV4 His_6VP1_8 $2A^{pro}$. In contrast with the genetic group A $2A^{pro}$, there was no ternary complex formation with initiation factors for HRV4 His_6VP1_8 $2A^{pro}$ C110S. We observed two separate peaks for eIF4E/eIF4GII$_{551\text{-}745}$ complex and the $2A^{pro}$ (see figure 4.19 A). Moreover, HRV4 His_6VP1_8 $2A^{pro}$ C110S also did not bind to eIF4E. Peaks were analyzed with SDS-PAGE on 17.5 % SDS-PAGE gels and results were conclusive (see figure 4.19 B, C). Nevertheless, we wanted to repeat the experiment with HRV1A $2A^{pro}$ C106A to exclude any interference stemming from the buffer A at pH 9.0. Here, we state that HRV1A $2A^{pro}$ C106A forms a ternary complex with the initiation factors, whereas HRV4 His_6VP1_8 $2A^{pro}$ is incapable of doing so under the same conditions.

Interestingly, CVB4 $2A^{pro}$ does not form a binary complex with either eIF4E or eIF4GII$_{551\text{-}745}$, similar to HRV4 His_6VP1_8 $2A^{pro}$ C110S. Heterotrimeric complex formation was observed with CVB4 $2A^{pro}$/eIF4E/eIF4GII$_{551\text{-}745}$ (Aumayr et al., 2015) whereas HRV4 His_6VP1_8 $2A^{pro}$ failed to do so. Figure 5.4 B shows the sequence similarity between the $2A^{pro}$ of HRV4 and CVB4 in comparison to figure 5.4

A. Figure 5.2 shows the distance between two genetic groups of rhinoviral $2A^{pro}$ in a maximum likelihood phylogenetic tree. There are 0.86 amino acid substitutions per site in HRV4 $2A^{pro}$ sequence when compared to HRV1A (see figure 5.2 A) and they share little sequence homology (39 %) (figure 5.4 A). In a manner of interaction with initiation factors, the genetic group B $2A^{pro}$ behaves quite differently.

To summarize, we have observed important differences between HRV1A $2A^{pro}$ and HRV4 $2A^{pro}$. It will be important for more investigations about the initiation factor recognition and binding to be done to further illuminate this situation.

6 APPENDIX

6.1 List of amino acids

A	Ala	Alanine
C	Cys	Cysteine
D	Asp	Aspartic acid
E	Glu	Glutamic acid
F	Phe	Phenylalanine
G	Gly	Glycine
H	His	Histidine
I	Ile	Isoleucine
K	Lys	Lysine
L	Leu	Leucine
M	Met	Methionine
N	Asn	Asparagine
P	Pro	Proline
Q	Gln	Glutamine
R	Arg	Arginine
S	Ser	Serine
T	Thr	Threonine
V	Val	Valine
W	Trp	Tryptophan
Y	Tyr	Tyrosine

6.2 List of abbreviations

$2A^{pro}$	Proteinase 2A
Å	Angström
°C	Degrees celsius
μg	Microgram
μl	Microliter
μM	Micromolar

aa	Amino acid
Amp	Ampicillin
APS	Ammonium peroxidisulfate
ATP	Adenosine triphosphate
bp	Base pair
CDHR3	Cadherine-related family member 3
CIP	Calf intestine phophatase
CV	Coxsackievirus
dH_2O	Deionized water
DNA	Deoxyribonucleic acid
DNase	Deoxyribonuclease
dNTP	Deoxynucleotide triphosphate
DSP	Dithiobis(succinimidyl propionate)
DTT	Dithiothreitol
EDTA	Ethylenediaminetetraacetic acid
eIF	Eukaryotic initiation factor
FMDV	Foot-and-mouth disease virus
g	Gram
h	Hour
HAV	Hepatitis A virus
HeLa	Henrietta Lacks' cells
HRV	Human rhinovirus
ICAM-1	Intercellular adhesion molecule-1
ICTV	Internal committee on taxonomy of viruses
IRES	Internal ribosomal entry site
Kb	Kilobases
kDa	Kilo Dalton
l	Liter
L^{pro}	Leader proteinase
LB	Luria Bertani
LDL	Low-density-lipoprotein
LDLR	Low-density-lipoprotein receptor
LGS	Lower gel solution
M	Molar
min	Minutes
ml	Mililiter

mM	Milimolar
mRNA	Messenger RNA
nt	Nucleotide
NTP	Nucleotide triphosphate
NUP	Nuclear pore complex protein
ORF	Open reading frame
p	Proportion
PABP	Poly(A)-binding protein
PAGE	Polyacrylamide gel electrophoresis
PBS	Phosphate buffered saline
PCR	Polymerase chain reaction
PDB	Protein Data Bank
PNK	Polynuclotide kinase
PolyA	Poly adenylation
PV	Poliovirus
RNA	Ribonucleic acid
rpm	Rotations per minute
RT	Room temperature
SDS	Sodiumdodecylsulfate
SGBP	*Streptomyces griseus* proteinase B
TAE	Tris-acetate-EDTA
TB	Terrific Broth
TEMED	Tetramethylethylenediamine
UTR	Untranslated region
UV	Ultraviolet
VLDLR	Very low density lipoprotein receptor
VP	Viral protein
VPg	Viral protein genome linked
wt	Wild-type

REFERENCES

- http://viralzone.expasy.org/all_by_species/33.html
- http://www.picornaviridae.com/
- ICVT Master Species List 2015 v1 (http://ictvonline.org/index.asp)
- Ahlquist P., Kaesberg P., Determination of the length distribution of poly(A) at the 3' terminus of the virion RNAs of EMC virus, poliovirus, rhinovirus, RAV-61 and CPMV and of mouse globin mRNA, *Nucleic Acids Res* (1979), **7**, 5, 1195-1204
- Ambros V., Baltimore D., Protein is linked to the 5' end of poliovirus RNA by a phosphodiester linkage to tyrosine, *J Biol Chem* (1978), **253**, 15, 5263-5266
- Ambros V., Blatimore D., Purification and properties of HeLa cell enzyme able to remove 5'-terminal protein from poliovirus RNA, *J Biol Chem* (1980), **225**, 14, 6739-6744
- Aminev A. G., Amineva S. P., Pamenberg A. C., Encephalomyocarditis viral protein 2A localizes to nucleoli and inhibits cap-dependent mRNA translation, *Virus Research* (2003), **95**: 45-57
- Anderson E. C., Hunt S. L., Jackson R. J., Internal initiation of translation from the human rhinovirus-2 internal ribosome entry site requires the binding of Unr to two distinct sites on the 5' untranslated region, *J Gen Virol* (2007), **88**: 3043-3052
- Andino R., Rieckhof G. E., Baltimore D., A functional ribonucleoprotein complex forms around the 5' end of poliovirus RNA, *Cell* (1990), **63**(2): 369-80
- Andino R., Rieckhof G. E., Achacoso P. L., Baltimore D., Poliovirus RNA synthesis utilizes an RNP complex formed around the 5'-end of viral RNA, *EMBO J* (1993), **12**, 9, 3587-3598
- Aumayr M. (2012) Investigation of the 2A proteinase of human rhinovirus 1A and 14. *Masterarbeit*
- Aumayr M. (2015) Structural basis of eIF4G cleavage by picornaviral proteinases and the involvement of eIF4E. *Dissertation*
- Aumayr M., Fedosyuk S., Ruzicska K., Sousa-Blin C., Kontaxis G., Skern T., NMR analysis of the interaction of picornaviral proteinases lb and 2A with their substrate eukaryotic initiation factor 4GII, *Protein Sci* (2015), **24**(12): 1979-96
- Barrett, A., Rawlings N., Woessner J. (2013), *Handbook of proteolytic enzymes Volume 1* Rawlings N. D., Salvesen G. Y., (Ed.), San Diego, CA: Academic Press, Elsevier
- Barton D. J., Morasco B. J., Flanegan J. B., Translating ribosomes inhibit poliovirus negative-strand RNA synthesis, *J Virol* (1999), **73**, 12, 10104-10112
- Baxter N. J., Roetzer A., Liebig H.-D., Sedelnikova S. E., Hounslow A. M. et al., Structure and dynamics of coxsackievirus B4 2A proteinase, an enzyme involved in the etiology of heart disease, *J Virol* (2006), **80**: 1451-1462

- Bazan J. F., Fletterick R. J., Viral cysteine proteinases are homologous to the trypsin-like family of serine proteinases: Structural and function implications, *Proc Natl Acad Sci USA* (1988), **85**, 7872-7876
- Bedard K. M., Daijogo S., Semler B. L., A nucleo-cytoplasmic SR protein functions in viral IRES-mediated translation initiation, *EMBO J* (2007), **26**, 459-467
- Beneke T. W., Habermehl K. O., Diefenthal W., Buchholz M., Iodination of poliovirus capsid proteins, *J Gen Virol* (1977), **34**, 387-390
- Belov G. A., Lidsky P. V., Mikitas O. V., Egger D., Lukyanov K. A., Bienz K., Agol V. I., Bidirectional increase in permeability of nuclear envelope upon poliovirus infection and accompanying alterations of nuclear pores, *J Virol* (2004), **78**, 10166-10177
- Belsham G. J., Translation and replication of FMDV RNA, *Curr Top Microbiol Immunol* (2005), **288**: 43-70
- Bizzintino J., Lee W. M., Laing I. A., Vang F., Pappas T., Zhang G., Martin A. C., Khoo S. K., Cox D. W., Geelhoed G. C., McMinn P. C., Goldblatt J., Gern J. E., Le Souef P. N., Association between human rhinovirus C and severity of acute asthma in children, *Eur Respir J* (2011), **37**(5): 1037-42
- Blaas D., Fuchs R., Mechanism of human rhinovirus infections, *Mol Cell Pediatr*. (2016), **3**:21
- Bochkov Y. A., Watters K., Ashraf S., Griggs T. F., Devries M. K., Jackson D. J., Palmenberg A. C., Gern J. E., Cadherin-related family member 3, a childhood asthma susceptibility gene product, mediates rhinovirus C binding and replication, *PNAS* (2015), **112**, 17, 5485-5490
- Borman A., Jackson R. J., Initiation of translation of human rhinovirus RNA: mapping the internal ribosome entry site, *Virology* (1992), **188**(2): 685-96
- Borman A. M., Bailly J., L., Girard M., Kean K. M., Picornavirus internal ribosome entry segments comparison of translation efficiency and the requirements for optimal internal initiation of translation *in vitro*, *Nucleic Acids Res* (1995), **23**, 3656-3663
- Borman A. M., Kean K. M., Intact eukaryotic initiation factor 4G is required for hepatitis A virus internal initiation of translation, *Virology* (1997), **237**(1): 129-36
- Borman A. M., Le Mercier P., Girard M., Kean K. M., Comparison of picornaviral IRES-driven internal initiation of translation in cultured cells of different origins, *Nucleic Acid Res* (1997), **25**, 5, 925-932
- Branden C., Tooze J. (1999), *Introduction to Protein Structure* New York NY: Garland Science
- Collis P. S., O'Donnel B. J., Barton D. J., Rogers J. A., Flanegan J. B., Replication of poliovirus RNA and subgenomic RNA transcripts in transfected cells, *J Virol* (1992), **66**, 11, 6480-6488
- Costa S., Almeida A., Castro A., Domingues L., Fusion tags for protein solubility, purification ad immunogenicity in *Echerichia coli*: the novel Fh8 system, *Front Microbiol* (2014), **5**: 63
- Crooks G. E., Hon G., Chandonia J. M., Brenner S. E., WebLogo: a sequence logo generator, *Genome Res* (2004), **14**(6): 1188-90

- Dasgupta A., Yalamancholi P., Clark M., Kliewer S., Fradkin L., Rubinstein S., Das S., Shen Y., Weidman W. K., Banerjee R., Datta U., Igo M., Kundu P., Barat B., Berk A. J., Effects of picornavirus proteinases on host cell transcription, (2003), p. 321-335, *In* Semler B. L., Wimmer E. (Eds.), *Molecular biology of picornaviruses*, ASM Press, Washington, D.C.
- Davies M. V., Pelletier J., Meerovitch K., Sonenberg N., Kaufman R. J., Inhibition of DNA replication, RNA polymerase II transcription, and translation, *J Biol Chem* (1991), **226** (22), 14714-14720
- de Breyne S., Yu Y., Unbehaun A., Pestova T. V., Hellen C. U. T., Direct functional interaction of initiation factor eIF4G with type 1 internal ribosomal entry sites, *Proc Natl Acad Sci USA* (2009), **106**: 9197-9202
- Devaney M. A., Vakharia V. N., Lloyd R. E., Ehrenfeld E., Grubman M. J., Leader protein of foot-and-mouth disease virus is required for cleavage of the p220 component of the cap-binding protein complex, *J Virol* (1988), **62**, 11, 4407-4409
- Dever T. E., Translation initiation: adept at adapting, *Trends in Biochemical Sciences* (1999), **24**, 10, 398-403
- Do D. H., Laus S., Leber A., Marcon M. J., Jordan J. A., Martin J. M., Wadowsky R. M., A One-Step, Real-Time PCR Assay for Rapid Detection of Rhinovirus, *J Mol Diagn* (2010), **12**, 1
- Edsall J. T., Felsenfeld G., Goodman D. S., Gurd F. R. N., The association of imidazole with ions of zinc and cupric copper, *J Am Chem Soc* (1954), **76**(11): 3054-3061
- Etchison D., Milburn S. C., Edery I., Sonenberg N., Hershey J. W. B., Inhibition of HeLa cell protein synthesis following poliovirus infection correlates with the proteolysis of a 220,000-dalton polypeptide associated with eukaryotic initation factor 3 and a cap binding complex, *J Biol chem* (1982), **257**, 24, 14806-14810
- Fendrick A. M., Monto A. S., Nightengale B., Sarnes M., The economic burden of non-influenza-related viral respiratory tract infection in the United States, *Arch Intern Med* (2003), **163**: 487-494
- Fitzgerald K. D., Chase A. J., Cathcart A. L., Tran G. P., Semler B. L., Viral proteinase requirements for nucleocytoplasmic relocalization of cellular splicing factor SRp20 during picornavirus infections, *J Virol* (2013), **87**(5): 2390-2400
- Flanegan J. B., Petterson R. F., Ambros V., Hewlett M. J., Baltimore D., Covalent linkage of a protein to a defined nucleotide sequence at the 5'-terminus of virion and replicative intermediate RNAs of poliovirus, *Biochemistry* (1977), **74**, 3, 962-965
- Flather D., Semler B. L., Picornaviruses and nuclear function: targeting a cellular compartment distinct from the replication site of a positive-strand RNA virus, *Front Microbiol* (2015), **6**: 594
- Fields B. N., Knipe D. M., Howley P. M., (2007), *Fields' Virology*, Wolters Kluwer Health/Lippincott Williams & Wilkins, Philadelphia, PA

- Foxman E. F., Storer J. A., Fitzgerald M. E., Wasik B. R., Hou L., Zhao H., Turner P. E., Pyle A. M., Iwasaki A., Temperature-dependent innate defense against the common cold virus limits viral replication at warm temperature in mouse airway cells, *PNAS* (2014) **112**, 3, 837-832
- Fuchs R., Blaas D., Uncoating of human rhinoviruses, *Rev Med Virol* (2010), **210**: 281-297
- Gamarnik A.V., Andino R., Two functional complexes formed by KH domain containing proteins with the 5' noncoding region of poliovirus RNA, *RNA* (1997), **3**: 882-892
- Gamarnik A. V., Andino R., Switch from translation to RNA replication in a positive-stranded RNA virus, *Genes Dev* (1998), **12**(15): 2293-2304
- Gamarnik A. V., Andino R., Interactions of viral protein 3CD and poly(rC) binding protein with the 5' untranslated region of the poliovirus genome, *J Virol* (2000), **74**(5): 2219-26
- Gauss-Müller V., Deinhardt F., Effect of hepatitis A virus infection on cell metabolism in vitro, *Proc Soc Exp Biol Med* (1984), **175**(1): 10-5
- Ghildyal R., Jordan B., Li D., Dagher H., Bardin P. G., Gern J. E., Jans D. A., Rhinovirus 3C proteinase can localize in the nucleus and alter active and passive nucleocytoplasmic transport,
- Gingras A.-C., Raught B., Sonenberg N., eIF4 initiation factors: effectors of mRNA recruitment to ribosomes and regulators of translation (1999), **68**: 913-963
- Gorbalenya A., E., Donchenko A. P., Blinov V. M., Koonin E. V., Cysteine proteinases of positive strand RNA viruses and chymotrypsin-like serine proteinases. A distinct protein superfamily with a common cold structural fold, *FEBS Lett* (1989), **243**, 2, 103-114
- Gustin K. E., Sarnow P., Inhibition of nucleat import and alteration of nuclear pore complex composition by rhinovirus, *J Virol* (2002), **76**(17): 8787-96
- Gradi A., Imataka H., Svitkin Y. V., Rom E., Raught B., Morino S., Sonenberg N., A novel function human eukaryotic translation initiation factor 4G, *Mol Cell Biol* (1998a), **18**(1): 334-342
- Gradi A., Svitkin Y. V., Imataka H., Sonenberg N., Proteolysis of human eukaryotic translation initiation factor eIF4GII, but not eIF4GI, coincides with the shutoff of host protein synthesis after poliovirus infection, *PNAS* (1998b), **95**, 19, 11089-11094
- Gradi A., Svitkin Y. V., Sommergruber W., Imataka H., Morino S., Skern T., Sonenberg N., Human rhinovirus 2A proteinase cleavage sites in eukaryotic initiation factors (eIF) 4GI and eIF4GII are different, *J Virol* (2003), **77**(8): 5026-9
- Gradi A., Foeger N., Strong R., Svitkin R., Sonenberg N., Skern T., Belsham G. J., Cleavage of eukaryotic translation initiation factor 4GII within foot-and-mouth disease virus-infected cells: identification of the L-proteinase cleavage site in vitro, *J Virol* (2004), **78**(7): 3271-3278
- Greve J. M., Davis G., Meyer A. M., Forte C. P., Yost S. C., Marlor C. W., Kamarck M. E., McClelland A., The major human rhinovirus receptor is ICAM-1, *Cell Press* (1989), **56**, 5, 839-847
- Gustin K. E., Sarnow P., Effects of poliovirus infection on nucleo-cytoplasmic trafficking and

nuclear pore complex composition, *EMBO J* (2001), **20**(1-2): 240-9

- Gustin K. E., Sarnow P., Inhibition of nuclear import and alteration of nuclear pore complex composition by rhinovirus, *J Virol* (2002), **76**(17): 8787-96
- Haghighat A., Svitkin Y., Novoa I., Kuechler E., Skern T. Sonenberg N., The eIF4G-eIF4E complex is the target direct cleavage by the rhinovirus 2A proteinase, *J Virol* (1996), **70**, 12, 8444-8450
- Harris K. S., Xiang W., Alexander L., Lane W. S., Paul A. V., Wimmer E., Interaction of poliovirus polypeptide $3CD^{pro}$ with the 5' and 3' termini of the poliovirus genome, *J Biol Chem* (1994), **269**, 43, 27004-27014
- Hayden F. G., Turner R. B., Gwaltney J. M., Chi-Burris K., Gersten M., Hsyu P., Patick A. K., Smith G. J. 3rd, Zalman L. S., Phase II, randomized, double-blind, placebo-controlled studies of ruprintrivir nasal spray 2-percent suspension for prevention and treatment of experimentally induced rhinovirus colds in healthy volunteers, *Antimicrob Agents Chemother* (2003), **47**(12): 3907-16
- Herold J., Andino R., Poliovirus RNA replication requires genome circularization through a protein-protein bridge, *Mol Cell* (2001), **7**, 3, 581-591
- Hershey J. W. B., Merrick W. C., (2000) *The pathway and mechanism of initiation of protein synthesis* Hershey N., Matthews M. B., Sonenberg N. (Eds.), Cold Spring Harbor Monograph Archive, Woodbury, NY
- Hewat E. A., Neumann E., Conway J. F., Moser R., Ronacher B., Marlovits T. C., Blaas D., The cellular receptor of human rhinovirus 2 binds around the 5-fold axis not in the canyon: a structural view, *EMBO J* (2000), **19**: 6317-6325
- Hofer F., Gruenberger M., Kowalski H., Machat H., Huettinger M., Kuechler E., Blaas D., Members of the low density lipoprotein receptor family mediate cell entry of a minor-group common cold virus, *Proc Natl Acad Sci U S A* (1994), **91**(5): 1839-42
- Hogle J. M., Chow M., Filman D. J., Three-dimensional structure of poliovirus at 2.9 A resolution, *Science* (1985), **229**(4720): 1358-65
- Hordern J. S., Leonard J. D., Scraba D. G., Structure of the mengo virion. VI. Spatial relationships of the capsid polypeptides as determined by chemical cross-linking analyses, *Virology* (1979), **1**, 131-140
- Hunt S. L., Jackson R. J., Polypyrimidine tract-binding protein (PTB) is necessary, but not sufficient, for efficient internal initiation of translation of human rhinovirus-2 RNA, *RNA* (1999), **5**(3): 344-359
- Jackson R. J., Kaminski A., Internal initiation of translation in eukaryotes: the picornavirus paradigm and beyond, *RNA* (1995), **1**(10): 985-1000
- Jackson R. J., Hellen C. U. T., Pestova T. V., The mechanism of eukaryotic translation initiation

and principles of its regulation, *Nature Rev Mol Cell Biol* (2010), **11**, 113-127

- Jacobson M. F., Baltimore D., Morphogenesis of poliovirus. I. Association of the viral RNA with coat protein, *J Mol Biol* (1968), **33**(2): 369-78
- Jacobson M. F., Asso J., Baltimore D., Further evidence on the formation of poliovirus proteins, *J Mol Biol* (1970), **49**, 657-699
- Jacobson S. E., Lamson D. M., St George K., Walsh T. J., Human rhinoviruses, *Clin Microbiol Rev* (2013), **26**(1): 135-162
- Jiang P., Liu Y., Ma H., Paul A. V., Wimmer E., Picornavirus Morphogenesis, *Microbiol Mol Biol Rev*. (2014), **78**, 418-437
- Joachims M., Breugel P. C. V., Lloyd R. E., Cleavage of poly(A)binding protein by enterovirus proteinases concurrent with inhibition of translation *in vitro*, *J Virol* (1999), **73**, 718-727
- Imataka H., Gradi A., Sonenberg N., A newly identified N-terminal amino acid sequence of human eIF4G binds poly(A)-binding protein and functions in poly(A)-dependent translation, *EMBO J* (1998), **17**(24): 7480-9
- Izumi R. E., Valdez B., Banerjee R., Srivastava M., Dasgupta A., Nucleolin stimulates viral internal ribosome entry site-mediated translation, *Virus Res* (2001), **76**(1): 17-29
- Kaariainen L., Ranki M., Inhibition of cell functions by RNA-virus infections, *Annu Rev Microbiol* (1984), **38**: 91-109
- Kafasla P., Mogner N., Robinson C. V., Jackson R. J., Polypyrimidine tract-binding protein stimulates the poliovirus IRES by modulating eIF4G binding, *EMBO J* (2010), **29**, 3710-3722
- Kirchweger R., Ziegler E., Lamphear B. J., Waters D., Liebig H.-D., Sommergruber W., Sobrino F., Hohenadl C., Blaas D., Rhoads R. E., et al., Footh-and-mouth disease virus leader proteinase: purification of the Lb form and determination of its cleavage site on eIF-4 gamma, *J Virol* (1994), **68**(9): 5677-84
- König H., Rosenwirth B., Purification and partial characterization of poliovirus proteinase 2A by means of a functional assay, *J Virol* (1988), **62**, 4, 1243-1250
- Kuge S., Saito I., Nomoto A., Primary structure of poliovirus defective-interfering particle genomes and possible generation mechanisms of the particles, *J Mol Biol* (1986), **192**, 3, 473-487
- Lamphear B. J., Yan R., Yang F., Waters D., Liebig H.-D., Klump H., Kuechler E., Skern T., Rhoads R. E., Mapping the cleavage site in protein synthesis initiation factor eIF-4g of the 2A proteinases from human coxsackievirus and rhinovirus, *J Biol Chem* (1993), **268**, 26, 19200-19203
- Lamphear B. J., Kirchweger R., Skern T., Rhoads R. E., Mapping of functional domains in eukaryotic protein synthesis initiation factor 4G (eIF4G) with picornaviral proteinases, *J Biol Chem* (1995), **270**, 21975-21983
- Lawson M. A., Semler B. L., Alternate poliovirus nonstructural protein processing cascades generated by primary sites of 3C proteinase cleavage, *Virology* (1992), **191**, 309-320

- Lee Y. F., Nomoto A., Detjen B. M., Wimmer E., A protein covalently linked to poliovirus genome RNA, *Biochemistry* (1977), **74**, 1 59-63
- Lee W., Watters K. E., Troupis A. T., Reinen N. M., Suchy F. P., Moyer K. L., Frederick R. O., Tonelli M., Aceti D. J., Palmenberg A. C., Markley J. L., Solution structure of the 2A proteinase from a common cold agent, human rhinovirus c2, strain w12, *PLoS ONE* (2014), **9**(6): e91298
- Liebig H. D., Ziegler E., Yan R., Hartmuth K., Klump H., Kowalski H., Blaas D., Sommergruber W., Frasel L., Lamphear B., et al., Purification of two picornaviral 2A proteinases: interaction with eIF-4 g and influence on in vitro translation, *Biochemistry* (1993), **32**(29): 7581-8
- Llyod R. E., Toyoda H., Etchison D., Wimmer E., Ehrenfeld E., Cleavage of the cap binding protein complex polypeptide p220 is not effected by the second poliovirus proteinase 2A, *Virology* (1986), **150**(1): 299-303
- Lonberg-Holm K., Butterworth B. E., Investigation of the Structure of Polio- and Human Rhinovirions through the Use of Selective Chemical Reactivity, *Virology* (1976), **71**, 1, 207-216
- Lyons T., Murray K. E., Roberts A. W., Barton D. J., Poliovirus 5'-terminal cloverleaf RNA is required in cis for VPg uridylylation and the initiation of negative-strand RNA synthesis, *J Virol* (2001), **75**(22): 10696-708
- Mahy B. W. J., van Regenmortel M. H. V. (2010), *Desk Encyclopedia of General Virology,* San Diego, CA: Academic Press, Elsevier
- Marongiu M. E., Pani A., Corrias M. V., Sau M., La Colla P., Poliovirus morphogenesis I. Identification of 80S dissociable particles and evidence for the artifactual production of procapsids, *J Virol* (1981), **39**, 2, 341-347
- Mclntyre C. L., Knowles N. J., Simmonds P., Proposals for the classification of human rhinovirus species A, B and C into genotypically assigned types, *J Gen Virol* (2013), **94**, 1792-1806
- Merrill M. K., Dobrikova E. Y., Gromeier M., Cell-type-specific repression of internal ribosome entry site activity by double-stranded RNA-binding protein 76, *J Virol* (2006), **80**, 3147-3156
- Merrill M. K., Gromeier M., The double-stranded RNA binding protein 76: NF45 heterodimer inhibits translation at the rhinovirus type 2 internal ribosome entry site, *J Virol* (2006), **80**, 1570-1585
- Mischak H., Neubauer C., Berger B., Kuechler E., Blaas D., Detection of human rhinovirus minor group receptor on renaturing western blots, *J Gen Virol* (1988), **69**, 2653-2656
- Neubauer C., Kuechler E., Blaas D., Mechanism of entry of human rhinovirus 2 into HeLa cells, *Virol* (1987), **158**(1): 255-8
- Neubauer D. (2013) Investifating the substrate specificity of enteroviral 2A proteinases- an attempt to solve high resolution structures of enzyme-substrate complexes. *Dissertation*
- Neubauer D., Aumayr M., Gösler I., Skern T., Specificity of human rhinovirus $2A^{pro}$ is determined by combined spatial properties of four cleavage site residues, *J Gen Virol* (2013), **94**(Pt 7): 1535-

1546

- Nomoto A., Lee Y. F., Wimmer E., The 5' end of poliovirus mRNA is not capped with m7G(5')ppp(5')Np, *Proc Natl Acad Sci U S A* (1976), **73**(2): 375-380
- Novak J. E., Kirkegaard K., Improved method for detecting poliovirus negative strands used to demonstrate specificity of positive-strand encapsidation and the ratio of positive to negative strands in infected cells, *J Virol* (1991), **65**, 6, 3384-3387
- Novak J. E., Kirkegaard K., Coupling between genome translation and replication in an RNA virus, *Genes Dev* (1994), **8**: 1726-1737
- Nugent C. I., Kirkegaard K., RNA binding properties of poliovirus subviral particles, *J Virol* (1995), **69**, 1, 13-22
- Ohlmann T., Rau M., Pain V. M., Morley S. J., The C-terminal domain of eukaryotic protein synthesis initiation factor (eIF) 4G is sufficient to support cap-independent translation in the absence of eIF4E, *EMBO J* (1996), **15**, 1371
- Olson N. H., Kolatkar P. R., Oliveira M. A., Cheng R. H., Greve J. M., McClelland A., Baker T. S., Rossmann M. G., Structure of a human rhinovirus complexed with its receptor molecule, *Proc Natl Acad Sci U S A* (1993), **90**(2): 507-511
- Onodera S., Phillips S. A., A novel method for obtaining poliovirus 14 S pentamers from procapsids and their self-assembly into virus-like shells, *Virology* (1987), **159**(2): 278-87
- Palmenberg, A. C., M. Pallansch, and R. R. Rueckert, Proteinase required for processing picornaviral coat protein resides in the viral replicase gene, *J Virol* (1979), **32**: 770-778.
- Palmenberg A. C., In vitro synthesis and assembly of picornaviral capsid intermediate structures, *J Virol* (1982), **44**, 3, 900-906
- Palmenberg A. C., Spiro D., Kuzmickas R., Wang S., Djikeng A., Rathe J. A., Fraser-Liggett C. M., Liggett S. B., Sequencing and analyses of all known human rhinovirus genomes reveal structure and evolution, *Science* (2009), **324**(5923): 55-59
- Pappas D. E., Hendly J. O., Hayden F. G., Winter B., Symptom profile of common colds in school-aged children, *Pediatr Infect Dis J* (2008), **27**: 8-11
- Park N., Skern T., Gustin K. E., Specific cleavage of the nuclear pore complex protein Nup62 by a viral proteinase, *J Biol Chem* (2010), **285**(37): 28796-28805
- Parsley T. B., Towner J. S., Blyn L. B., Ehrenfeld E., Semler B.i L., Poly (rC) binding protein 2 forms a ternary complex with the 5'-terminal sequences of poliovirus RNA and the viral 3CD proteinase, *RNA* (1997), **3**: 1124-1134
- Pelletier J., Sonenberg N., Internal initiation of translation of eukaryotic mRNA directed by a sequence derived from poliovirus RNA, *Nature* (1988), **334**(6180): 320-5
- Pestova T. V., Hellen C. U. T., Shatsky I. N., Canonical eukaryotic initiation factors determine initiation of translation by internal ribosomal entry, *Mol Cell Biol* (1996), **16**: 6859-6869

- Petersen J. F. W., Cherney M. M., Liebig H.-D., Skern T., Kuechler E., James M. N. G., The structure of the 2A proteinase from a common cold virus: a proteinase responsible for the shut off of host cell protein synthesis, *EMBO J* (1999), **18**, 20, 5463-5475
- Pilipenko E. V., Blinov V. M., Chernov B. K., Dmitrieva T. M., Agol V. I., Conservation of the secondary structure of the 5'-untranslated region of cardio- and aphthovirus RNAs, *Nucleic Acids Res* (1989), **17**, 14
- Pilipenko E. V., Blinov V. M., Agol V. I., Gross rearrangements within the 5'-untranslated region of picornaviral genomes, *Nucleic Acids Res* (1990), **18**, 11, 3371
- Prchla E., Kuechler E., Blaas D., Fuchs R., Uncoating of human rhinovirus serotype 2 from late endosomes, *J Virol* (1994), **68**, 6, 3713-3723
- Rombaut B., Vrijsen R., Boeye A., In vitro assembly of poliovirus empty capsids: antigenic consequences and immunological assay of the morphopoietic factor, *Virology* (1984), **135**(2): 546-50
- Rombaut B., Vrijsen R., Boeye A., A pH-dependent dissociation of poliovirus procapsids, *Virology* (1987), **157**, 1, 245-247
- Rombaut B., Boeye A., In vitro assembly of poliovirus 14 S subunits: disoxaril stabilization as a model for the antigenicit conferring activity of infected cell extracts, *Virology* (1991), **180**(2): 788-792
- Rott R., Siddell S., One hundred years of animal virology, *J Gen Virol* (1998), **79**, 2871-2874
- Rossmann M. G., Arnold E., Erickson J. W., Frankenberger E. A., Griffith J. P., Hecht H.-J., Johnson J. E., Kamer G., Luo M., Mosser A. G., Rueckert R. R., Sherry B., Vriend G., Structure of a human common cold virus and functional relationship to other picornaviruses, *Nature* (1985), **317**, 145-153
- Royston L., Tapparel C., Rhinoviruses and Respiratory Enteroviruses: Not as Simple as ABC, *Viruses* (2016), **8**, 16
- Rueckert R. R., Wimmer E., Systematic nomenclature of picornavirus proteins, *J Virol* (1984), **50**, 3, 957-959
- San-Miguel T., Bermúdez, Gavidia I., Production of soluble eukaryotic recombinant proteins in *E. coli* is favored in early log-phase cultures induced at low temperature, *Springerplus* (2013), **2**: 89
- Sarkany Z., Skern T., Polgar L., Characterization of the active site thiol group of rhinovirus 2A proteinase, *FEBS Lett* (2000), **481**, 289-292
- Sarnow P., Role of 3'-end sequences in infectivity of poliovirus transcripts made in vitro, *J Virol* (1989), **63**, 1, 467-470
- Sharma r., Raychaudhuri S., Dasgupta A., Nuclear entry of poliovirus proteinase-polymerase precursor 3CD: implications for host cell transcription shut-off, *Virology* (2004), **320**, 195-205

- Simmonds P., Mclntyre C., Savolanien-Kopra C., Tapparel C., Mackay I. M., Hovi T., Proposals for the classification of human rhinovirus species C into gentoypically assigned types, *J Gen Virol* (2010), **91**, 2409-2419
- Skern T., Sommergruber W., Auer H., Volkmann P., Zorn M., Liebig D.-H., Fessl F., Blaas D., Kuechler E., Substrate requirements of a human rhinoviral 2A proteinase, *Virology* (1991), **181**(1): 46-54
- Sommergruber W., Zorn M., Blaas D., Fessl F., Volkmann P., Maurer-Fogy I., Pallai P., Merluzzi V., Matteo M., Skern T. et al., Polypeptide 2A of human rhinovirus type 2: identification as a proteinase and characterization by mutational analysis, *Virology* (1989), **169**(1): 68-77
- Sommergruber W., Ahorn H., Zöphel A., Maurer-Fogy I., Fessl F., Schnorrenberg G., Liebig H.-D., Blaas D., Kuechler E., Skern T., Cleavage specificity on synthetic peptide substrates of human rhinovirus 2 proteinase 2A, *J Biol Chem* (1992), **267**, 31, 22639-22644
- Sommergruber W., Ahorn H., Klump H., Seipelt J., Zoephel A., Fessl F., Krystek E., Blaas D., Kuechler E., Liebig H.-D., Skern T., 2A proteinases of coxsackie- and rhinovirus cleave peptides derived from eIF-4γ via a common recognition motif, *Virology* (1994a), **198**, 2, 741-745
- Sommergruber W., Casari G., Fessl F., Seipelt J., Skern T., The 2A proteinase of human rhinovirus is a zinc containing enzyme, *Virology* (1994b), **204**(2): 815-8
- Sommergruber W., Seipelt J., Fessl F., Skern T., Liebig H.-D., Casari G., Mutational Analyses support a model for the HRV2 2A proteinase, *Virology* (1997), **234**, 203-214
- Sonenberg N., Morgan M. A., Merrick W. C., Shatkin A. J., A polypeptide in eukaryotic initiation factors that crosslinks specifically to the 5'-terminal cap in mRNA, *Proc NAtl Acad Sci USA* (1978), **75**(10): 4843-7
- Spector D. H., Baltimore D., Requirement of 3'-terminal poly(adenylic acid) for the infectivity of poliovirus RNA, *Proc Natl Acad Sci USA* (1974), **71**, 8, 2983-2987
- Svitkin Y. V., Herdy B., Costa-Mattioli M., Gingras A. C., Raught B., Sonenberg N., Eukaryotic translation initiation factor 4E availability controls the switch between cap-dependent and internal ribosomal entry site-mediated translation, *Mol Cell Biol* (2005), **25**(23): 10556-65
- Toyoda H., Nicklin M. J., Murray M. G., Anderson C. W., Dunn J. J., Studier F. W., Wimmer E., A second virus-encoded proteinase involved in proteolytic processing of poliovirus polyprotein, *Cell* (1986), **45**: 761-770
- Tsukada H., Blow D. M., Structure of alpha-chymotrypsin refined at 1.68 A resolution, *J Mol Biol* (1985), **184**(4): 703-11
- Turner R. B., Rhinovirus: More than Just a Common Cold Virus, *J Infect Dis* (2007); **195**: 765-6
- Virgen-Slane R., Rozovics J. M., Fitzgerald K. D., Ngo T., Chou W., van der Heden van Noort G. J., Filippov D. V., Gershon P. D., Semler B. L., An RNA virus hijacks an incognito function of DNA repair enzyme, *Proc Natl Acad Sci U S A* (2012), **109**(36): 14634-9

- Vogt D. A., Andino R., An RNA element at the 5'-end of the poliovirus genome functions as a general promoter for RNA synthesis, *PLoS Phathog* (2010), **6**(6): e1000936
- Voss T., Meyer R., Sommergruber W., Spectroscopic characterization of rhinoviral proteinase 2A: Zn is essential for the structural integrity, *Protein Sci* (1995), **4**(12): 2526-31
- Vlasak M., Roivainen M., Reithmayer M., Goesler I., Laine P., Snyers L., Hovi T., Blaas D., The minor receptor group of human rhinovirus (HRV) includes HRV23 and HRV25, but the presence of a Lys in the VP1 HI loop is not sufficient for receptor binding, *J Virol* (2005), **79**, 12, 7389-7395
- Vlasak M., Blomqvist S., Hovi T., Hewat E., Blaas D., Sequence and structure of human rhinoviruses reveal the basis of receptor discrimination, *J Virol* (2003), **77**(12): 6923-6930
- Waggoner S., Sarnow P., Viral ribonucleoprotein complex formation and nucleolar-cytoplasmic relocalization of nucleolin in poliovirus-infected cells, *J Virol* (1998), **72**(8): 6699-709
- Watters K., Palmenberg A. C., Differential processing of nuclear porecomplex proteins by rhinovirus 2A proteinases from different species and serotypes, *J Virol* (2011), **85**(20): 10874-83
- Wetz K., Habermehl K. O., Specific Cross-linking of Capsid Proteins to Virus RNA by Ultraviolet Irradiation of Poliovirus, *J Gen Virol* (1982), **59**, 397-401
- Whitton J. L., Cornell C. T., Feuer R., Host and virus determinants of picornavirus pathogenesis and tropism, *Nature Reviews* (2005), **3**, 765-776
- Wingfield P. T., Protein precipitation using ammonium sulphate, *Curr Protoc Protein Sci* (2001), Appendix-3F
- Zoll J., Heus H. A., van Kuppeveld F. J., Mechers W. J., The structure-function relationship of the enterovirus 3'-UTR, *Virus Res* (2009), **139**: 209-216